

UNIVERSITY OF CALIFORNIA, SAN DIEGO

An Empirical Chaos Expansion Method for Uncertainty Quantification

A Dissertation submitted in partial satisfaction of the
requirements for the degree
Doctor of Philosophy

in

Mathematics with a Specialization in Computational Science

by

Gautam Wilkins

Committee in charge:

Professor Melvin Leok, Chair
Professor Scott Baden
Professor Philip Gill
Professor Michael Holst
Professor Daniel Tartakovsky

2016

Copyright
Gautam Wilkins, 2016
All rights reserved.

The Dissertation of Gautam Wilkins is approved, and it is acceptable in quality and form for publication on microfilm and electronically:

Chair

University of California, San Diego

2016

DEDICATION

To my wonderful fiancée Jennifer and to my parents for all of their encouragement and support. And to my dog Kenny for sitting beside me on the couch during many days and nights of research and revisions.

TABLE OF CONTENTS

	Signature Page	iii
	Dedication	iv
	Table of Contents	v
	List of Figures	viii
	Acknowledgements	xi
	Vita	xii
	Abstract of the Dissertation	xiii
Chapter 1	Introduction	1
	1.1 Introduction	2
	1.1.1 Polynomial Chaos	2
	1.1.2 General Basis	5
	1.1.3 Conversion Between Bases	8
Chapter 2	Empirical Chaos Expansion	10
	2.1 Empirical Bases	11
	2.1.1 Sampling Trajectories	12
	2.1.2 Model Reduction	13
	2.1.3 Proper Orthogonal Decomposition	14
	2.1.4 Empirical Chaos Expansion	16
	2.1.5 Convergence	18
	2.2 One Dimensional Wave Equation	22
	2.2.1 Polynomial Chaos Expansion	22
	2.2.2 Empirical Chaos Expansion	26
	2.2.3 Running Time	33
	2.2.4 Basis Function Evolution	34
	2.3 Two Dimensional Wave Equation	37
	2.3.1 Polynomial Chaos Expansion	37
	2.3.2 Sparse Grid Quadrature	41
	2.3.3 Empirical Chaos Expansion	43
	2.3.4 Running Time	44
	2.4 Diffusion Equation	45
	2.4.1 Polynomial Chaos Expansion	46
	2.4.2 Empirical Chaos Expansion	48
	2.4.3 Running Time	51
	2.4.4 Basis Function Evolution	52

	2.5	Advection-Reaction Equation	59
	2.5.1	Polynomial Chaos Expansion	60
	2.5.2	Empirical Chaos Expansion	66
	2.5.3	Running Time	70
	2.5.4	Basis Function Evolution	71
	2.6	Reaction-Diffusion Equation	75
	2.6.1	Polynomial Chaos Expansion	76
	2.6.2	Empirical Chaos Expansion	82
	2.6.3	Running Time	87
	2.6.4	Basis Function Evolution	88
	2.7	Acknowledgements	91
Chapter 3		Empirical Basis Evolution Operator	92
	3.1	Empirical Basis Evolution	93
	3.1.1	One Dimensional Wave Equation	95
	3.1.2	Diffusion Equation	100
	3.2	Acknowledgements	103
Chapter 4		Stochastic Collocation	104
	4.1	One Dimensional Wave Equation	108
	4.1.1	Polynomial Chaos Expansion	108
	4.1.2	Empirical Chaos Expansion	109
	4.1.3	Running Time	112
	4.1.4	Basis Function Evolution	113
	4.2	Diffusion Equation	115
	4.2.1	Polynomial Chaos Expansion	115
	4.2.2	Empirical Chaos Expansion	116
	4.2.3	Running Time	118
	4.2.4	Basis Function Evolution	119
	4.3	Advection-Reaction Equation	123
	4.3.1	Polynomial Chaos Expansion	123
	4.3.2	Empirical Chaos Expansion	124
	4.3.3	Running Time	126
	4.3.4	Basis Function Evolution	127
	4.4	Reaction-Diffusion Equation	129
	4.4.1	Polynomial Chaos Expansion	129
	4.4.2	Empirical Chaos Expansion	130
	4.4.3	Running Time	132
	4.4.4	Basis Function Evolution	133
	4.5	Acknowledgements	136

Chapter 5	Conclusion	137
	5.1 Future Work	138
Bibliography	141

LIST OF FIGURES

Figure 2.1:	One dimensional wave mean square expectation at $x = 0$ from gPC . . .	24
Figure 2.2:	One dimensional wave mean square expectation at $x = 0$ from gPC . . .	25
Figure 2.3:	One dimensional wave mean square expectation at $x = 0$ from gPC . . .	25
Figure 2.4:	One dimensional wave mean square expectation at $x = 0$ from gPC . . .	26
Figure 2.5:	One dimensional wave mean square expectation at $x = 0$	30
Figure 2.6:	One dimensional wave singular values from POD	31
Figure 2.7:	One dimensional wave mean square expectation at $x = 0$	31
Figure 2.8:	One dimensional wave mean square expectation at $x = 0$	32
Figure 2.9:	Number of empirical basis functions for varying timestep sizes	33
Figure 2.10:	One dimensional wave running time comparison	34
Figure 2.11:	One dimensional wave basis function evolution	35
Figure 2.12:	One dimensional wave evolution of singular values from POD	36
Figure 2.13:	One dimensional wave basis function evolution	36
Figure 2.14:	Two dimensional wave mean square expectation at $x = 0$ from gPC . . .	41
Figure 2.15:	Two dimensional wave mean square expectation at $x = 0$	43
Figure 2.16:	Two dimensional wave running time	44
Figure 2.17:	Diffusion equation mean square expectation at $x = 1$ from gPC	48
Figure 2.18:	Diffusion equation mean square expectation at $x = 1$	50
Figure 2.19:	Diffusion equation running time comparison	52
Figure 2.20:	Number of empirical basis functions for varying timestep sizes	54
Figure 2.21:	Diffusion equation first basis function evolution	54
Figure 2.22:	Diffusion equation first basis function evolution	55
Figure 2.23:	Diffusion equation second basis function evolution	55
Figure 2.24:	Diffusion equation second basis function evolution	56
Figure 2.25:	Diffusion equation singular values from POD	57
Figure 2.26:	Diffusion equation evolution of singular values from POD	58
Figure 2.27:	Advection-reaction mean square expectation $x = 0$ from gPC	63
Figure 2.28:	Advection-reaction mean square expectation $x = 0$ from gPC	64
Figure 2.29:	Advection-reaction mean square expectation $x = 0$ from gPC	64
Figure 2.30:	Advection-reaction mean square expectation $x = 0$ from gPC	65
Figure 2.31:	Advection-reaction mean square expectation at $x = 0$	68
Figure 2.32:	Advection-reaction mean square expectation at $x = 0$	69
Figure 2.33:	Advection-reaction singular values from POD	69
Figure 2.34:	Advection-reaction evolution of singular values from POD	70
Figure 2.35:	Advection-reaction running time comparison	71
Figure 2.36:	Advection-reaction basis function evolution	72
Figure 2.37:	Advection-reaction basis function evolution	73
Figure 2.38:	Advection-reaction basis function evolution	73
Figure 2.39:	Advection-reaction evolution of singular values from POD	74
Figure 2.40:	Reaction-diffusion mean square expectation $x = 1$ from gPC	80
Figure 2.41:	Reaction-diffusion mean square expectation $x = 1$ from gPC	80

Figure 2.42: Reaction-diffusion mean square expectation $x = 1$ from gPC	81
Figure 2.43: Reaction-diffusion mean square expectation at $x = 1$	85
Figure 2.44: Reaction-diffusion mean square expectation at $x = 1$	86
Figure 2.45: Reaction-diffusion singular values from POD	87
Figure 2.46: Reaction-diffusion running time comparison	88
Figure 2.47: Reaction-diffusion basis function evolution	89
Figure 2.48: Reaction-diffusion basis function evolution	89
Figure 2.49: Reaction-diffusion evolution of singular values from POD	90
Figure 3.1: One dimensional wave mean square expectation at $x = 0$	97
Figure 3.2: One dimensional wave mean square expectation at $x = 0$	97
Figure 3.3: One dimensional wave mean square expectation at $x = 0$	99
Figure 3.4: One dimensional wave mean square expectation at $x = 0$	99
Figure 3.5: Diffusion equation mean square expectation at $x = 1$	102
Figure 3.6: Diffusion equation mean square expectation at $x = 1$	102
Figure 4.1: One dimensional wave mean square expectation at $x = 0$ from gPC . . .	109
Figure 4.2: One dimensional wave mean square expectation at $x = 0$	111
Figure 4.3: One dimensional wave singular values from POD	111
Figure 4.4: One dimensional wave running time comparison	112
Figure 4.5: One dimensional wave basis function evolution	113
Figure 4.6: One dimensional wave evolution of singular values from POD	114
Figure 4.7: One dimensional wave basis function evolution	114
Figure 4.8: Diffusion equation mean square expectation at $x = 1$ from gPC	116
Figure 4.9: Diffusion equation mean square expectation at $x = 1$	117
Figure 4.10: Diffusion equation singular values from POD	118
Figure 4.11: Diffusion equation running time comparison	119
Figure 4.12: Diffusion equation first basis function evolution	120
Figure 4.13: Diffusion equation second basis function evolution	120
Figure 4.14: Diffusion equation first basis function evolution	121
Figure 4.15: Diffusion equation second basis function evolution	121
Figure 4.16: Diffusion equation evolution of singular values from POD	122
Figure 4.17: Advection-reaction mean square expectation $x = 0$ from gPC	124
Figure 4.18: Advection-reaction mean square expectation at $x = 0$	125
Figure 4.19: Advection-reaction singular values from POD	126
Figure 4.20: Advection-reaction running time comparison	127
Figure 4.21: Advection-reaction basis function evolution	128
Figure 4.22: Advection-reaction evolution of singular values from POD	128
Figure 4.23: Reaction-diffusion mean square expectation $x = 1$ from gPC	130
Figure 4.24: Reaction-diffusion mean square expectation at $x = 1$	131
Figure 4.25: Reaction-diffusion singular values from POD	132
Figure 4.26: Reaction-diffusion running time comparison	133
Figure 4.27: Reaction-diffusion basis function evolution	134
Figure 4.28: Reaction-diffusion basis function evolution	134

Figure 4.29: Reaction-diffusion evolution of singular values from POD 135

ACKNOWLEDGEMENTS

I would like to thank my advisor, Professor Melvin Leok, for his guidance and support during my time at UC San Diego. Much of my progress as a mathematician over the last few years is due to his guidance, and for that I will remain forever grateful.

I would also like to thank Professor Daniel Tartakovsky for a number of enlightening discussions and correspondence regarding polynomial chaos and uncertainty quantification.

And lastly I would like to thank Professors Gerardo Dominguez, Ming Gu, and Jason Lee, who encouraged me to pursue both an education and research in the field of computational mathematics.

The material in Chapters 2, 3, and 4 is in preparation for submission for publication and was co-authored with Professor Melvin Leok. The dissertation author was the primary investigator and author of this material.

VITA

- 2010 B. A. in Mathematics, University of California, Berkeley
- 2010 B. A. in Computer Science, University of California, Berkeley
- 2013 M. A. in Mathematics (Applied), University of California, San Diego
- 2016 Ph. D. in Mathematics with a Specialization in Computational Science, University of California, San Diego

PUBLICATIONS

G Wilkins and M Gu. "A Modified Brent's Method for Finding Zeros of Functions", *Numerische Mathematik*, Vol. 123, 177-188, 2013

G Dominguez, G Wilkins, and M Thiemens. "reply", *Nature*, Vol. 482, 2012

G Dominguez, G Wilkins, and M Thiemens. "On the Soret Effect and Isotopic Fractionation in High-Temperature Silicate Melts", *Nature*, Vol. 473, 70-73, 2011

G Dominguez, G Wilkins, and M Thiemens. "A Photochemical Model and Sensitivity Study of the Triple-Oxygen $\Delta^{17}\text{O}$ Isotopic Composition of NO_y , HO_x , and H_2O_2 in a Polluted Boundary Layer", *Atmospheric Chemistry and Physics Discussions*, Vol. 9 13355-13406, 2009

ABSTRACT OF THE DISSERTATION

An Empirical Chaos Expansion Method for Uncertainty Quantification

by

Gautam Wilkins

Doctor of Philosophy in Mathematics with a Specialization in Computational Science

University of California, San Diego, 2016

Professor Melvin Leok, Chair

Uncertainty quantification seeks to provide a quantitative means to understand complex systems that are impacted by uncertainty in their parameters. The polynomial chaos method is a computational approach to solve stochastic partial differential equations (SPDE) by projecting the solution onto a space of orthogonal polynomials of the stochastic variables and solving for the deterministic coefficients. Polynomial chaos can be more efficient than Monte Carlo methods when the number of stochastic variables is low, and the integration time is not too large. When performing long-term integration, however, achieving accurate solutions often requires the space of polynomial functions to become unacceptably

large. This dissertation presents an alternative approach, where sets of empirical basis functions are constructed by examining the behavior of the solution for fixed values of the random variables. The empirical basis functions are evolved over time, which means that the total number can be kept small, even when performing long-term integration. We introduce this method of empirical chaos expansion, and apply it to a number of model equations, demonstrating that the computational time scales linearly with the final integration time. That is not the case for polynomial chaos in general, since achieving accuracy for long-term integration usually requires larger polynomial bases, causing a nonlinear scaling with the final integration time. We also present an analytical method that uses the dynamics of the SPDE to predict the evolution of the empirical basis functions and demonstrate how it can be applied to evolve the empirical basis functions without needing to resample realizations of the original SPDE.

Chapter 1

Introduction

1.1 Introduction

Consider the stochastic initial boundary value partial differential equation (SPDE) model problem:

$$u_t(x, t, \xi) = L(u, x, t, \xi), \quad (1.1)$$

where x is a spatial variable, t is time, ξ is a random variable with known distribution on probability space Ω , and L is a linear or nonlinear differential operator. SPDEs are used to model systems that contain small scale stochastic components along with large scale deterministic components. Frequently the deterministic components arise from governing physics, while the stochastic components are due to measurement errors or some other form of underlying uncertainty. Assuming that the distribution of the stochastic variables is known, we wish to determine information about the distribution of the solution u . SPDEs have frequently demonstrated their use in modeling physical phenomena such as wave propagation [61, 38], diffusion [63, 62, 32], Burgers and Navier-Stokes equations with random forcing [4, 78, 80, 79, 51, 12, 10, 13, 69, 68], multivariable predictive control [54, 46, 47, 48], and chemical reactors with uncertainties [74].

1.1.1 Polynomial Chaos

The original polynomial chaos formulation was introduced by Wiener [81, 82], who used Hermite polynomial functionals to model a Gaussian random process. Polynomial chaos methods begin by choosing a space of polynomial functions that are orthonormal with respect to the distribution of the random variable ξ . Such polynomial spaces are known for standard distributions. If we let $\{P_i\}_{i=1}^{\infty}$ be the orthogonal polynomial basis functions, then

we can project the solution u onto the basis functions as:

$$\hat{u}^i(x,t) = \langle u, P_i \rangle := \int_{\Omega} u(x,t,\xi) P_i(\xi) d\mu,$$

where μ is the measure of the probability space Ω . We can then represent the solution u as:

$$u(x,t,\xi) = \sum_{i=1}^{\infty} \hat{u}^i(x,t) P_i(\xi), \quad (1.2)$$

If the coefficients $\hat{u}^i(x,t)$ were known, then (1.2) would be an exact representation of the true solution. Since the initial conditions are known, they can be projected onto the basis functions to get initial values for the $\hat{u}^i(x,t)$ functions. The expansion (1.2) can then be substituted into the original model problem (1.1) to obtain:

$$\sum_{i=1}^{\infty} \hat{u}_t^i(x,t) P_i(\xi) = L \left(\sum_{i=1}^{\infty} \hat{u}^i(x,t) P_i(\xi), x, t, \xi \right).$$

We can then multiply by a test function P_j and take an expectation over Ω to get:

$$\begin{aligned} \sum_{i=1}^{\infty} \hat{u}_t^i(x,t) P_i(\xi) P_j(\xi) &= L \left(\sum_{i=1}^{\infty} \hat{u}^i(x,t) P_i(\xi), x, t, \xi \right) P_j(\xi) \\ \implies E \left[\sum_{i=1}^{\infty} \hat{u}_t^i(x,t) P_i(\xi) P_j(\xi) \right] &= E \left[L \left(\sum_{i=1}^{\infty} \hat{u}^i(x,t) P_i(\xi), x, t, \xi \right) P_j(\xi) \right] \\ \implies \hat{u}_t^j(x,t) &= E \left[L \left(\sum_{i=1}^{\infty} \hat{u}^i(x,t) P_i(\xi), x, t, \xi \right) P_j(\xi) \right], \end{aligned}$$

where the expectation on the left side simplified due to the P_i 's being orthonormal. We can

then truncate the infinite expansion on the right hand side at some finite value N , to get:

$$\hat{u}_i^j(x, t) = E \left[L \left(\sum_{i=1}^N \hat{u}^i(x, t) P_i(\xi), x, t, \xi \right) P_j(\xi) \right] \quad 1 \leq j \leq N. \quad (1.3)$$

In practice the right hand side can usually be simplified as well, but it depends on the form of the differential operator L . This results in a system of coupled deterministic differential equations for the unknown \hat{u}^i 's. Solving the system will give an approximation of the true solution u . This is known as the stochastic Galerkin method [26].

A result by Cameron and Martin [6] established that the series (1.2) converges strongly to L_2 functionals, which implies that the series converges for stochastic processes with finite second moments. The work in [26] coupled the Hermite polynomial expansions with finite element methods for solving SPDEs, and the method was applied to model uncertainty in a variety of physical systems [24, 71, 89, 14], and a number of papers were written on the convergence properties [49, 8, 60, 20] of polynomial chaos methods for various SPDEs. An extension by Xiu and Karniadakis [88] proposed the use of orthogonal polynomials in the Askey scheme [1] for a variety of other random variable distributions, including uniform and beta distributions. The work also established the same strong convergence results that held for Hermite polynomial expansions of normal random variables. This method is known as generalized polynomial chaos (gPC), and an overview is provided in [85]. gPC methods have been applied to a variety of problems in uncertainty quantification, including problems in fluid dynamics and solid mechanics [87, 90, 91, 66, 15, 45, 42].

Since their introduction, two well-known issues have become apparent with the gPC method. First, if the number of random variables is too large, then the resulting stochastic Galerkin system becomes too expensive to solve, and Monte Carlo methods outperform gPC methods [75, 27]. This is the curse of dimensionality, and in this case is due to the

need to introduce multidimensional polynomials, one dimension for each random variable. Including even modest orders of high dimensional polynomial functions can quickly become prohibitively expensive. Methods have been proposed to limit the growth rate, including sparse truncation [29] that selectively eliminates high order polynomials, modifications of stochastic collocation methods [16], multi-element gPC expansions [75, 76, 21], and model reduction to project a high dimensional random space onto a lower dimensional one while still preserving important dynamics [15, 25, 58, 59]. While these methods slow the curse of dimensionality, none of them entirely eliminate it, and for systems with a high number of random variables it is more efficient to turn to Monte Carlo methods, which have a convergence rate independent of the dimension of the random space.

The second issue with the gPC method is that in order to accurately approximate a solution with unsteady dynamics over a long time interval, a large number of basis functions must be used (i.e. we must choose a large value for N in equation (1.3)) [27, 53, 29]. This is not particularly surprising, but it is problematic since the amount of work does not scale linearly with the order of the polynomial basis functions; this issue becomes particularly troublesome as the number of random variables increases. While multi-element gPC expansions [75, 76] have been suggested as an option, they do not entirely solve this issue. Another approach is the time-dependent polynomial chaos method [23, 28], which integrates for a short period of time, then treats the solution as a new random variable and attempts to numerically derive an orthogonal polynomial basis for the new random variable.

1.1.2 General Basis

The above results can be extended in a straightforward manner to non-orthonormal bases as well. Consider any set of functions $\{\Psi^i\}_{i=1}^{\infty}$ that form a basis for $L^2(\Omega)$, but are not

necessarily orthonormal. Then there exist coefficients $\hat{u}^i(x, t)$ such that:

$$u(x, t, \xi) = \sum_{i=1}^{\infty} \hat{u}^i(x, t) \Psi^i(\xi),$$

which implies that:

$$\begin{aligned} \langle u, \Psi^i \rangle &= \left\langle \sum_{j=1}^{\infty} \hat{u}^j \Psi^j, \Psi^i \right\rangle \\ &= \sum_{j=1}^{\infty} \hat{u}^j \langle \Psi^j, \Psi^i \rangle. \end{aligned}$$

If we let:

$$A_{ji} = \langle \Psi^j, \Psi^i \rangle, \quad \hat{u} = \begin{pmatrix} \hat{u}^1 \\ \hat{u}^2 \\ \vdots \end{pmatrix}, \quad \text{and} \quad f = \begin{pmatrix} \langle u, \Psi^1 \rangle \\ \langle u, \Psi^2 \rangle \\ \vdots \end{pmatrix},$$

then we can write the above system as:

$$A\hat{u} = f, \tag{1.4}$$

where the \hat{u} vector is unknown, and the A and f matrices can be computed by inner products (if u is known). Since the model problem is an initial boundary value problem we can compute the initial values for the \hat{u}_i 's. Just like with standard polynomial chaos we can derive a stochastic Galerkin method by substituting the expansion into the model

problem (1.1), multiplying by a test function Ψ^j , and taking an expectation over Ω :

$$\begin{aligned} \sum_{i=1}^{\infty} \hat{u}_t^i(x,t) \Psi^i(\xi) \Psi^j(\xi) &= L \left(\sum_{i=1}^{\infty} \hat{u}^i(x,t) \Psi^i(\xi), x, t, \xi \right) \Psi^j(\xi) \\ \implies E \left[\sum_{i=1}^{\infty} \hat{u}_t^i(x,t) \Psi^i(\xi) \Psi^j(\xi) \right] &= E \left[L \left(\sum_{i=1}^{\infty} \hat{u}^i(x,t) \Psi^i(\xi), x, t, \xi \right) \Psi^j(\xi) \right]. \end{aligned}$$

If we truncate the expansion at finite value N we get:

$$E \left[\sum_{i=1}^N \hat{u}_t^i(x,t) \Psi^i(\xi) \Psi^j(\xi) \right] = E \left[L \left(\sum_{i=1}^N \hat{u}^i(x,t) \Psi^i(\xi), x, t, \xi \right) \Psi^j(\xi) \right] \quad (1.5)$$

Now if we let:

$$\tilde{A}_{ji} = \langle \Psi^j, \Psi^i \rangle, \quad \hat{u} = \begin{pmatrix} \hat{u}^1 \\ \hat{u}^2 \\ \vdots \\ \hat{u}^n \end{pmatrix}, \quad \text{and} \quad b_j = E \left[L \left(\sum_{i=1}^N \hat{u}^i(x,t) \Psi^i(\xi), x, t, \xi \right) \Psi^j(\xi) \right],$$

then we get the system

$$\tilde{A} \hat{u}_t = b, \quad (1.6)$$

which is a deterministic differential algebraic equation (DAE) whose solution is the values of the unknown \hat{u}^i coefficients.

1.1.3 Conversion Between Bases

Assume we have two distinct bases $\{\Psi^i\}_{i=1}^{\infty}$ and $\{\Phi^i\}_{i=1}^{\infty}$ for $L^2(\Omega)$, such that:

$$u(x, t, \xi) = \sum_{i=1}^{\infty} \hat{u}_{\Phi}^i(x, t) \Phi^i(\xi), \quad \text{and}$$

$$u(x, t, \xi) = \sum_{i=1}^{\infty} \hat{u}_{\Psi}^i(x, t) \Psi^i(\xi).$$

Then if we know the values of \hat{u}_{Ψ}^i , we can compute the values of \hat{u}_{Φ}^i with a standard change of basis operation:

$$\begin{aligned} \langle u, \Phi^j \rangle &= \sum_{i=1}^{\infty} \langle \hat{u}_{\Psi}^i(x, t) \Psi^i, \Phi^j \rangle \\ &= \sum_{i=1}^{\infty} \hat{u}_{\Psi}^i(x, t) \langle \Psi^i, \Phi^j \rangle. \end{aligned}$$

Letting

$$M_{ji} = \langle \Psi^i, \Phi^j \rangle \quad \text{and} \quad b_j = \langle u, \Phi^j \rangle$$

implies that

$$b = M \hat{u}_{\Psi}. \tag{1.7}$$

The right hand side is a straightforward computation since \hat{u}_{Ψ} is known, and we can use equation (1.4) to compute the values of the \hat{u}_{Φ} coefficients.

The same computation will work when the two bases are finite dimensional instead of infinite dimensional. If the bases are instead: $\{\Psi^i\}_{i=1}^N$ and $\{\Phi^i\}_{i=1}^M$, then we can project

$u(x, t, \xi)$ onto the first and second bases:

$$u(x, t, \xi) \approx \bar{u}_\Phi(x, t, \xi) := \sum_{i=1}^N \hat{u}_\Phi^i(x, t) \Phi^i(\xi)$$

$$u(x, t, \xi) \approx \bar{u}_\Psi(x, t, \xi) := \sum_{i=1}^M \hat{u}_\Psi^i(x, t) \Psi^i(\xi).$$

If we know the values of the \hat{u}_Ψ^i coefficients, then we can compute an approximation of the \hat{u}_Φ^i coefficients with the same change of basis operation as in the infinite dimensional case:

$$\begin{aligned} \langle u, \Phi^j \rangle &\approx \sum_{i=1}^N \langle \hat{u}_\Phi^i(x, t) \Phi^i(\xi), \Phi^j \rangle \\ &= \sum_{i=1}^N \hat{u}_\Phi^i(x, t) \langle \Phi^i(\xi), \Phi^j \rangle \end{aligned}$$

Letting

$$M_{ji} = \langle \Psi^i, \Phi^j \rangle \quad \text{and} \quad b_j = \langle u, \Phi^j \rangle$$

implies that

$$b = M \hat{u}_\Psi.$$

As we know the values of the \hat{u}_Ψ coefficients, the right hand side can again be computed and we may use equation (1.4) to compute an approximation to the values of the \hat{u}_Φ coefficients. Note that the operations described above first project u onto the subspace spanned by $\{\Psi^j\}$, and then project that projection onto the subspace spanned by $\{\Phi^i\}$.

Chapter 2

Empirical Chaos Expansion

2.1 Empirical Bases

We now seek to resolve the issue of long-term integration for gPC methods, using the following general approach.

First, come up with a finite and small set of basis functions that result in a low projection error over a short time interval (say $0 \leq t \leq \tau_0$). Then, perform a stochastic Galerkin method via equation (1.5) in order to approximate the solution up to time τ . This will give values for the \hat{u}^i coefficients. Now, come up with a different set of basis functions that result in a low projection error over the short time interval $\tau_0 \leq t \leq \tau_1$. We can use the previous solution at τ_0 as the initial condition, and calculate the initial values of the \hat{u}^i 's in the new basis by equation (1.7). We can then perform another stochastic Galerkin method over the new basis to compute the solution up to time τ_1 . Continuing this process iteratively will allow us to compute the solution out to a long time t with a low error, and at each individual step we will only be dealing with a relatively small basis.

The principal issue, then, is determining a subspace spanned by a small number of basis functions for each interval $\tau_i \leq t \leq \tau_{i+1}$, such that the solution u will have a low projection error in the subspace. Once we have such a set of basis functions for each time interval, then we can follow the approach outlined above to solve the SPDE on a relatively small set of basis functions.

The work of [23] makes a similar attempt, but relies on integrating the solution to a small time in the future, and then treating the solution as a new random variable that must be added to the gPC expansion before integrating out to a later time. This entails numerically deriving a new set of orthogonal polynomial basis functions that are inferred from the numerical probability distribution of the solution. In this dissertation we present an alternate approach, where we no longer require the basis functions to be orthonormal, and

instead use techniques of model reduction to construct an empirically optimal set of basis functions at each given timestep.

2.1.1 Sampling Trajectories

Consider fixing a single point in space x_0 and time t_0 , and then examining how the function $u(x_0, t_0, \xi)$ varies in ξ . This will give a single trajectory of the solution as a function of the random variable ξ . If we examine many such trajectories then it is reasonable to assume that a good subspace into which to project the solution should have a low projection error for most or all of the trajectories.

We can find such trajectories by choosing a set of fixed values for ξ (call them $\{\xi_k\}_{k=1}^K$), and then solving the resulting deterministic PDE for each ξ_k , much like Monte Carlo methods. The difference, however, is that Monte Carlo methods require solving the PDE for an extremely large number of values of ξ before they converge, and we sample a much smaller number of trajectories. Once we know the solutions for each of the values of $\{\xi_k\}$, we can construct the following matrix, assuming that we have discretized space and time into the set of points $\{(x_i, t_j)\}_{(i,j)=(1,1)}^{(M,N)}$:

$$T = \begin{pmatrix} u(x_1, t_1, \xi_1) & u(x_1, t_1, \xi_2) & \dots & u(x_1, t_1, \xi_K) \\ u(x_1, t_2, \xi_1) & u(x_1, t_2, \xi_2) & \dots & u(x_1, t_2, \xi_K) \\ \vdots & & & \\ u(x_1, t_N, \xi_1) & u(x_1, t_N, \xi_2) & \dots & u(x_1, t_N, \xi_K) \\ u(x_2, t_1, \xi_1) & u(x_2, t_1, \xi_2) & \dots & u(x_2, t_1, \xi_K) \\ \vdots & & & \\ u(x_M, t_N, \xi_1) & u(x_M, t_N, \xi_2) & \dots & u(x_M, t_N, \xi_K). \end{pmatrix} \quad (2.1)$$

Each row of the matrix T represents a discrete trajectory of the solution as a function of the random variable ξ . Note that in general this matrix will have far more rows than columns. We now seek a (hopefully small) set of basis functions in ξ that will result in a low projection error for each of the rows of T . The motivating assumption is that such a set of basis functions will also result in a low projection error for the true solution $u(x, t, \xi)$.

2.1.2 Model Reduction

The field of model reduction focuses primarily on effective methods to solve problems that exist in very high dimensional spaces by constructing a lower dimensional space, projecting from the high dimensional space onto the lower dimensional space, and solving the problem on the lower dimensional space. A key concern is choosing the lower dimensional space in such a way that the important dynamics of the system are retained [56]. A low dimensional space with a high projection error is useless. One of the classic problems is to efficiently solve a linear dynamical system that is both observable and controllable [73]:

$$\dot{x}_t = Ax + Bu$$

$$y = Cx,$$

where $x \in \mathbb{R}^n$ is a state space vector in a very high dimensional space, $A \in \mathbb{R}^n \times \mathbb{R}^n$ is a constant matrix, $B \in \mathbb{R}^n \times \mathbb{R}^k$ is a constant matrix, $u \in \mathbb{R}^k$ is a control vector whose value can be changed at different points in time, $C \in \mathbb{R}^m \times \mathbb{R}^n$ is a constant matrix, and y is the observation vector. In many dynamical systems the full state cannot be directly observed, only part of it, and that is what y represents. The problem cannot be effectively solved due to the high dimension of the space that the vector x resides in. A standard and well-studied

task in the field of model reduction is how to construct a subspace of the state space that x resides in such that the projection error is low. In this specific case a low projection error would mean that if we solve the original problem on the lower dimensional subspace with the same initial conditions and control input, the observed values y would have a small error compared to the values of y if we computed a solution on the full state space. In the SPDEs studied in this work the state space is fully observable, so there is no need for the y term.

To frame the problem of constructing an empirical basis in terms of model reduction, we have to move slightly away from the standard linear dynamical system model. In the standard model, a trajectory would involve changing values of the x state space vector through time. In our case, an individual column of the T matrix in the previous section can be thought of as a single value of the high dimensional state space vector x . Now, however, instead of varying in time, the state space vector varies as a function of the random variable ξ .

In principle we could take every row of the T matrix, and treat it as an individual basis function of the random variable ξ by constructing an interpolating function. But since the number of rows will, in general, be extremely large, this is not computationally practical. What we would instead prefer is a small set of vectors such that when we project any individual row vector from the T matrix onto their span, it has a low projection error. This is effectively a model reduction problem on a fully observable system.

2.1.3 Proper Orthogonal Decomposition

Proper Orthogonal Decomposition (POD) is a standard tool in the field of model reduction [7, 37] and is also known as the Karhunen-Loève transform [36, 41], or Principal Component Analysis [65] in the finite dimensional case. It is often used to construct

low dimensional representations of very high dimensional spaces that preserve the most important dynamics [43, 44, 83].

Following the exposition from [43], in the discrete case we have T in $\mathbb{R}^n \times \mathbb{R}^m$ from equation 2.1, where we can view each row of T as a sample from a random vector that takes values in the space \mathbb{R}^m . We then seek a set of $k < m$ basis vectors such that the rows of T can be projected with minimum mean square error onto the k basis vectors. The optimization problem can be expressed as:

$$\min_{P_k} E \left[\|v - P_k v\|^2 \right]$$

where v is a random vector from the space sampled by the rows of T , the expectation is over the rows of T , $P_k v$ is the projection of v onto the optimal choice of k basis vectors, and the minimization is over all sets of k basis vectors. In practice we can perform a singular value decomposition of the T matrix in order to compute the POD:

$$T = U \Sigma V^T.$$

Then the first k columns of the right singular matrix V are the set of k basis vectors that minimize the mean square error when we project the m rows of the T matrix onto their span. This will give us a set of k vectors that span a subspace that will result in a low projection error for all of the rows of the T matrix. We can now construct a basis function in ξ for each row of the V matrix by constructing an interpolating function through its values at each of the ξ_k points.

2.1.4 Empirical Chaos Expansion

At this point we can construct a general algorithm to solve the SPDE model problem (1.1) using successive sets of empirical basis functions. We refer to this method as empirical chaos expansion. We begin by choosing a set, $\{\xi_k\}_{k=1}^M$, from the range of the random variable ξ . If there were multiple random variables then we would choose a set of random vectors from the product space of the random variables. If we wish to solve the SPDE from time t_0 to time t_f , then we partition the interval as: $\{t_0, \tau_1, \tau_2, \dots, \tau_{n-1}, t_f\}$. We then solve the deterministic partial differential equation for each fixed value of ξ in the set $\{\xi_k\}_{k=1}^M$, starting at time t_0 and ending at time τ_1 . Assuming that the solutions are computed using a finite difference method, we will then have values for the solution $u(x, t, \xi)$ at a set of points (x_i, t_i, ξ_k) . Fixing a point in space and time then varying the value of ξ , we get a single row of the matrix T in Section 2.1.1, and we can use the full set of solutions to construct the full T matrix. We then perform a POD of the T matrix by computing its singular value decomposition, and choose the first N_1 columns of the right singular value matrix to be the set of basis functions. In practice N_1 is chosen so that the $N_1 + 1$ st singular value is small relative to the largest singular value. Note that each column of the right singular value matrix can be viewed as a table of values for the basis function at each of the ξ values from the set $\{\xi_k\}$. We could construct an interpolating function for each of the basis column vectors, though it is computationally faster to simply use the values for a numerical quadrature formula. We will refer to the set of empirical basis functions generated for the time interval $[t_0, \tau_1]$ as $\{\Psi_1^i(\xi)\}_{i=1}^{N_1}$, where each Ψ_1^i is an individual basis function. For the first time interval $[t_0, \tau_1]$, we thus approximate the true solution u as:

$$u(x, t, \xi) \approx \sum_{i=1}^{N_1} \hat{u}^i(x, t) \Psi_1^i(\xi).$$

To determine the initial values of the unknown \hat{u}^i coefficients, we project the initial condition onto each of the basis functions:

$$\hat{u}^i(x, t_0) = \langle u(x, t_0), \Psi_1^i \rangle.$$

The inner product is actually an integral, and since we have a table of values for Ψ_1^i , we can compute the inner product using numerical quadrature. Once we have the initial values of the \hat{u}^i coefficients we solve the propagation equation (1.6) for the stochastic Galerkin system for the SPDE, which computes the values of the \hat{u}^i coefficients up to time τ_1 . Note that setting up the system for the propagation equation will require us to compute expectations, which we can compute using numerical quadrature.

The solution at the final time τ_1 can be used as the initial condition to compute solutions on the interval $[\tau_1, \tau_2]$. We begin by computing the solution to the deterministic partial differential equation for each fixed value of ξ in the set $\{\xi_k\}_{k=1}^m$, starting at time τ_1 and ending at time τ_2 . We now use the computed solutions to construct a new T matrix that has trajectories over the time interval $[\tau_1, \tau_2]$. We then perform a POD of the T matrix by computing its singular value decomposition, and choose the first N_2 columns of the right singular value matrix to be the set of basis functions. This gives a set of empirical basis functions $\{\Psi_2^i(\xi)\}_{i=1}^{N_2}$. Although we have values $\hat{u}^i(x, t)$ up to time τ_1 , these are the coefficients with respect to the old basis $\{\Psi_1^i(\xi)\}$. We can convert them to coefficients with respect to the new basis $\{\Psi_2^i(\xi)\}$ by following the method described in Section 1.1.3. Recall that applying the method requires us to compute entries of the matrix:

$$M_{ji} = \langle \Psi_1^i, \Psi_2^j \rangle.$$

Again, these inner products can be computed using numerical quadrature. Once we construct the M matrix, we multiply it by the coefficient vector \hat{u} for the old basis and the result is the initial coefficient vector for the new basis. Now the true solution u is approximated as:

$$u(x, t, \xi) \approx \sum_{i=1}^N \hat{u}^i(x, t) \Psi_2^i(\xi),$$

on the interval $[\tau_2, \tau_2]$. Since we only have the values of the \hat{u}^i coefficients at time τ_1 , we solve the propagation equation (1.6), which computes the values of the \hat{u}^i coefficients up to time τ_2 .

At this point we repeat the procedure in the previous paragraph to generate a new set of empirical basis functions for the interval $[\tau_2, \tau_3]$, project the old coefficients onto the new basis, and solve the new propagation equation to obtain a solution up to time τ_3 . This process is then repeated for every timestep until we reach the final integration time.

2.1.5 Convergence

Let $u_m^k = \sum_{i=1}^m \hat{u}^i(x, t) \Psi^i(\xi)$ be the approximation to the true solution on a time interval $[\tau_i, \tau_{i+1}]$ constructed through empirical chaos by sampling a discrete set of k trajectories in the space of random variables, $\{\xi_k\}_{i=1}^k$. Let \bar{u}_m^k be the projection of the true solution u onto the span of the k trajectories. Note that the projection error at any of the ξ_k points will be zero. Then from the triangle inequality we have:

$$\|u - u_m^k\| \leq \|u - \bar{u}_m^k\| + \|\bar{u}_m^k - u_m^k\|,$$

in some appropriate norm. The error in the first term can be controlled by choosing the set $\{\xi_k\}$ as interpolation nodes and increasing k . This follows from applying standard

interpolation theory, assuming sufficient regularity of the solution u . The error in the second term is due to POD, where instead of projecting u onto the full span of the trajectories, we project onto a lower dimensional subspace with m basis functions. This error can be controlled by increasing m .

Computational Cost

In order to fully solve the SPDE at an intermediate timestep $i + 1$ (i.e. any timestep other than the first), we must perform the following operations:

1. Solve the deterministic PDE for each value of ξ in the set $\{\xi_k\}_{k=1}^m$. If solving a single instance of the deterministic PDE takes time $O(n)$, then this operation will take time $O(mn)$. However, it is trivial to parallelize this operation which can dramatically reduce the computational time.
2. Compute the POD of the T matrix by computing its singular value decomposition. The T matrix will always have m columns, but the number of rows depends on the number of finite difference grid points and is almost always much larger than m . Since we only need the right singular values, which will be an $m \times m$ matrix, we can reduce the cost of the SVD operation by only computing the singular value matrix σ , and the right singular value matrix V .
3. Project the old \hat{u}^i coefficients onto the new set of basis functions. This operation requires us to compute the M matrix, which will be $N_{i+1} \times N_i$ (where N_i and N_{i+1} are the number of empirical basis functions for the i th and $i + 1$ st timesteps, respectively). Each entry of the matrix is computed by calculating an inner product with a numerical quadrature method. We then multiply the M matrix by the old \hat{u}^i coefficient values.

4. Compute the left and right hand sides of the propagation equation (1.6). This will require computing expectations, which can be done with numerical quadrature. The exact cost of this operation depends on the number of basis functions and also how complicated the differential operator L is.
5. Solve the propagation equation to advance the solution to the next timestep. Again the cost of this operation is highly dependent on the differential operator L . In some cases solving the propagation equation is no harder than solving the deterministic PDE, and in others it is far more computationally expensive. In either case, it will be a coupled system of N_{i+1} PDEs.

The key advantage of this approach is that we can control the number of empirical basis functions by adjusting the size of the timestep. gPC uses the same set of basis functions for every point in time, and for many practical SPDEs this means that achieving accuracy in the solution out to long integration times requires using a very large set of basis functions. By contrast, each set of empirical basis functions only needs to have a low projection error over its corresponding time interval, which can be quite short. This allows the empirical chaos expansion method to run in linear time as a function of the final integration time, i.e., if we want to double the final integration time, it will take about twice as long to compute a solution using empirical chaos expansion.

Computing Solution Statistics

If there are k total timesteps then we will need to keep track of a set of k sets of basis functions and their associated coefficients in order to fully reconstruct the solution. In the end we still have a fully analytic representation of the true solution u , and we can use it to compute any desired solution statistics. The actual computations will be more complex

than those for gPC, due to the fact that the basis functions are not orthogonal, and there are multiple sets of basis functions (one for each timestep). Let $\{\Psi_j^i\}_{i=1}^{N_j}$ be the set of N_j basis functions for timestep j , and let $\{\hat{u}_j^i\}_{i=1}^{N_j}$ be the corresponding set of coefficients.

If we want to compute the mean of the true solution, then we compute:

$$\begin{aligned} E[u(x, t, \xi)] &= E \left[\sum_{i=1}^{N_{k^*}} \hat{u}_{k^*}^i \Psi_{k^*}^i \right] \\ &= \sum_{i=1}^{N_{k^*}} \hat{u}_{k^*}^i E[\Psi_{k^*}^i]. \end{aligned}$$

where k^* is the timestep that contains the time t , and $E[\Psi_{k^*}^i]$ can be computed using numerical quadrature.

If we want to compute the mean square expectation of the true solution, then we compute:

$$\begin{aligned} E[u(x, t, \xi)] &= E \left[\left(\sum_{i=1}^{N_{k^*}} \hat{u}_{k^*}^i \Psi_{k^*}^i \right)^2 \right] \\ &= E \left[\sum_{i=1}^{N_{k^*}} \sum_{j=1}^{N_{k^*}} \hat{u}_{k^*}^i \hat{u}_{k^*}^j \Psi_{k^*}^i \Psi_{k^*}^j \right] \\ &= \sum_{i=1}^{N_{k^*}} \sum_{j=1}^{N_{k^*}} \hat{u}_{k^*}^i \hat{u}_{k^*}^j E[\Psi_{k^*}^i \Psi_{k^*}^j] \end{aligned}$$

where k^* is the timestep that contains the time t , and $E[\Psi_{k^*}^i \Psi_{k^*}^j]$ can be computed using numerical quadrature. Other solution statistics can be computed in a similar manner.

2.2 One Dimensional Wave Equation

Consider the SPDE:

$$u_t(x, t, \xi) = \xi u_x(x, t, \xi), \quad 0 \leq x \leq 2\pi, \quad t \geq 0 \quad (2.2)$$

$$u(x, 0, \xi) = \cos(x), \quad (2.3)$$

with periodic boundary conditions, and where ξ is uniformly distributed in $[-1, 1]$. The exact solution is:

$$\cos(x - \xi t). \quad (2.4)$$

Note that over the space for this problem:

$$\langle f, g \rangle := \int_{-1}^1 f(\xi)g(\xi)(1/2)d\xi$$

$$E[f] := \int_{-1}^1 f(\xi)(1/2)d\xi$$

This hyperbolic SPDE was analyzed in [27], and one of the findings was that for a fixed polynomial basis, the error will scale linearly with final integration time, thus requiring that the gPC expansion continually add additional terms in order to achieve accurate long-term solutions.

2.2.1 Polynomial Chaos Expansion

If we use gPC then we choose the normalized Legendre polynomials to be our basis functions. Letting $\{L_i\}$ be the i^{th} normalized Legendre polynomial function, we can perform

a stochastic Galerkin method as in Section 1.1.1. The true solution is expanded as:

$$u(x, t, \xi) = \sum_{i=1}^{\infty} \hat{u}^i(x, t) L^i(\xi).$$

Substituting this into Equation 2.2, then multiplying by a test function $L^j(\xi)$, and taking the expectation of both sides gives:

$$\begin{aligned} \sum_{i=1}^{\infty} \hat{u}_t^i(x, t) L^i(\xi) &= \xi \sum_{i=1}^{\infty} \hat{u}_x^i(x, t) L^i(\xi) \\ \implies E \left[\sum_{i=1}^{\infty} \hat{u}_t^i(x, t) L^i(\xi) L^j(\xi) \right] &= E \left[\xi \sum_{i=1}^{\infty} \hat{u}_x^i(x, t) L^i(\xi) L^j(\xi) \right] \\ \implies \sum_{i=1}^{\infty} \hat{u}_t^i(x, t) E [L^i(\xi) L^j(\xi)] &= \sum_{i=1}^{\infty} \hat{u}_x^i(x, t) E [\xi L^i(\xi) L^j(\xi)] \\ &\implies \hat{u}_t^j = \sum_{i=1}^{\infty} \hat{u}_x^i(x, t) E [\xi L^i(\xi) L^j(\xi)] \end{aligned}$$

Letting

$$A_{ji} = E [\xi L_j L_i] \quad \text{and} \quad \hat{u} = \begin{pmatrix} \hat{u}^1(x, t) \\ \hat{u}^2(x, t) \\ \vdots \end{pmatrix}$$

simplifies the previous system to:

$$\hat{u}_t = A \hat{u}_x. \tag{2.5}$$

Since the initial condition is deterministic, $\hat{u}^1(x, 0) = \cos(x)$, and $\hat{u}^i(x, 0) = 0$ for $i > 1$.

We can then truncate the infinite system at some finite value N and solve the resulting deterministic system of PDEs. To examine the accuracy of the solution we can look at the mean square expectation at $x = 0$. The exact value is:

$$\begin{aligned}
 E [(u(0,t,\xi))^2] &= \int_{-1}^1 (\cos^2(\xi t))(1/2)d\xi \\
 &= \frac{1}{2} \left(1 + \frac{\cos(t) \sin(t)}{t} \right).
 \end{aligned} \tag{2.6}$$

See Figures (2.1, 2.2, 2.3) for a comparison of the exact value of the mean square expectation with the numerical value computed by applying the stochastic Galerkin method to expansions truncated at different values of N . It is clear that past a certain point in time all of the PC expansions diverge from the exact value.

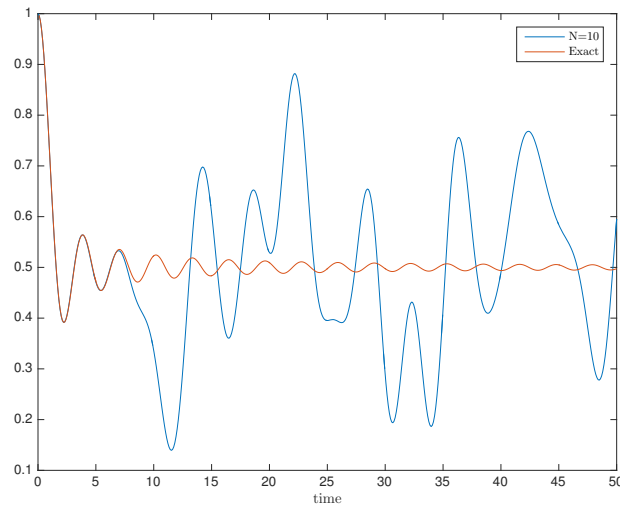


Figure 2.1: Mean Square Expectation at $x = 0$ of solution to (2.2), computed using gPC with stochastic Galerkin using Legendre polynomials up to order 10

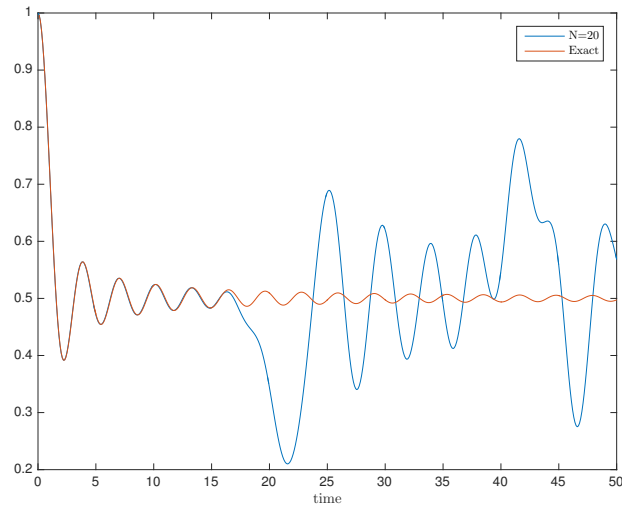


Figure 2.2: Mean Square Expectation at $x = 0$ of solution to (2.2), computed using gPC with stochastic Galerkin using Legendre polynomials up to order 20

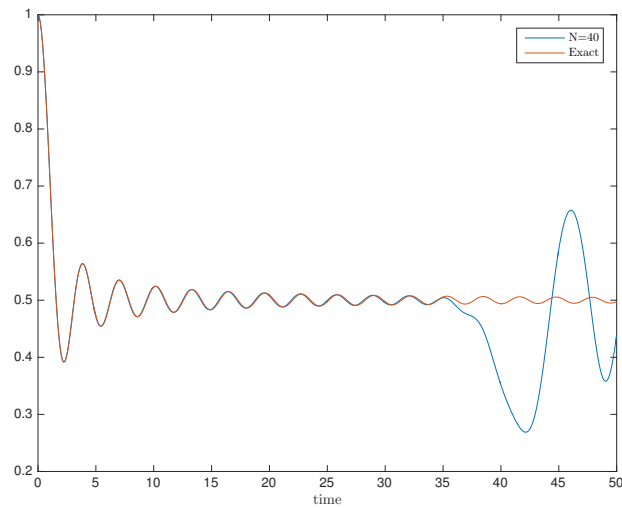


Figure 2.3: Mean Square Expectation at $x = 0$ of solution to (2.2), computed using gPC with stochastic Galerkin using Legendre polynomials up to order 40

This is not an issue with the stochastic Galerkin method. In fact, even if we project the exact solution (2.4) onto the space of Legendre polynomials (see Figure 2.4) and compute its mean square expectation, we can see that more and more polynomial basis functions are needed to accurately project the exact solution.

This raises another important concern with standard polynomial chaos techniques. If the initial condition is allowed to be stochastic, then it might be the case that we need a large number of polynomial functions *just to accurately project the initial condition*. For example, if we were to make the initial condition of the problem equal to the exact solution $\cos(x - \xi t)$ for a large value of t , then we would need a large number of Legendre polynomial basis functions even to accurately compute the solution over a short time interval.

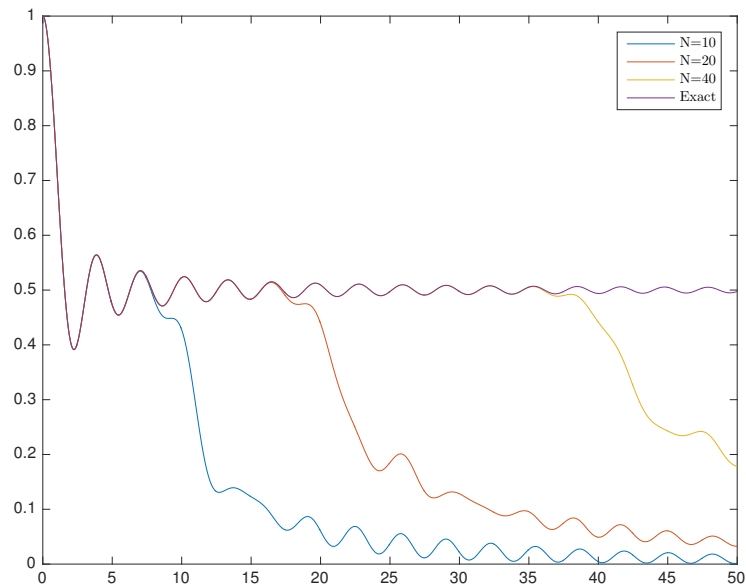


Figure 2.4: Mean Square Expectation $x = 0$ of the projection of the exact solution to (2.2) onto gPC basis functions for increasing polynomial order N .

2.2.2 Empirical Chaos Expansion

In order to apply an empirical chaos expansion, we must account for the fact that the basis functions might no longer be orthogonal. This results in the stochastic Galerkin system becoming slightly more complicated than the one for gPC. If we let $\{\Psi^i(\xi)\}_{i=1}^N$ be a set of possibly non-orthogonal basis functions, then we can express the exact solution to

Equation (2.2) as:

$$u(x, t, \xi) \approx \sum_{i=1}^N \hat{u}^i(x, t) \Psi^i(\xi).$$

Substituting this expansion into Equation (2.2) results in:

$$\sum_{i=1}^N \hat{u}_t^i(x, t) \Psi^i(\xi) = \xi \sum_{i=1}^N \hat{u}_x^i(x, t) \Psi^i(\xi)$$

We then multiply by a test function $\Psi^j(\xi)$, and take an expectation over Ω of both sides, resulting in:

$$\begin{aligned} & \sum_{i=1}^N \hat{u}_t^i(x, t) \Psi^i(\xi) \Psi^j(\xi) = \sum_{i=1}^N \hat{u}_x^i(x, t) \Psi^i(\xi) \Psi^j(\xi) \xi \\ \implies & E \left[\sum_{i=1}^N \hat{u}_t^i(x, t) \Psi^i(\xi) \Psi^j(\xi) \right] = E \left[\sum_{i=1}^N \hat{u}_x^i(x, t) \Psi^i(\xi) \Psi^j(\xi) \xi \right] \\ \implies & \sum_{i=1}^N \hat{u}_t^i(x, t) E [\Psi^i(\xi) \Psi^j(\xi)] = \sum_{i=1}^N \hat{u}_x^i(x, t) E [\Psi^i(\xi) \Psi^j(\xi) \xi]. \end{aligned} \quad (2.7)$$

Letting

$$M_{ji} = E [\Psi^i(\xi) \Psi^j(\xi)], \quad A_{ji} = E [\Psi^i(\xi) \Psi^j(\xi) \xi], \quad \text{and} \quad u = \begin{pmatrix} u^1(x, t) \\ u^2(x, t) \\ \vdots \\ u^N(x, t) \end{pmatrix},$$

Equation (2.7) can be expressed as:

$$Mu_t = Au_x. \quad (2.8)$$

If we know the actual values of the empirical basis functions Ψ^i and the initial value of the \hat{u}^i coefficients, then the matrices M and A can both be computed, and the system in (2.8) can be solved to obtain the values of the coefficients at later times.

We can follow the method in section 2.1 to construct empirical basis functions over small time intervals by sampling trajectories and applying POD. We begin by choosing a fixed set of values for the random variable ξ , and solve equation (2.2) for each of the fixed ξ values, starting at time zero and ending at time τ_1 . Fixing ξ makes the PDE deterministic, and it can be solved with any number of existing numerical methods. Here, we use a method of lines discretization to approximate the spatial derivative and then apply a fourth-order Runge-Kutta method to perform the time integration (*ode45* in Matlab). If we take the discrete solutions at a fixed point in space and time and vary the value of ξ , then it can be viewed as a trajectory through the random space. We use these discrete trajectories as the rows of the T matrix from section 2.1.3, and perform POD by computing the singular values of T . We then scale the singular values so that the maximum value has magnitude 1, and cut off the expansion once the magnitude of the corresponding singular values drops below 10^{-4} . The value of 10^{-4} is arbitrary and was determined empirically by cutting off the expansion at varying values. Once the empirical basis functions $\{\Psi^i(\xi)\}$ have been generated, we do not explicitly construct an interpolant, but instead use the discrete values as interpolation nodes for a composite trapezoidal quadrature rule in order to compute the necessary expectations and inner products. On the first timestep we project the initial condition $u_0(x, \xi)$ onto the basis functions by computing:

$$\hat{u}^i(x, 0) = \langle u_0(x, \xi), \Psi^i(\xi) \rangle_{\Omega} = \int_{\Omega} u_0(x, \xi) \Psi^i(\xi) (1/2) d\xi.$$

This gives us the initial values of the \hat{u}^i coefficients. From there, we compute the entries

of the M and A matrices in equation (2.8), and solve the system numerically up to the first timestep, τ_1 . At that point, we have values for the \hat{u}^i coefficients up to time τ_1 , and thus an analytic approximation of the true solution $u(x, t, \xi)$ up to time τ_1 . We use the solution at time τ_1 as an initial condition, and then solve the deterministic PDE up to the second timestep, τ_2 , for the same fixed set of values for ξ as in the first step. The solutions now give a set of trajectories in the random space for times between τ_1 and τ_2 . We apply POD to these trajectories to obtain a new set of basis functions, $\{\Phi^i\}_{i=1}^M$. We then follow the method in section 1.1.3 to project the coefficients of the solution at time τ_1 , which are coefficients for the old basis, $\{\Psi^i\}$, into coefficients for the new basis, $\{\Phi^i\}$ and use them as the initial values of the \hat{u}^i coefficients. We then use the new basis functions Φ^i to compute new values for the M and A matrices from equation (2.8) and solve the DAE up to time τ_2 .

We now repeat the above process iteratively for times τ_2 to τ_3 , then τ_3 to τ_4 , and so on, up to the final integration time. In general, choosing smaller timesteps results in fewer empirical basis functions, while larger timesteps require more empirical basis functions. Figure 2.5 shows the result of applying this method with a timestep of size 1, using 120 Chebyshev nodes for values of ξ between -1 and 1 to compute trajectories for the empirical basis functions. The numerical solution was then used to estimate the mean square expectation of the true solution at the point $x = 0$. The maximum number of empirical basis functions used on any given step was 9.

In order to determine an appropriate number of basis functions to use for a given timestep, we can examine the singular values from the POD. See figure 2.6, which shows the singular values for the POD from the first timestep, scaled so that the first singular value has magnitude 1. There is a sharp drop-off in the magnitude of the singular values around the fifth singular value. The code for the empirical chaos expansion truncates the expansion

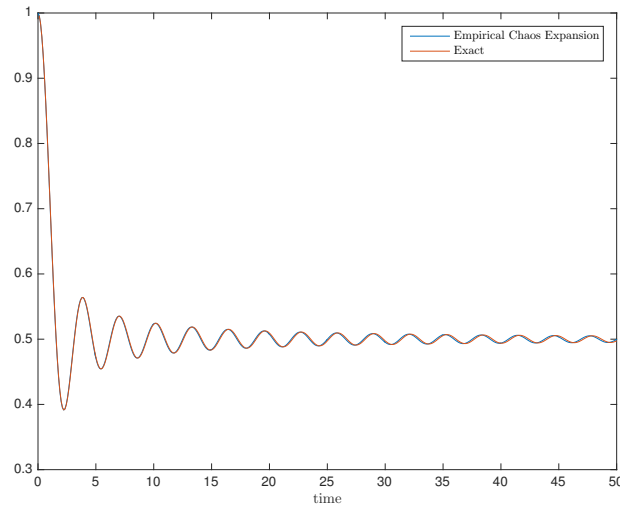


Figure 2.5: Mean Square Expectation at $x = 0$ of solution to 2.2, computed using empirical chaos expansion with stochastic Galerkin. Maximum of 9 empirical basis functions on each timestep.

once the scaled value of the singular values has dropped below 10^{-4} . Past that point adding additional basis functions does not appear to increase the accuracy. See figures 2.7 and 2.8, which show the result of applying the empirical chaos expansion to the one dimensional wave equation but with only 4 and 5 basis functions, respectively. In both of those cases the number of empirical basis functions is too low and results in large projection errors. Note that the cutoff criterion we used results in using 9 basis functions (see figure 2.5).

As mentioned earlier, choosing a larger timestep for the empirical chaos expansion results in growth of the required number of basis functions for each timestep. This is unsurprising, since we observe the same behavior with gPC; in order to accurately capture solution behavior for long time periods, we need more and more basis functions. This presents an interesting optimization challenge for empirical chaos expansion, since a smaller basis results in a smaller stochastic Galerkin system, but a smaller timestep means that we must re-compute more empirical bases. Computing an empirical basis involves sampling

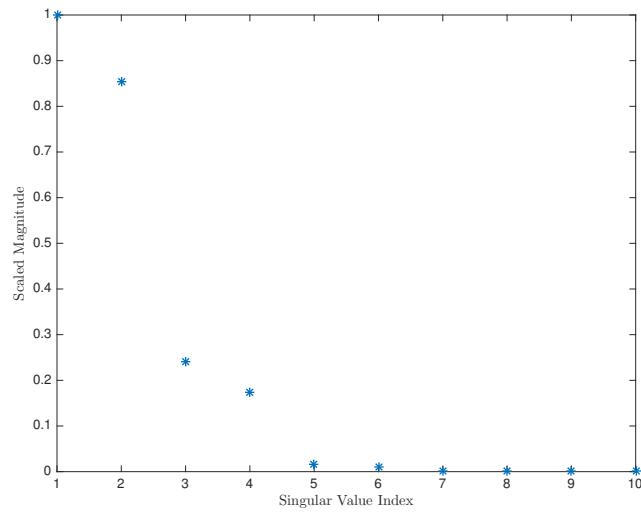


Figure 2.6: Singular values from POD for the first timestep when performing empirical chaos expansion to solve (2.2). Singular values are scaled so that the maximum singular value has magnitude 1.

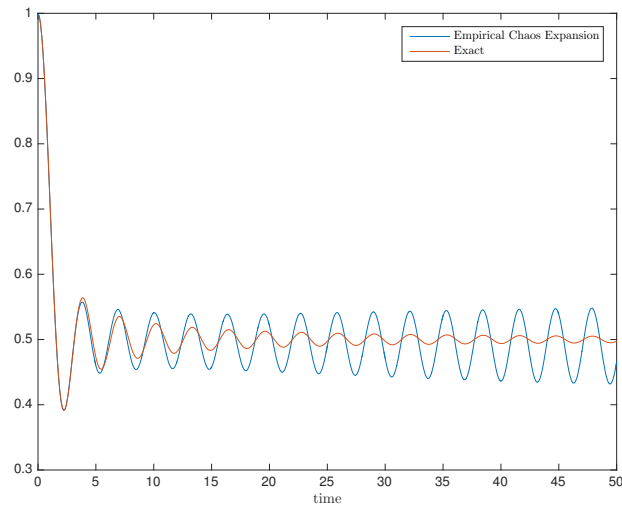


Figure 2.7: Mean Square Expectation at $x = 0$ of solution to 2.2, computed using empirical chaos expansion with stochastic Galerkin. Maximum of 4 empirical basis functions on each timestep.

trajectories of the SPDE, then computing the POD of the trajectories and using it to construct an empirical basis, and finally projecting the initial condition onto the set of basis functions. Thus, a smaller timestep reduces the cost of solving the stochastic Galerkin system, but

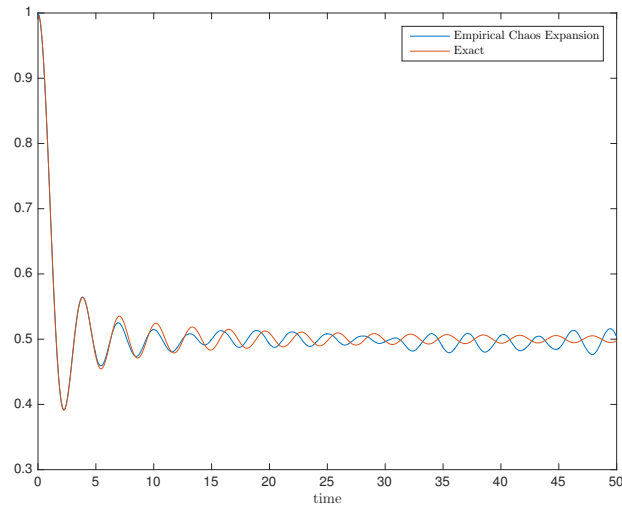


Figure 2.8: Mean Square Expectation at $x = 0$ of solution to 2.2, computed using empirical chaos expansion with stochastic Galerkin. Maximum of 5 empirical basis functions on each timestep.

increases the cost of generating the empirical bases. For the model problem of this section, a timestep of size 4 appeared to be the optimal choice. Figure 2.9 shows the required number of basis functions for different choices of timesteps.

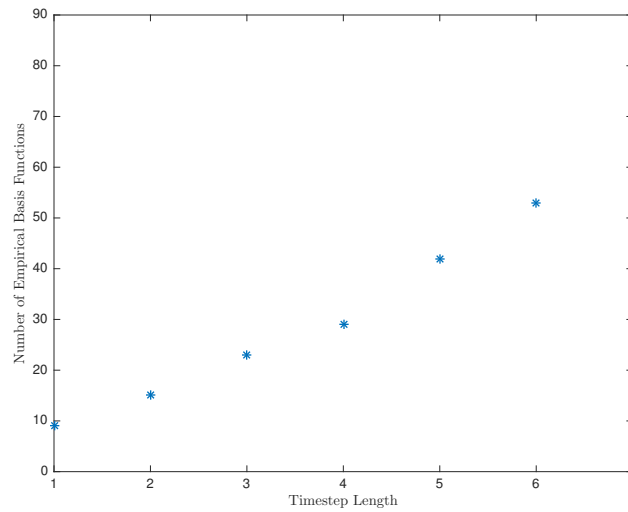


Figure 2.9: Number of empirical basis functions required for varying timestep sizes in order to accurately solve the one dimensional wave equation (2.2) using a stochastic Galerkin method. Note that the size of the timestep has a strong influence on the total number of empirical basis functions.

2.2.3 Running Time

As long as the number of empirical basis functions does not noticeably grow as the number of timesteps increases, we can expect the execution time for the empirical expansion method to scale linearly with the final integration time (see figure 2.10). When compared to the gPC method, we can note the superlinear growth of the running time for gPC. For the timescales examined, however, gPC outperforms the empirical chaos method due to the fixed overhead cost of generating a new set of basis functions and then projecting the solution from the old set of basis functions onto the new set of basis functions when applying an empirical chaos expansion.

Since the Legendre polynomials and the A matrix in (2.5) can be precomputed for gPC, the running time to construct them is not included in the gPC running time. However, as the order gets larger, the running time to construct the A matrix is far larger than the actual time required to execute the gPC code, due to the $O(n^2)$ time required to compute

all of the entries. In the simulations presented, the Legendre polynomials were generated symbolically and integrated exactly to avoid any error. In order to integrate out to time 200 accurately, we had to use 220 basis functions, and the time required to compute the A matrix was around 10 hours. In contrast, the empirical chaos method requires no pre-computation and instead computes its basis functions directly from the sampled trajectories.

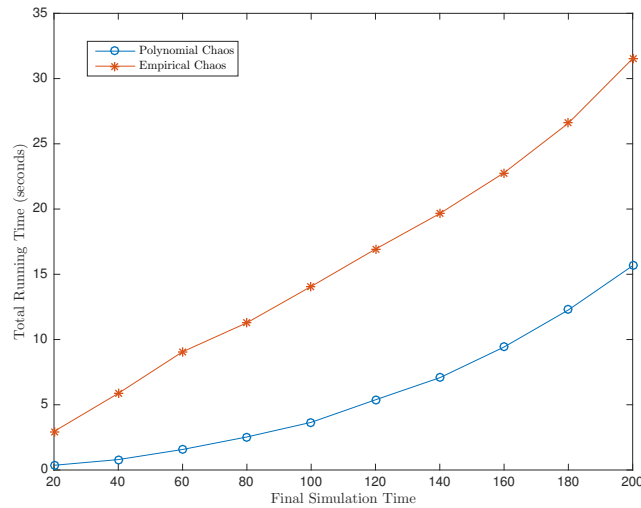


Figure 2.10: Comparison of total running times for solutions of (2.2) computed to the same accuracy using empirical chaos expansion and gPC with stochastic Galerkin.

2.2.4 Basis Function Evolution

Since a new set of basis functions is computed at every timestep in the empirical expansion, it is natural to examine how they change over time. In order to closely monitor their evolution, we set the timestep size for the wave equation to 0.1, and examine the values of the basis functions over time. Figure 2.11 shows the basis function that corresponds to the largest singular value from POD for the first 5 timesteps (each of size 0.1).

The basis function evolves smoothly over time, although at singular value crossings

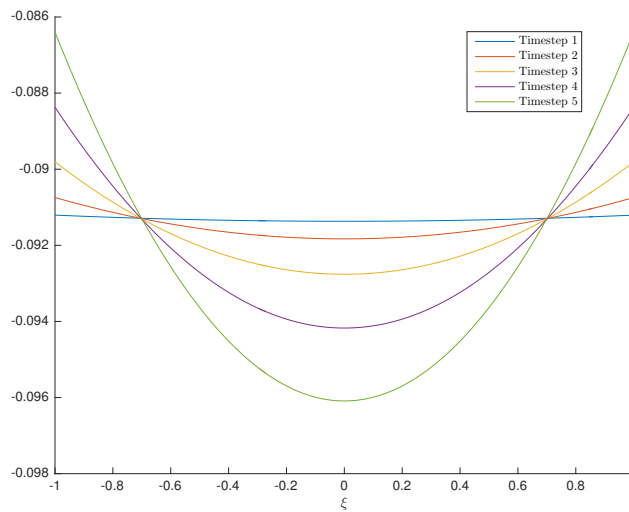


Figure 2.11: Evolution of the first basis function from POD for the first five timesteps in the solution to (2.2) using empirical chaos expansion.

it becomes the function associated with the second largest singular value. Figure 2.12 shows the magnitudes of the first and second singular values from POD for 100 timesteps, and there are multiple singular value crossings. Figure 2.13 gives a three dimensional view of the basis function evolution, where the x -axis is the value of the random variable, and the y -axis is time. From this figure we can also observe the smooth evolution of this basis function. In a later chapter we will explore how to take advantage of this smooth evolution.

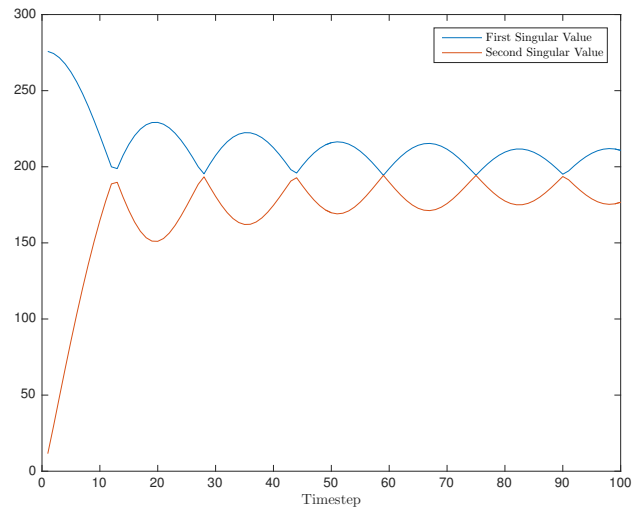


Figure 2.12: Evolution of the magnitude of the first two singular values from POD in the solution to (2.2) using empirical chaos expansion.

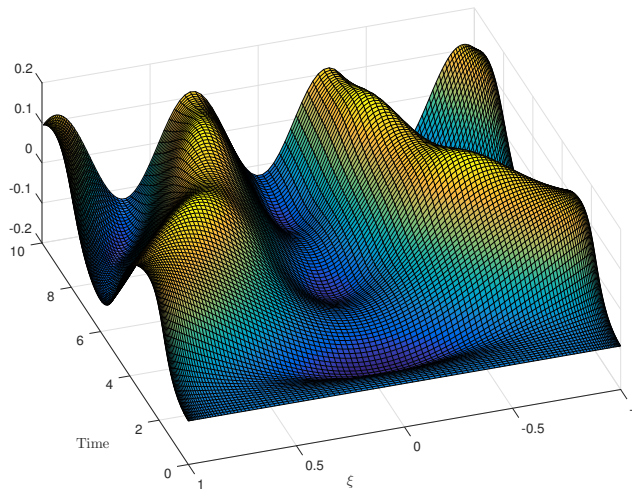


Figure 2.13: Evolution of the first basis function from POD for the first 100 timesteps in the solution to (2.2) using empirical chaos expansion.

2.3 Two Dimensional Wave Equation

To illustrate the poor scaling of polynomial chaos methods with multiple variables, we can consider a slightly modified version of the wave equation (2.2) with two random variables:

$$u_t(x, t, \xi_1, \xi_2) = (\xi_1 \xi_2) u_x(x, t, \xi), \quad 0 \leq x \leq 2\pi, \quad t \geq 0 \quad (2.9)$$

$$u(x, 0, \xi_1, \xi_2) = \cos(x), \quad (2.10)$$

with periodic boundary conditions, and where ξ_1 and ξ_2 are independent and uniformly distributed in $[-1, 1]$. The exact solution is:

$$u(x, t, \xi_1, \xi_2) = \cos(x - \xi_1 \xi_2 t),$$

Note that over the space for this problem:

$$\begin{aligned} \langle f, g \rangle &:= \int_{-1}^1 \int_{-1}^1 f(\xi_1, \xi_2) g(\xi_1, \xi_2) (1/4) d\xi_1 d\xi_2 \\ E[f] &:= \int_{-1}^1 \int_{-1}^1 f(\xi_1, \xi_2) (1/4) d\xi_1 d\xi_2 \end{aligned}$$

2.3.1 Polynomial Chaos Expansion

We may project the solution onto the space of multidimensional Legendre polynomials, which are constructed by taking tensor products of the single variable Legendre polynomials over each of the two random variables. For example, the first 10 basis functions

are:

$$L_1^2(\xi_1, \xi_2) = L_1(\xi_1)L_1(\xi_2)$$

$$L_2^2(\xi_1, \xi_2) = L_1(\xi_1)L_2(\xi_2)$$

$$L_3^2(\xi_1, \xi_2) = L_2(\xi_1)L_1(\xi_2)$$

$$L_4^2(\xi_1, \xi_2) = L_1(\xi_1)L_3(\xi_2)$$

$$L_5^2(\xi_1, \xi_2) = L_2(\xi_1)L_2(\xi_2)$$

$$L_6^2(\xi_1, \xi_2) = L_3(\xi_1)L_1(\xi_2)$$

$$L_7^2(\xi_1, \xi_2) = L_1(\xi_1)L_4(\xi_2)$$

$$L_8^2(\xi_1, \xi_2) = L_2(\xi_1)L_3(\xi_2)$$

$$L_9^2(\xi_1, \xi_2) = L_3(\xi_1)L_2(\xi_2)$$

$$L_{10}^2(\xi_1, \xi_2) = L_4(\xi_1)L_1(\xi_2),$$

where L_i^2 is the i^{th} two variable Legendre polynomial, and L_i is the i^{th} single variable Legendre polynomial. Just like their single variable counterparts, the multidimensional Legendre polynomials are orthonormal, and they form a basis over the random variable space $[-1, 1] \times [-1, 1]$.

We are taking combinations of two single variable Legendre polynomials to construct the multidimensional Legendre polynomials, so if we want multidimensional polynomials up to order n then we need $O(n^2)$ basis functions in total. This also means that the complexity of the operations to precompute the basis functions and the A matrix will run in $O(n^4)$ time. The big-O complexity will get even worse if we add additional random variables.

We can again perform a stochastic Galerkin method as in section 1.1.1 by substituting the expansion:

$$u(x, t, \xi_1, \xi_2) = \sum_{i=1}^{\infty} \hat{u}^i(x, t) L_i^2(\xi_1, \xi_2)$$

into Equation 2.9, then multiplying by a test function L_j^2 , and taking an expectation:

$$\begin{aligned} \sum_{i=1}^{\infty} \hat{u}_t^i(x, t) L_i^2(\xi_1, \xi_2) &= \xi_1 \xi_2 \sum_{i=1}^{\infty} \hat{u}_x^i(x, t) L_i^2(\xi_1, \xi_2) \\ \implies E \left[\sum_{i=1}^{\infty} \hat{u}_t^i(x, t) L_i^2(\xi_1, \xi_2) L_j^2(\xi_1, \xi_2) \right] &= E \left[\xi_1 \xi_2 \sum_{i=1}^{\infty} \hat{u}_x^i(x, t) L_i^2(\xi_1, \xi_2) L_j^2(\xi_1, \xi_2) \right] \\ \implies \sum_{i=1}^{\infty} \hat{u}_t^i(x, t) E [L_i^2(\xi_1, \xi_2) L_j^2(\xi_1, \xi_2)] &= \sum_{i=1}^{\infty} \hat{u}_x^i(x, t) E [\xi_1 \xi_2 L_i^2(\xi_1, \xi_2) L_j^2(\xi_1, \xi_2)] \\ \implies \hat{u}_t^j(x, t) &= \sum_{i=1}^{\infty} \hat{u}_x^i(x, t) E [\xi_1 \xi_2 L_i^2(\xi_1, \xi_2) L_j^2(\xi_1, \xi_2)] \end{aligned} \tag{2.11}$$

Letting

$$A_{ji} = E [\xi_1 \xi_2 L_j^2 L_i^2] \quad \text{and} \quad \hat{u} = \begin{pmatrix} \hat{u}^1(x, t) \\ \hat{u}^2(x, t) \\ \vdots \end{pmatrix}$$

simplifies Equation 2.11 to:

$$\hat{u}_t = A \hat{u}_x. \tag{2.12}$$

Since the initial condition is deterministic, $\hat{u}^1(x, 0) = \cos(x)$, and $\hat{u}^i(x, 0) = 0$ for $i > 1$.

We can then truncate the infinite system at some finite value N and solve the resulting deterministic system. To examine the solution we can look at the mean square expectation at $x = 0$. The exact value is:

$$\begin{aligned}
E [(u(0,t,\xi))^2] &= \int_{-1}^1 \int_{-1}^1 (\cos^2(\xi_1 \xi_2 t)) (1/2) d\xi_1 d\xi_2 \\
&= \frac{1}{2} \left(1 + \frac{\text{Si}(2t)}{2t} \right).
\end{aligned} \tag{2.13}$$

where Si is the sine integral:

$$\text{Si}(z) := \int_0^z \frac{\sin t}{t} dt.$$

See figure 2.14 for a comparison of the performance of standard polynomial chaos as the order increases. For order 40, the number of basis functions is 820. Similar to the one dimensional wave equation with a single random variable, we need an increasingly higher order polynomial basis in order to accurately capture the solution out to long time intervals.

Once the matrix A from equation (2.12) has been precomputed, the actual running time of the polynomial chaos method is fast (though it scales quadratically) for orders up to 40. However, the current code that we use to generate the Legendre polynomials starts incurring a prohibitive computational cost at this point, which is why we do not present gPC results for orders past 40 in the two dimensional case.

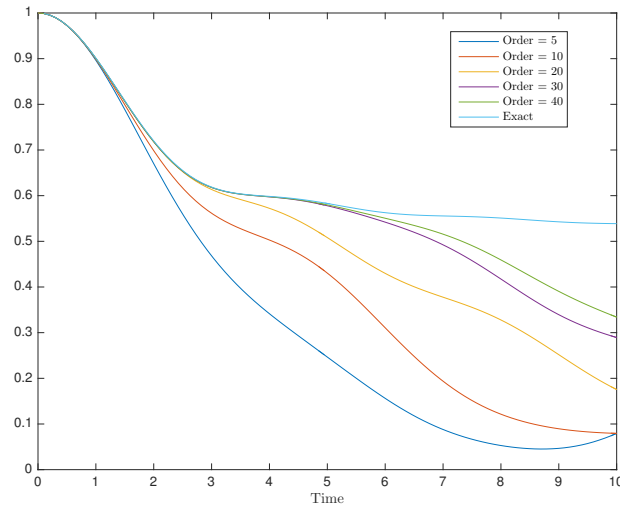


Figure 2.14: Mean Square Expectation at $x = 0$ of solution to (2.9), computed using gPC with stochastic Galerkin using two dimensional Legendre polynomials of varying order.

2.3.2 Sparse Grid Quadrature

Before we can effectively construct an empirical chaos expansion to solve equation (2.9), we must first determine an appropriate set of two dimensional random vectors $\{\bar{\xi}_i\}_{i=1}^m$ at which to solve the deterministic version of equation (2.9). In the case where there was a single random variable we chose Chebyshev nodes on the interval, and determining the value of the empirical basis functions at those points allowed us to apply numerical quadrature methods to compute the necessary inner products and expectations. In the two variable case we have a similar requirement: if we know the values of the empirical basis functions only at each of the random vectors in the set $\{\bar{\xi}_i\}_{i=1}^m$, we must be able to apply a numerical cubature method to compute inner products and expectations involving the basis functions, or be able to interpolate the basis functions. We could choose to evaluate the solutions on a uniform two-dimensional grid, but sampling m points in each dimension results in $O(m^2)$ total points. The situation becomes even worse as the total number of random variables

grows. To reduce the cost of solving problems on multi-dimensional random spaces, we can use sparse quadrature methods.

Sparse grid methods were first developed in [70]. While sparse grid methods are based on tensor product constructions, they avoid taking the full tensor product, and thus their growth rate scales far slower than the growth rate for full tensor product grids. The interpolating function is of the form (Lemma 1 from [77]):

$$U_q = \sum_{1 \leq \mathbf{i}, q-d+1 \leq |\mathbf{i}| \leq q} (-1)^{q-|\mathbf{i}|} \binom{d-1}{q-|\mathbf{i}|} \bigotimes_{k=1}^d U_{i_k},$$

where d is the dimension of the space, q is the level of the sparse grid, the multi-index $\mathbf{i} = (i_1, i_2, \dots, i_d)$, $|\mathbf{i}| := \sum_{k=1}^d i_k$, and U_{i_k} is an interpolating function in dimension k over i_k nodes. The condition $q - d + 1 \leq |\mathbf{i}| \leq q$ in the summation makes it so that we do not take the full tensor product.

The construction of sparse grids depends on the choice of interpolating nodes for each of the U_{i_k} . We use Clenshaw-Curtis sparse grids [11], which use extrema of the Chebyshev polynomials for the interpolation nodes in each individual dimension. A detailed discussion of their construction and implementation may be found in [19] and [22]. There are a number of convergence results regarding sparse grid quadrature, and a result from [3] establishes that for functions on the space

$$F_d^l = \{f : [-1, 1]^d \rightarrow \mathbb{R} \mid \partial^{\mathbf{i}} f \text{ continuous, } i_j \leq l \forall 1 \leq j \leq d\},$$

the following error bound holds:

$$\|f - U_M\|_{\infty} \leq C_{d,l} M^{-l} (\log M)^{(l+2)(d-1)+1},$$

where U_M is an interpolating polynomial of f on M nodal points, and $C_{d,l}$ is a constant that depends on d and l .

For the computations presented in the following sections, we use a sparse grid library written in Matlab [40, 39].

2.3.3 Empirical Chaos Expansion

We can again follow the method in Section 2.1 to construct empirical basis functions over small time intervals. Since the trajectories are over two random dimensions we use Clenshaw-Curtis sparse grids to determine at which values of ξ_1 and ξ_2 we should sample the solution. See figure 2.15 for a plot of the results. The plot was generated using a grid depth of 10 (which results in 7196 sampled points) and a timestep size of 1.

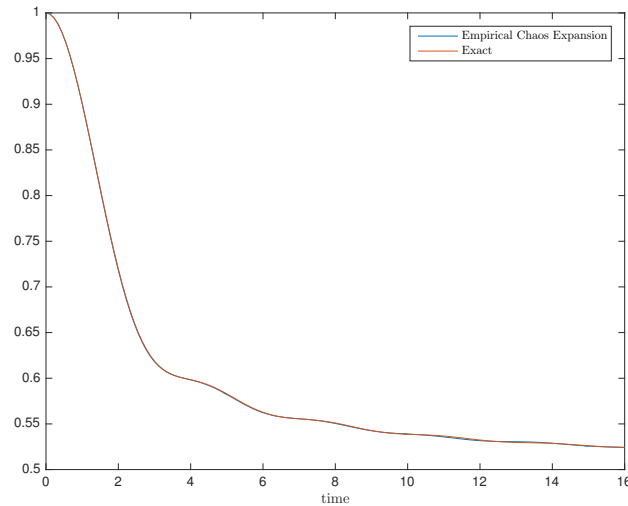


Figure 2.15: Mean Square Expectation at $x = 0$ of solution to (2.9), computed using empirical chaos expansion with stochastic Galerkin.

2.3.4 Running Time

The library that we currently use for the sparse grid interpolation and projection runs rather slowly, so in the two dimensional case the projection operation between the bases at each timestep dominates the computational time (approximately 92% of the running time is spent projecting the bases). While the cost of each projection is high, the computational time still scales linearly as the final simulation time is increased (see figure 2.16). With a more highly optimized multidimensional integration library the main computational cost should be incurred by sampling trajectories, as is true in the one dimensional case. We do not have gPC results to compare to the empirical chaos running times as the offline cost to precompute the A matrix in 2.12 is prohibitive past order 40, which prevents us from obtaining accurate solutions past a final integration time of about 8 with gPC.

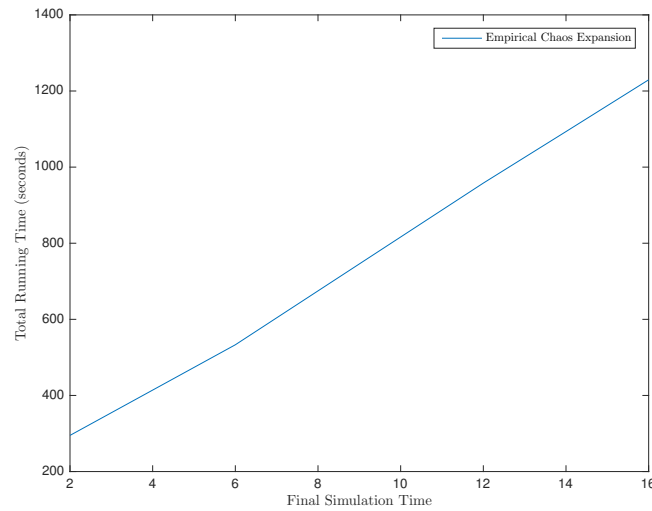


Figure 2.16: Total running times for solutions of (2.12) computed using empirical chaos expansion with stochastic Galerkin.

2.4 Diffusion Equation

Consider the SPDE:

$$u_t(x, t, \xi) = \xi u_{xx}(x, t, \xi), \quad 0 \leq x \leq 6, \quad t \geq 0 \quad (2.14)$$

$$u(x, 0, \xi) = 3I_{[2,4]}, \quad (2.15)$$

with homogeneous Dirichlet boundary conditions, i.e.

$$u(0, t, \xi) = u(6, t, \xi) = 0.$$

$I_{[a,b]}$ is the indicator function on the interval $[a, b]$ and ξ is a random variable uniformly distributed on $[0, 1]$. Since the solution to the diffusion equation with these initial conditions will eventually converge, gPC does quite well. Integrating out to long times accurately does not require continually increasing the number of basis functions. Even though existing techniques solve this equation efficiently, it is interesting to examine how the basis functions for the empirical chaos expansion change over time. The true solution converges to a fixed value as time goes to infinity, so it is reasonable to expect the empirical basis functions to converge as well. This turns out to be true, as we will see in the following sections.

Note that over the space of this problem:

$$\langle f, g \rangle := \int_0^1 f(\xi)g(\xi)d\xi$$

$$E[f] := \int_0^1 f(\xi)d\xi$$

2.4.1 Polynomial Chaos Expansion

Since the random variable ξ is uniformly distributed, we again use the Legendre polynomials $\{L^i(\xi)\}_{i=1}^{\infty}$ as the set of orthogonal polynomial basis functions. The domain of the random space is the interval $[0, 1]$, so we must use shifted Legendre polynomials, since the standard Legendre polynomials are orthogonal over the interval $[-1, 1]$. The true solution can be expressed as:

$$u(x, t, \xi) = \sum_{i=1}^{\infty} \hat{u}^i(x, t) L^i(\xi),$$

and substituting this expression into equation (2.14) gives:

$$\sum_{i=1}^{\infty} \hat{u}_t^i(x, t) L^i(\xi) = \xi \sum_{i=1}^{\infty} \hat{u}_{xx}^i(x, t) L^i(\xi)$$

Multiplying by a test function $L^j(\xi)$ and taking the expectation gives:

$$\begin{aligned} \sum_{i=1}^{\infty} \hat{u}_t^i(x, t) L^i(\xi) L^j(\xi) &= \xi \sum_{i=1}^{\infty} \hat{u}_{xx}^i(x, t) L^i(\xi) L^j(\xi) \\ \implies E \left[\sum_{i=1}^{\infty} \hat{u}_t^i(x, t) L^i(\xi) L^j(\xi) \right] &= E \left[\xi \sum_{i=1}^{\infty} \hat{u}_{xx}^i(x, t) L^i(\xi) L^j(\xi) \right] \\ \implies \sum_{i=1}^{\infty} \hat{u}_t^i(x, t) E [L^i(\xi) L^j(\xi)] &= \sum_{i=1}^{\infty} \hat{u}_{xx}^i(x, t) E [\xi L^i(\xi) L^j(\xi)] \\ \implies \hat{u}^j(x, t) &= \sum_{i=1}^{\infty} \hat{u}_{xx}^i(x, t) E [\xi L^i(\xi) L^j(\xi)] \end{aligned} \quad (2.16)$$

Letting

$$A_{ji} = E [\xi L^i(\xi) L^j(\xi)] \quad \text{and} \quad \hat{u} = \begin{pmatrix} \hat{u}^1(x, t) \\ \hat{u}^2(x, t) \\ \vdots \end{pmatrix},$$

equation (2.16) can be simplified to:

$$\hat{u}_t = A\hat{u}_x x. \quad (2.17)$$

The infinite system in (2.17) can then be truncated at a finite value N , which results in a coupled system of N deterministic PDEs. Since the initial condition is deterministic, the initial values for the \hat{u}^i 's are:

$$\hat{u}^1(x, 0) = 3I_{[2,4]}, \quad \hat{u}^i(x, 0) = 0 \text{ for all } i > 1.$$

Using the initial condition, we can solve the truncated system from equation 2.17, which gives the evolution of the unknown \hat{u}^i coefficients in time. In figure 2.17 we plot the mean square expectation of the solution at $x = 1$, computed using the stochastic Galerkin method for different polynomial orders. The exact solution was computed by running Monte Carlo sampling until it converged ($\sim 30,000$ iterations). The mean square expectation at $x = 1$ can be computed as:

$$E [u(1, t, \xi)^2] \approx E \left[\left(\sum_{i=1}^N \hat{u}^i(x, t) L^i(\xi) \right)^2 \right] = \sum_{i=1}^N E [(\hat{u}^i)^2].$$

Unlike the one dimensional wave equation in section 2.2, the solution of which is a travelling wave, the solutions to the diffusion equation all converge to the same final value. The result is that polynomial chaos is accurate out to long times even with a small set of basis functions. Note that in figure 2.17, using 10 polynomial functions captures the solution behavior very well out to a final time of 100, and using 15 polynomial functions makes the computed solution almost indistinguishable from the exact solution.

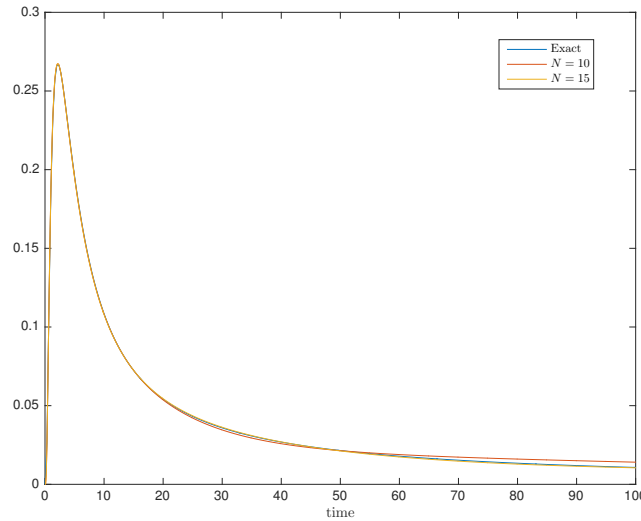


Figure 2.17: Mean Square Expectation at $x = 1$ of solution to (2.14), computed using gPC with stochastic Galerkin using Legendre polynomials of varying order N .

2.4.2 Empirical Chaos Expansion

Just as before, we can follow the approach of section 2.1 to construct an empirical basis and solve the diffusion equation. First, we must analytically derive the stochastic Galerkin system for an arbitrary basis $\{\Psi^i(\xi)\}_{i=1}^N$. We approximate the true solution as:

$$u(x, t, \xi) \approx \sum_{i=1}^N \hat{u}^i(x, t) \Psi^i(\xi),$$

where $\{\Psi^i\}_{i=1}^N$ is the set of non-orthogonal empirical basis functions. Substituting this expansion into equation (2.14) gives:

$$\sum_{i=1}^N \hat{u}_t^i(x, t) \Psi^i(\xi) = \xi \sum_{i=1}^N \hat{u}_{xx}^i(x, t) \Psi^i(\xi)$$

then multiplying by a test function Ψ^j and taking the expectation:

$$\begin{aligned}
\sum_{i=1}^N \hat{u}_t^i(x,t) \Psi^i(\xi) \Psi^j(\xi) &= \xi \sum_{i=1}^N \hat{u}_{xx}^i(x,t) \Psi^i(\xi) \Psi^j(\xi) \\
E \left[\sum_{i=1}^N \hat{u}_t^i(x,t) \Psi^i(\xi) \Psi^j(\xi) \right] &= E \left[\xi \sum_{i=1}^N \hat{u}_{xx}^i(x,t) \Psi^i(\xi) \Psi^j(\xi) \right] \\
\sum_{i=1}^N \hat{u}_t^i(x,t) E [\Psi^i(\xi) \Psi^j(\xi)] &= \sum_{i=1}^N \hat{u}_{xx}^i(x,t) E [\xi \Psi^i(\xi) \Psi^j(\xi)]
\end{aligned} \tag{2.18}$$

Letting

$$M_{ji} = E [\Psi^i(\xi) \Psi^j(\xi)], \quad A_{ji} = E [\xi \Psi^i(\xi) \Psi^j(\xi)], \quad \text{and} \quad \hat{u} = \begin{pmatrix} \hat{u}^1(x,t) \\ \hat{u}^2(x,t) \\ \vdots \\ \hat{u}^N(x,t) \end{pmatrix},$$

simplifies equation (2.18) to:

$$M \hat{u}_t = A \hat{u}_{xx}. \tag{2.19}$$

We can use the solution of (2.19) to compute the values of the unknown \hat{u}^i coefficients at later times. Just as with the one dimensional wave equation in section 2.2, we begin by picking a set of values of ξ , this time in the interval $[0, 1]$, and solve the diffusion equation (2.14) from time 0 to time τ_1 for each of the values of ξ . In this case we chose the set of values of ξ to be 200 Chebyshev nodes in the interval $[0, 1]$. Next, we perform POD on the numerical solutions in order to derive a set of empirical basis functions. Again, we truncate the basis functions when the corresponding scaled singular value drops below 10^{-4} . For the first timestep, we project the initial condition onto each empirical basis function by

numerically computing:

$$\hat{u}^i(x,0) = \langle u(x,0,\xi), \Psi^i(\xi) \rangle = \int_0^1 u(x,0,\xi) \Psi^i(\xi) d\xi,$$

for all i from 1 to N . We then use the empirical basis functions to compute the M and A matrices in equation (2.18), and solve the system from time 0 to time τ_1 . However, for computational efficiency we do not recompute trajectories to find a new empirical basis for the time interval $[\tau_1, \tau_2]$. Just as with gPC, we can obtain accurate solutions to the diffusion equation by using a fixed basis. Since we fix the basis, the cost of solving the diffusion equation is much lower than the cost of solving the one dimensional wave equation, since we only need to compute trajectories over a short time interval instead of over the entire integration time.

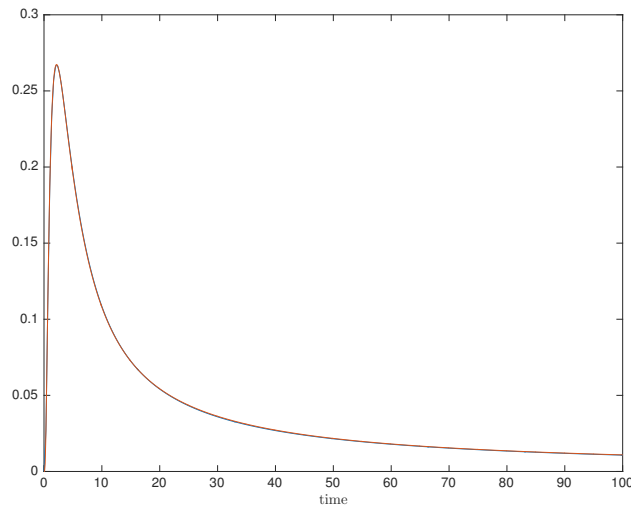


Figure 2.18: Mean square expectation at $x = 1$ of the solution to the diffusion equation (2.14) computed using an empirical chaos expansion with stochastic Galerkin. The empirical basis functions were generated by solving trajectories up to time $t = 1$, and then fixing them for the entire integration time. The number of basis functions used was 12.

2.4.3 Running Time

Figure 2.19 shows a comparison between the total running times of polynomial chaos and empirical chaos expansion methods when solving the diffusion equation 2.14. The computational time for the polynomial chaos method scales roughly linearly with the final simulation time because we can leave the total number of basis functions fixed at 15. This can be contrasted with the situation for the one dimensional wave equation where we needed to increase the number of basis functions in order to accurately solve the SPDE out to longer times. Similarly, the running time for the empirical chaos expansion method also scales linearly with the final simulation time. For computational efficiency we only compute the empirical basis functions by sampling trajectories up to time $t = 1$ and then leave them fixed for the remaining integration time.

We do not include the cost of pre-computing the A matrix from Equation 2.17 or the normalized Legendre polynomials in the running time plots. Both methods use roughly the same number of basis functions. The polynomial chaos expansion uses 15 basis functions and the empirical chaos expansion uses 12 basis functions. Polynomial chaos slightly outperforms the empirical chaos expansion due to the cost of generating the set of empirical basis functions as well as the cost of projecting the initial condition onto the empirical basis functions. Since the initial condition is deterministic it becomes the coefficient of the first Legendre polynomial (i.e. $L_1 = 1$) and we do not need to perform any projections when performing polynomial chaos.

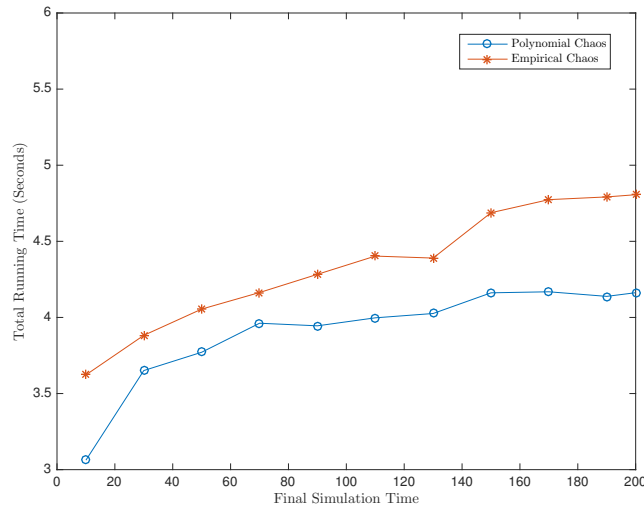


Figure 2.19: Comparison of total running times for solutions of (2.14) computed to the same accuracy using empirical chaos expansion and gPC with stochastic Galerkin.

2.4.4 Basis Function Evolution

Even though we do not need to evolve the empirical basis functions to accurately solve the diffusion equation, we can examine how they change over time if we do re-compute them at each timestep. For the results in this section we sample trajectories and apply POD to compute empirical basis functions up to time τ_1 , but then instead of leaving the basis fixed, we then use the final solution at time τ_1 as an initial condition, and solve the diffusion equation (2.14) from time τ_1 to time τ_2 for each value of ξ to compute trajectories. We then apply a POD to the trajectories to construct a new empirical basis $\{\Phi^i\}_{i=1}^N$. We then take the final solution at time τ_1 , which is expressed in terms of coefficients \hat{u}^i corresponding to the old basis $\{\Psi^i\}$, and apply the basis transformation from section 1.1.3 to convert them into coefficients for the new basis $\{\Phi^i\}$. We then use the new basis $\{\Phi^i\}$ to recompute the A and M matrices in equation 2.19, and solve it again to advance the solution up to time τ_2 . We then repeat this process iteratively until we have reached the final integration time.

Unlike the case for the one dimensional wave, increasing the timestep size does not have a strong impact on the required number of empirical basis functions. Recall we decide the number of empirical basis functions by examining the relative magnitudes of the singular values from POD. As the solution to the diffusion equation converges, we do not need a growing set of basis functions to accurately capture the solution behavior at later times. Figure 2.18 shows the computed mean square expectation at $x = 1$ for an empirical chaos expansion with timestep size 100. Since the final integration time was also 100, only one timestep was performed. Even in that case it only used 17 empirical basis functions. This can be contrasted with the behavior of the one dimensional wave, where a timestep of size 7 required 83 empirical basis functions.

We set the timestep size to 0.1 in order to closely monitor the evolution of the basis functions, and integrated out to time 40. Figure 2.21 shows the basis functions for the first five timesteps for the basis function corresponding to the largest singular value from POD, and Figure 2.22 shows the basis functions for timesteps 400 and 500. For those 100 timesteps the basis functions only slightly change. The same is also true for the basis functions associated with the smaller singular values. Figures 2.23 and 2.24 show the evolution of the basis function associated with the second largest singular value, and this basis function converges as well.

Figure 2.20 shows how the number of empirical basis functions changes as we increase the timestep when solving equation (2.14) using an empirical chaos expansion. Unlike the one dimensional wave equation, the number of basis functions required does not greatly increase as we increase the size of the timesteps.

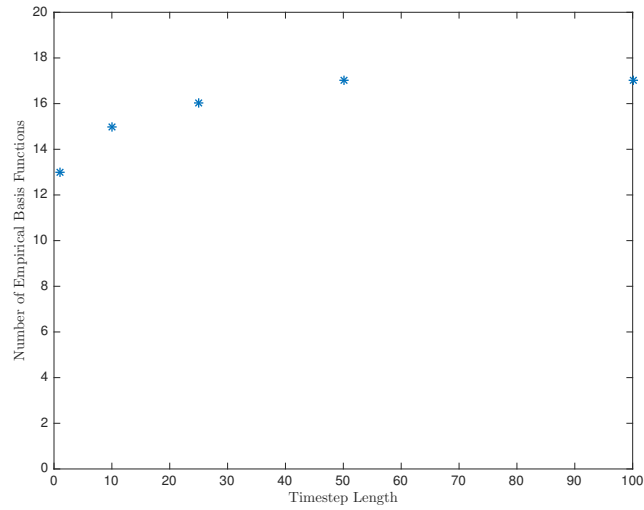


Figure 2.20: Number of empirical basis functions required for varying timestep sizes in order to accurately solve the diffusion equation (2.14) using a stochastic Galerkin method. Note that the size of the timestep does not have a strong influence on the total number of empirical basis functions.

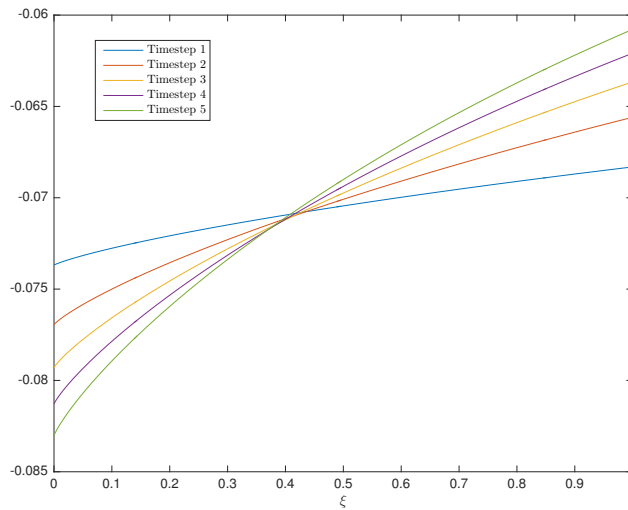


Figure 2.21: Evolution of the first basis function from POD for the first five timesteps in the solution to (2.14) using empirical chaos expansion.

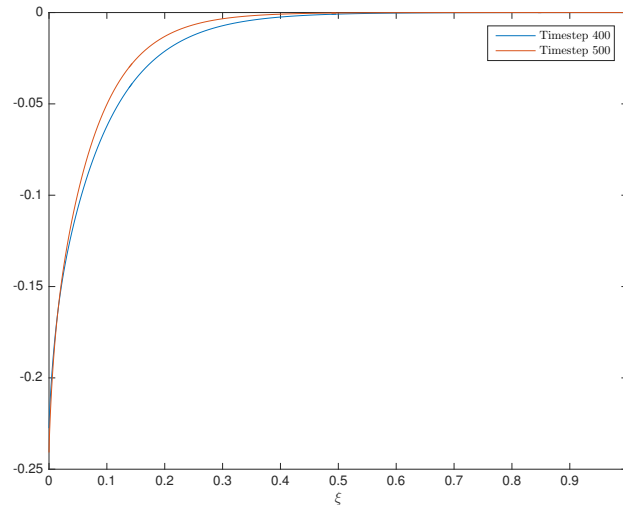


Figure 2.22: Evolution of the first basis function from POD for timesteps 400 and 500 in the solution to (2.14) using empirical chaos expansion.

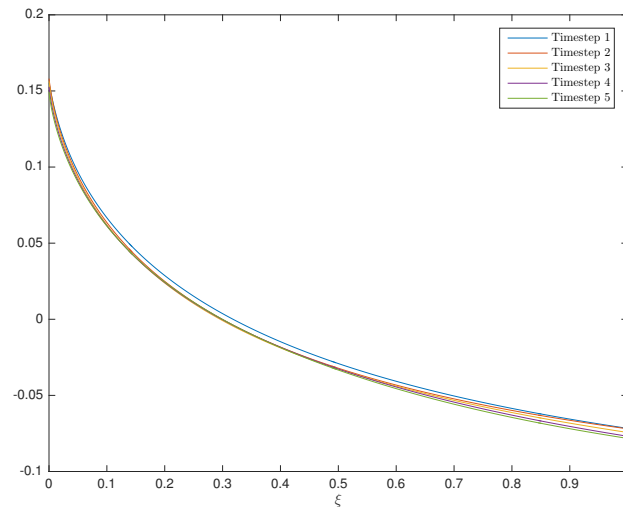


Figure 2.23: Evolution of the second basis function from POD for the first five timesteps in the solution to (2.14) using empirical chaos expansion.

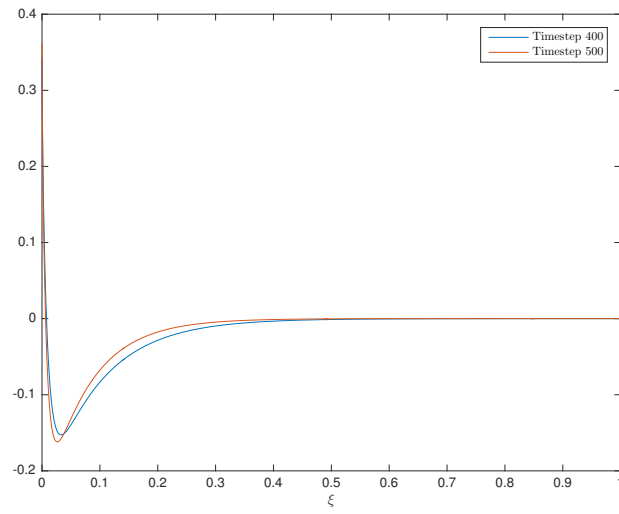


Figure 2.24: Evolution of the second basis function from POD for timesteps 400 and 500 in the solution to (2.14) using empirical chaos expansion.

Just as with the wave equation, there is a marked drop-off in the magnitudes of the singular values from POD, which provides a very natural way to automatically choose the number of empirical basis functions at every timestep (see figure 2.25). Unlike the wave equation, the largest singular values from POD for the diffusion equation do not seem to cross, which makes it easier to track the evolution of individual basis functions (see figure 2.26).

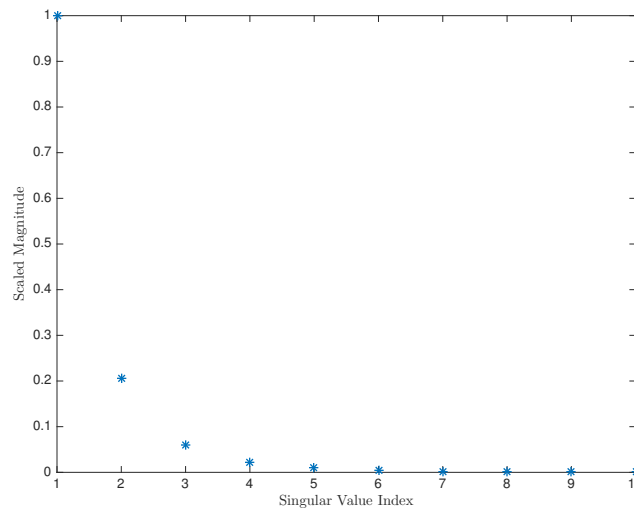


Figure 2.25: Singular values from POD for timestep 10 when performing empirical chaos expansion to solve (2.14). Singular values are scaled so that the maximum singular value has magnitude 1.

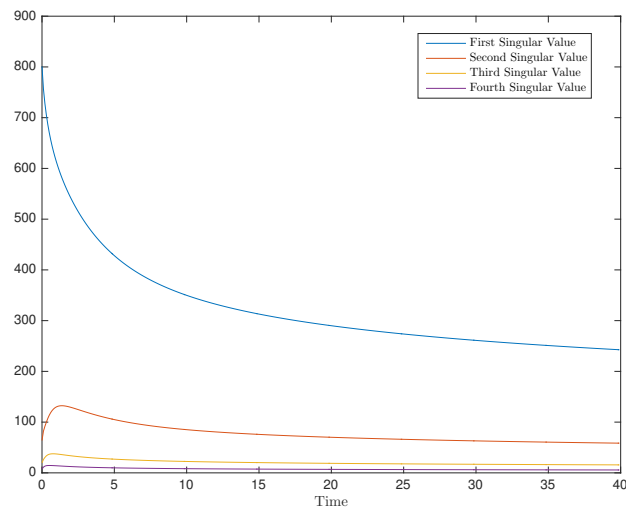


Figure 2.26: Evolution of the magnitude of the first four singular values from POD in the solution to (2.2) using empirical chaos expansion.

2.5 Advection-Reaction Equation

In the previous sections, the gPC method outperforms the empirical chaos expansion even though it uses a far larger polynomial basis for the wave equation. There are two reasons for this. First, the stochastic Galerkin PDE systems were relatively straightforward to solve, even when they were high-dimensional. Additionally, the polynomial chaos expansions rely on pre-computing the A matrix in Equation 2.5 since it always uses the fixed set of Legendre polynomials as its orthogonal basis. This accounts for much of the efficiency observed in previous sections.

If we consider the advection-reaction equation:

$$u_t(x, t, \xi) = \xi u_x(x, t, \xi) + f(x, u),$$

where the function $f(x, u)$ is nonlinear and not a simple polynomial expression such as u^2 , then the resulting stochastic Galerkin system becomes more difficult to evaluate than the original system, as we will see in subsequent sections. If the order of the polynomial basis becomes large, then the stochastic Galerkin system for standard polynomial chaos quickly becomes computationally intractable. In this instance, the benefit of the empirical chaos expansion becomes evident. Since it limits the number of basis functions to a small number, the stochastic Galerkin system remains small at each timestep and it remains relatively inexpensive to solve even when the final integration time is large.

In the subsequent sections we consider the model advection-reaction SPDE:

$$u_t(x, t, \xi) = \xi u_x(x, t, \xi) + 0.1 |u|^{\frac{1}{2}}, \quad 0 \leq x \leq 2\pi, \quad t \geq 0 \quad (2.20)$$

$$u(x, 0, \xi) = \cos(x) + \frac{3}{2}, \quad (2.21)$$

with periodic boundary conditions and where ξ is uniformly distributed on $[-1, 1]$. Note that over the space for this problem:

$$\langle f, g \rangle := \int_{-1}^1 f(\xi)g(\xi)(1/2)d\xi$$

$$E[f] := \int_{-1}^1 f(\xi)(1/2)d\xi$$

We do not have an analytic solution for this SPDE, so we run Monte Carlo simulations until they converge in order to check the accuracy of the solutions computed from the polynomial chaos expansion and the empirical chaos expansion.

2.5.1 Polynomial Chaos Expansion

If we use gPC then we choose the normalized Legendre polynomials to be our basis functions. Letting $\{L^i\}$ be the i^{th} normalized Legendre polynomial, we can perform a stochastic Galerkin method as in section 1.1.1. The true solution to Equation 2.20 is expanded as:

$$u(x, t, \xi) = \sum_{i=1}^{\infty} \hat{u}^i(x, t) L^i(\xi).$$

Substituting this into equation 2.20, then multiplying by a test function $L^j(\xi)$, and taking the expectation of both sides gives:

$$\begin{aligned}
& \sum_{i=1}^{\infty} \hat{u}_t^i(x,t) L^i(\xi) = \xi \sum_{i=1}^{\infty} \hat{u}_x^i(x,t) L^i(\xi) + 0.1 \left| \sum_{i=1}^{\infty} \hat{u}_x^i(x,t) L^i(\xi) \right|^{\frac{1}{2}} \\
\implies E \left[\sum_{i=1}^{\infty} \hat{u}_t^i(x,t) L^i(\xi) L^j(\xi) \right] &= E \left[\xi \sum_{i=1}^{\infty} \hat{u}_x^i(x,t) L^i(\xi) L^j(\xi) \right] \\
& \quad + 0.1 E \left[\left| \sum_{i=1}^{\infty} \hat{u}_x^i(x,t) L^i(\xi) \right|^{\frac{1}{2}} L^j(\xi) \right] \\
\implies \sum_{i=1}^{\infty} \hat{u}_t^i(x,t) E [L^i(\xi) L^j(\xi)] &= \sum_{i=1}^{\infty} \hat{u}_x^i(x,t) E [\xi L^i(\xi) L^j(\xi)] \\
& \quad + 0.1 E \left[\left| \sum_{i=1}^{\infty} \hat{u}_x^i(x,t) L^i(\xi) \right|^{\frac{1}{2}} L^j(\xi) \right] \\
\implies \hat{u}_t^j &= \sum_{i=1}^{\infty} \hat{u}_x^i(x,t) E [\xi L^i(\xi) L^j(\xi)] \\
& \quad + 0.1 E \left[\left| \sum_{i=1}^{\infty} \hat{u}_x^i(x,t) L^i(\xi) \right|^{\frac{1}{2}} L^j(\xi) \right]
\end{aligned}$$

Letting

$$\begin{aligned}
A_{ji} &= E [\xi L_j L_i] \\
\hat{f}_j &= 0.1 E \left[\left| \sum_{i=1}^{\infty} \hat{u}_x^i(x,t) L^i(\xi) \right|^{\frac{1}{2}} L^j(\xi) \right] \\
\hat{u} &= \begin{pmatrix} \hat{u}^1(x,t) \\ \hat{u}^2(x,t) \\ \vdots \end{pmatrix}
\end{aligned}$$

simplifies the previous system to:

$$\hat{u}_t = A\hat{u}_x + \hat{f}. \quad (2.22)$$

Since the initial condition is deterministic,

$$\hat{u}^1(x, 0) = \cos(x) + \frac{3}{2}, \text{ and } \hat{u}^i(x, 0) = 0 \text{ for } i > 1.$$

We can then truncate the infinite system at some finite value N and solve the resulting deterministic system of PDEs.

The stochastic Galerkin system in equation (2.22) is more difficult to solve than the original SPDE system in Equation 2.20 due to the nonlinear \hat{f} term. The expectations inside cannot be pre-computed since they depend on the values of the \hat{u}^i coefficients at each point in space and in time. We can compute \hat{f} at each timestep with numerical quadrature, but it requires us to compute N expectations, where N is the number of polynomial basis functions. If we solve the stochastic Galerkin system using a method of lines discretization or some other finite difference based approach, we will need to compute N expectations for every timestep of the numerical solver. This becomes very expensive as N grows. In order to compute the expectations in the \hat{f} vector we use a composite trapezoidal quadrature method that uses 300 Chebyshev nodes on the interval $[-1, 1]$. The Legendre polynomials and the A matrix in equation (2.22) are pre-computed using symbolic arithmetic to avoid any error.

To examine the accuracy of the solution we can look at the mean square expectation at $x = 0$, computed from the numerical solution to the stochastic Galerkin system in equation (2.22). Figures 2.27, 2.28, 2.29, and 2.30 show the numerical gPC results compared to exact solutions generated by performing 100,000 Monte Carlo iterations. For the short final time of 10 in figure 2.27, a small number of polynomial basis functions performs well.

When integrating out to a final time of 100 in figures 2.28, 2.29, and 2.30, however, a much higher number of basis functions are required for the solution to be accurate. To numerically solve the differential equations, we use a method of lines discretization coupled with a fourth order Runge-Kutta integrator (*ode45* in Matlab).

We include results up to polynomial order 40, but for higher orders the stochastic Galerkin system became unstable. It is not clear at this point whether the instability was due to the numerical method we used to solve the PDE system, or if the underlying system itself became unstable for higher polynomial orders.

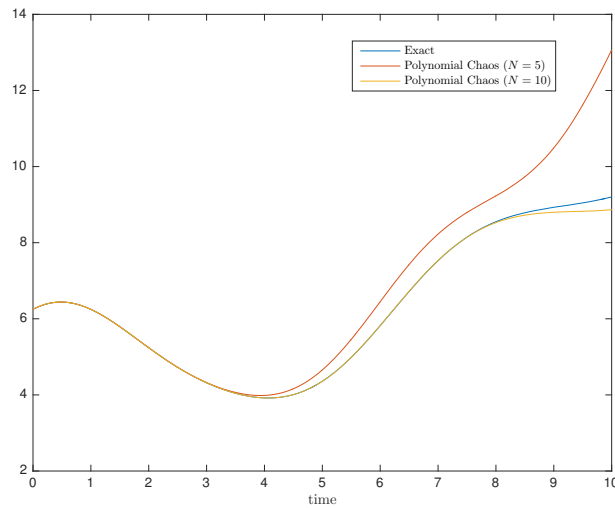


Figure 2.27: Mean square expectation $x = 0$ of solution to (2.20), computed using gPC with stochastic Galerkin. N is the total number of polynomial basis functions that were used. The exact solution was generated by performing Monte Carlo sampling with 100,000 realizations.

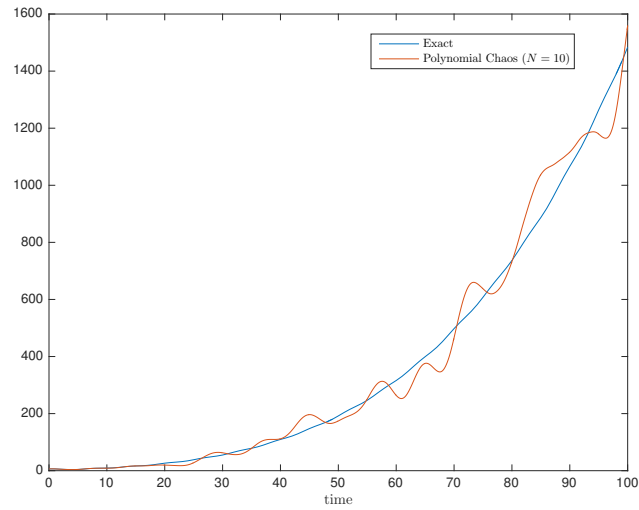


Figure 2.28: Mean square expectation $x = 0$ of solution to (2.20), computed using gPC with stochastic Galerkin, using Legendre polynomials up to order 10. The exact solution was generated by performing Monte Carlo sampling with 100,000 realizations.

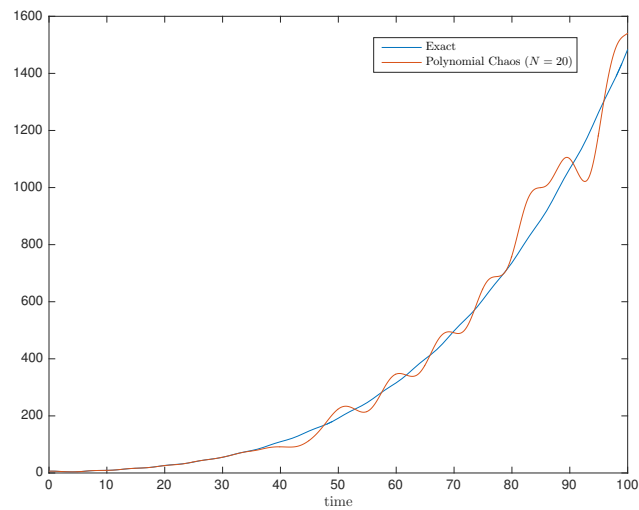


Figure 2.29: Mean square expectation $x = 0$ of solution to (2.20), computed using gPC with stochastic Galerkin, using Legendre polynomials up to order 20. The exact solution was generated by performing Monte Carlo sampling with 100,000 realizations.

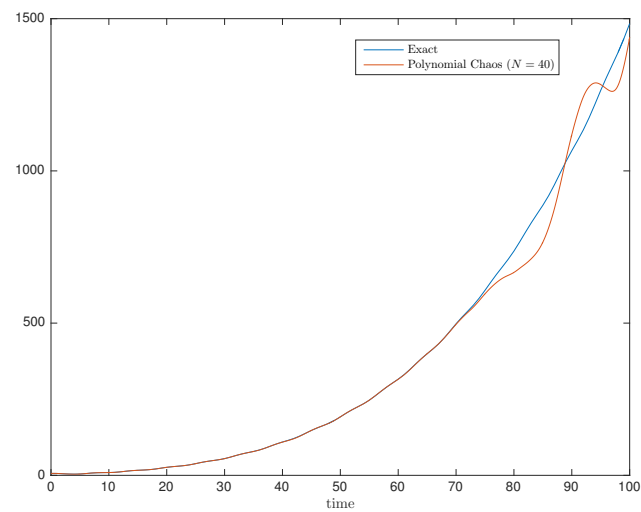


Figure 2.30: Mean square expectation $x = 0$ of solution to (2.20), computed using gPC with stochastic Galerkin, using Legendre polynomials up to order 40. The exact solution was generated by performing Monte Carlo sampling with 100,000 realizations.

2.5.2 Empirical Chaos Expansion

If we let $\{\Psi^i(\xi)\}_{i=1}^N$ be the set of empirical basis functions, we can perform a stochastic Galerkin method as in section 1.1.1. The true solution to equation (2.20) is approximated as:

$$u(x, t, \xi) = \sum_{i=1}^N \hat{u}^i(x, t) \Psi^i(\xi).$$

Substituting this into equation (2.20), then multiplying by a test function $\Psi^j(\xi)$, and taking the expectation of both sides gives:

$$\begin{aligned} \sum_{i=1}^N \hat{u}_t^i(x, t) \Psi^i(\xi) &= \xi \sum_{i=1}^N \hat{u}_x^i(x, t) \Psi^i(\xi) + 0.1 \left| \sum_{i=1}^N \hat{u}_x^i(x, t) \Psi^i(\xi) \right|^{\frac{1}{2}} \\ \implies E \left[\sum_{i=1}^N \hat{u}_t^i(x, t) \Psi^i(\xi) \Psi^j(\xi) \right] &= E \left[\xi \sum_{i=1}^N \hat{u}_x^i(x, t) \Psi^i(\xi) \Psi^j(\xi) \right] \\ &\quad + 0.1 E \left[\left| \sum_{i=1}^N \hat{u}_x^i(x, t) \Psi^i(\xi) \right|^{\frac{1}{2}} \Psi^j(\xi) \right] \\ \implies \sum_{i=1}^N \hat{u}_t^i(x, t) E [\Psi^i(\xi) \Psi^j(\xi)] &= \sum_{i=1}^N \hat{u}_x^i(x, t) E [\xi \Psi^i(\xi) \Psi^j(\xi)] \\ &\quad + 0.1 E \left[\left| \sum_{i=1}^N \hat{u}_x^i(x, t) \Psi^i(\xi) \right|^{\frac{1}{2}} \Psi^j(\xi) \right] \end{aligned}$$

Letting

$$\begin{aligned}
 A_{ji} &= E [\xi \Psi_j \Psi_i] \\
 M_{ji} &= E [\Psi_j \Psi_i] \\
 \hat{f}_j &= 0.1 E \left[\left| \sum_{i=1}^N \hat{u}_x^i(x,t) \Psi^i(\xi) \right|^{\frac{1}{2}} \Psi^j(\xi) \right] \\
 \hat{u} &= \begin{pmatrix} \hat{u}^1(x,t) \\ \hat{u}^2(x,t) \\ \vdots \end{pmatrix}
 \end{aligned}$$

simplifies the previous system to:

$$M \hat{u}_t = A \hat{u}_x + \hat{f}. \quad (2.23)$$

We can follow the method in section 2.1 to construct empirical basis functions over small time intervals by sampling trajectories and applying POD, and then using those empirical basis functions to compute the M and A matrices and the \hat{f} vector in equation (2.23). We use 300 Chebyshev nodes on the interval $[-1, 1]$ as the set of values for ξ . We compute the intermediate expectations of the \hat{f} vector using the same composite trapezoidal quadrature rule that we used for gPC in order to have a fair comparison of the running times. We also use the same method of lines discretization coupled with a fourth order Runge-Kutta integrator (*ode45* in Matlab) to numerically solve the stochastic Galerkin system.

To examine the accuracy of the solution we look at the mean square expectation at $x = 0$, computed from the numerical solution to the stochastic Galerkin system in equation (2.23). Figures 2.31 and 2.32 show the numerical empirical chaos expansion results compared to

exact solutions generated by performing 100,000 Monte Carlo iterations. The sampling points were 300 Chebyshev nodes on the interval $[-1, 1]$

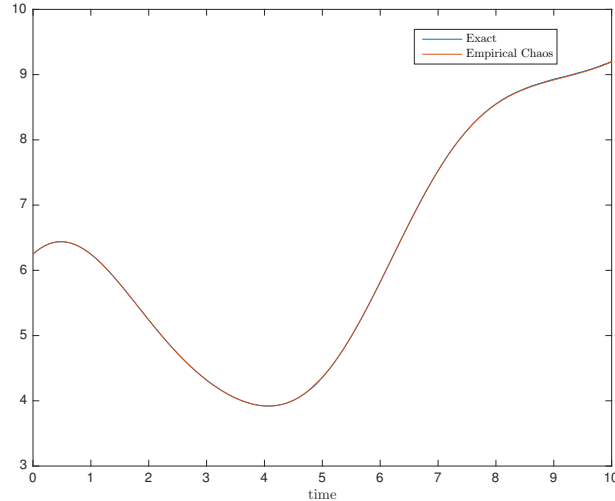


Figure 2.31: Mean square expectation at $x = 0$ of the solution to (2.20) computed using an empirical chaos expansion with stochastic Galerkin. The timestep size was 2, the basis functions were computed by solving the deterministic equation at 300 Chebyshev nodes on the interval $[-1, 1]$, and the maximum number of basis functions used at a single timestep was 33.

Just as in previous sections, we choose the number of empirical basis functions by examining the magnitude of the scaled singular values from POD. The overall number needed is higher for this SPDE than the previous ones, but there is still the same marked drop-off in the magnitude of the scaled singular values. Figure 2.33 shows the magnitude of the singular values from the POD that was computed at $t = 6$. There is a marked drop in the magnitude from the first to the second singular value, and by the sixth singular value the scaled magnitude has gotten quite small.

The initial mean square expectation fluctuates due to the presence of the advection term ξu_x , but the reaction term $|u|^{\frac{1}{2}}$ dominates the behavior out at long times. This can be seen when comparing the mean square expectations in Figures 2.31 and 2.32. In Figure 2.31

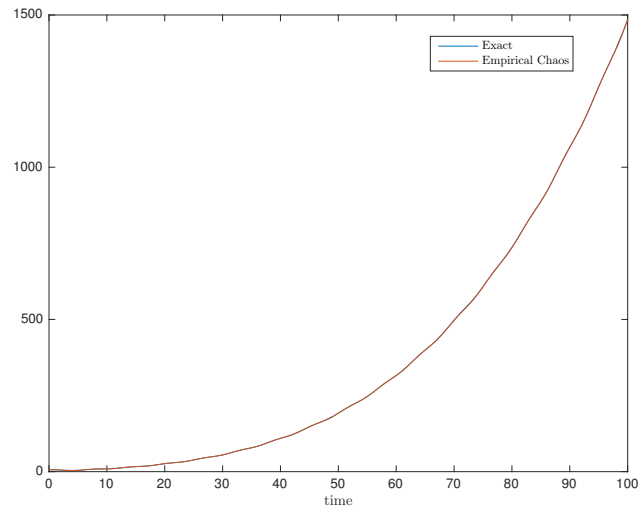


Figure 2.32: Mean square expectation at $x = 0$ of the solution to (2.20) computed using an empirical chaos expansion with stochastic Galerkin. The timestep size was 2, the basis functions were computed by solving the deterministic equation at 300 Chebyshev nodes on the interval $[-1, 1]$, and the maximum number of basis functions used at a single timestep was 33.

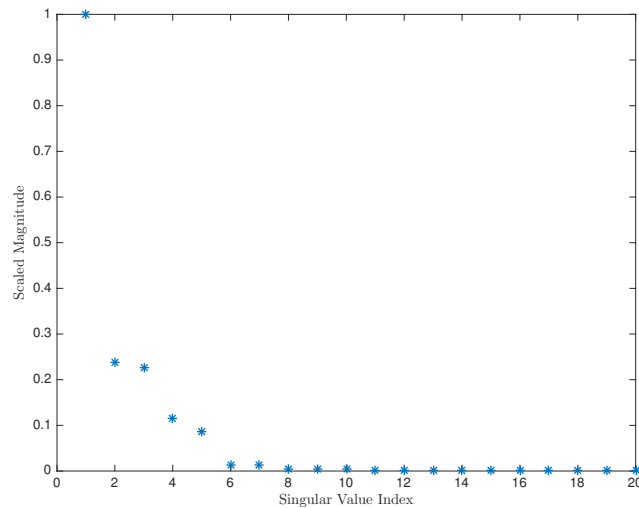


Figure 2.33: Singular values from POD for the third timestep when performing empirical chaos expansion to solve (2.20). Singular values are scaled so that the maximum singular value has magnitude 1.

the solution is integrated to final time 10, and there is a noticeable wave-like movement of the mean square expectation in time. In Figure 2.32, however, the solution is integrated to final

time 100, and though the wave-like motion is still present in the mean square expectation, it has been dominated by the total growth of the solution u due to the reaction term. The singular values from POD also reflect this behavior. In Figure 2.34, we plot the magnitudes of the first two singular values that were generated at each timestep of the empirical chaos expansion solver. As the time grows, the first singular value becomes completely dominant, which reflects the fact that the reaction term dominates the behavior at later times.

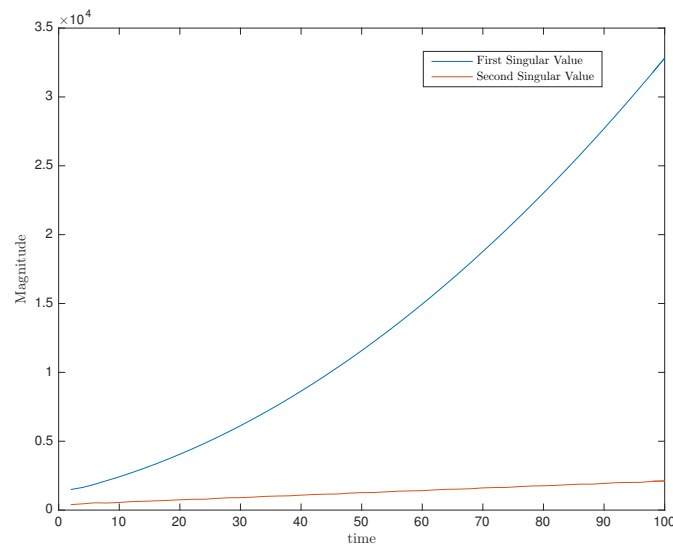


Figure 2.34: Evolution of the magnitude of the first two singular values from POD in the solution to (2.20) using empirical chaos expansion.

2.5.3 Running Time

Since the number of empirical basis functions does not dramatically grow as the number of timesteps increases, the execution time for the empirical expansion method scales linearly with the final integration time (see figure 2.10). We can also note the superlinear growth of the running time for gPC as a function of the final integration time. Although gPC outperforms the empirical chaos expansion for the smaller integration times, it is

outperformed by the empirical chaos expansion for final integration times larger than about 34.

We do not include the cost to pre-compute the A matrix in Equation 2.22, nor the cost to generate the required number of Legendre polynomials for the polynomial chaos expansion. As mentioned previously, however, the entries of the \hat{f} matrix cannot be pre-computed, and the computational effort to compute these entries grows as $O(N^2)$, where N is the number of basis functions. As the final simulation time increases, we must increase the number of polynomial basis functions in order to accurately solve the system, and this causes the computational cost to grow superlinearly.

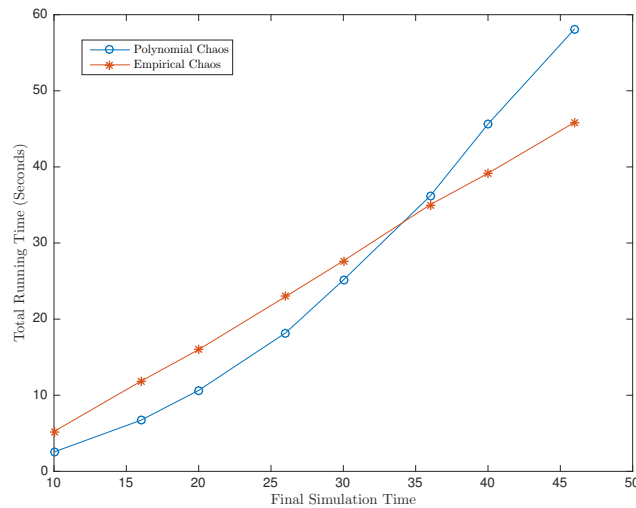


Figure 2.35: Comparison of total running times for solutions of (2.20) computed to the same accuracy using empirical chaos expansion and gPC with stochastic Galerkin.

2.5.4 Basis Function Evolution

To monitor the evolution of the basis functions, we set the timestep size for the advection-reaction equation (2.20) to 0.1, and examine the values of the basis functions

over time. Figure 2.36 shows the values of the basis function that corresponds to the largest singular value from POD for the first 5 timesteps (each of size 0.1).

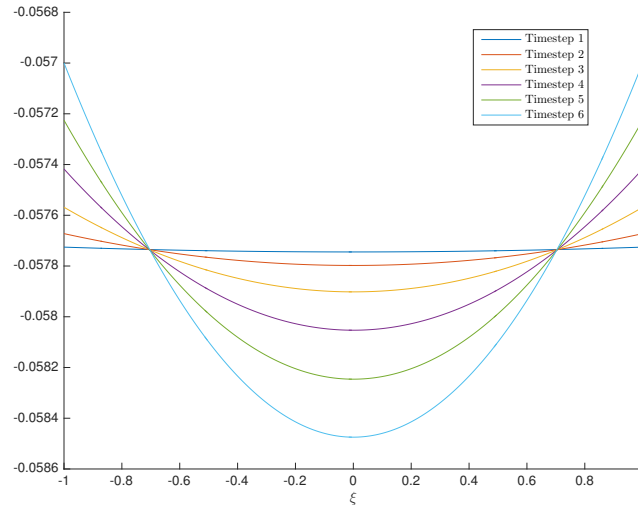


Figure 2.36: Evolution of the first basis function from POD for the first five timesteps in the solution to (2.20) using empirical chaos expansion.

The first basis function evolves smoothly over time, and since there are no crossings between the first and second singular value, it is straightforward to track the evolution of this basis function through time. We can also look at the second basis function evolution in Figures 2.37 and 2.38. The second basis function changes slowly, and thus in Figure 2.37, which shows the evolution of the second basis function over the first 3 timesteps, the functions are visually indistinguishable. If we instead look at Figure 2.38, which shows the evolution of the second basis function over the first 30 timesteps, we can visually observe its smooth evolution. The first and third singular values have multiple crossings, as we can see in Figure 2.39, which means that the second basis function will be associated either with the second or third singular value at different times.

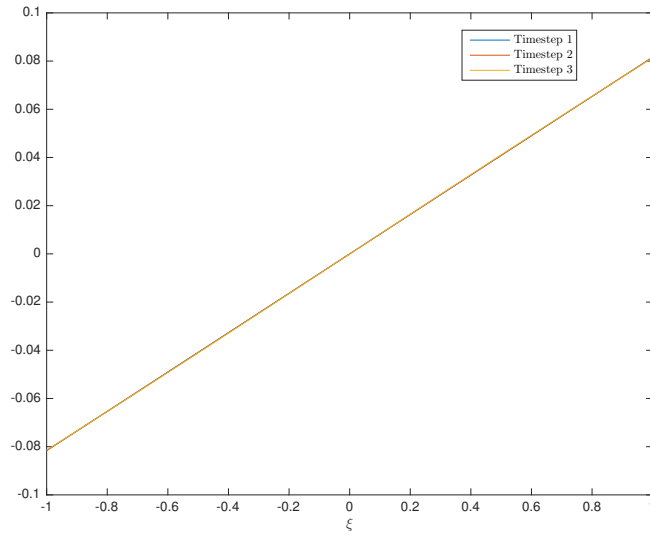


Figure 2.37: Evolution of the second basis function from POD for the first three timesteps in the solution to (2.20) using empirical chaos expansion.

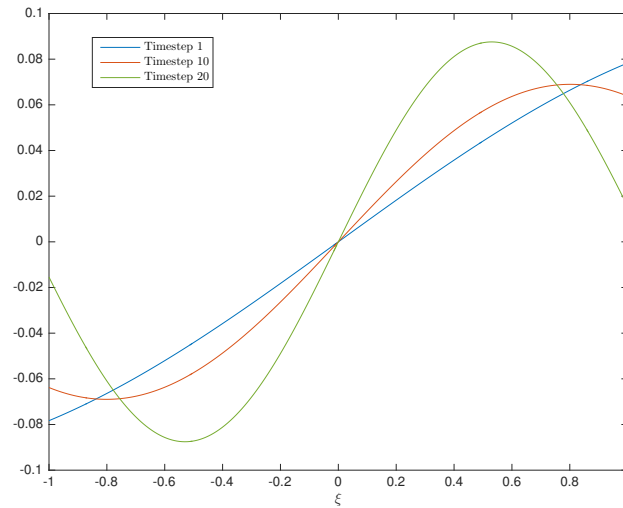


Figure 2.38: Evolution of the second basis function from POD for the first 30 timesteps in the solution to (2.20) using empirical chaos expansion.

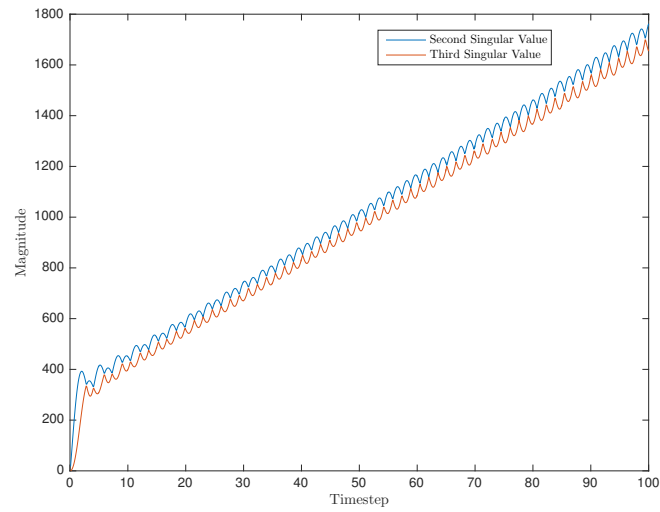


Figure 2.39: Evolution of the magnitude of the second and third singular values from POD in the solution to (2.20) using empirical chaos expansion.

2.6 Reaction-Diffusion Equation

In this section we consider a model reaction-diffusion equation:

$$u_t(x, t, \xi) = \xi u_{xx}(x, t, \xi) + 0.1 \left(u - |u|^{\frac{3}{2}} \right), \quad 0 \leq x \leq 6, \quad t \geq 0 \quad (2.24)$$

$$u(x, 0, \xi) = 3I_{[2,4]}, \quad (2.25)$$

with homogeneous Dirichlet boundary conditions, i.e.

$$u(0, t, \xi) = u(6, t, \xi) = 0.$$

$I_{[a,b]}$ is the indicator function on the interval $[a, b]$ and ξ is a random variable uniformly distributed on $[0, 1]$. Since the solution to the reaction-diffusion equation with these initial conditions will eventually converge, the gPC expansion can achieve high accuracy at long integration times without needing to include more and more basis functions. Similarly, the empirical chaos expansion does quite well with the first set of empirical basis functions that it generates, and does not need to update them by resampling solutions at later times. However, the inclusion of the nonlinear $|u|^{\frac{3}{2}}$ term greatly increases the cost of solving the stochastic Galerkin system compared to the system generated by the diffusion equation in Section 2.4.

Note that over the space for this problem:

$$\langle f, g \rangle := \int_0^1 f(\xi)g(\xi)d\xi$$

$$E[f] := \int_0^1 f(\xi)d\xi$$

We do not have an analytic solution for this SPDE, so we run Monte Carlo simulations until they converge in order to check the accuracy of the solutions computed from the polynomial chaos expansion and the empirical chaos expansion.

2.6.1 Polynomial Chaos Expansion

If we use gPC then we use normalized Legendre polynomials to be our basis functions. The domain of the random space is the interval $[0, 1]$, so we must use shifted Legendre polynomials, since the standard Legendre polynomials are orthogonal over the interval $[-1, 1]$. Letting $\{L^i\}$ be the i^{th} normalized shifted Legendre polynomial, we can perform a stochastic Galerkin method as in section 1.1.1. The true solution to equation (2.24) is expanded as:

$$u(x, t, \xi) = \sum_{i=1}^{\infty} \hat{u}^i(x, t) L^i(\xi).$$

Substituting this into equation (2.24), then multiplying by a test function $L^j(\xi)$, and taking the expectation of both sides gives:

$$\begin{aligned}
& \sum_{i=1}^{\infty} \hat{u}_t^i(x,t) L^i(\xi) = \xi \sum_{i=1}^{\infty} \hat{u}_{xx}^i(x,t) L^i(\xi) \\
& \quad + 0.1 \left(\sum_{i=1}^{\infty} \hat{u}^i(x,t) L^i(\xi) - \left| \sum_{i=1}^{\infty} \hat{u}^i(x,t) L^i(\xi) \right|^{\frac{3}{2}} \right) \\
\implies E \left[\sum_{i=1}^{\infty} \hat{u}_t^i(x,t) L^i(\xi) L^j(\xi) \right] &= E \left[\xi \sum_{i=1}^{\infty} \hat{u}_{xx}^i(x,t) L^i(\xi) L^j(\xi) \right] \\
& \quad + 0.1 E \left[\sum_{i=1}^{\infty} \hat{u}^i(x,t) L^i(\xi) - \left| \sum_{i=1}^{\infty} \hat{u}^i(x,t) L^i(\xi) \right|^{\frac{3}{2}} L^j(\xi) \right] \\
\implies \sum_{i=1}^{\infty} \hat{u}_t^i(x,t) E [L^i(\xi) L^j(\xi)] &= \sum_{i=1}^{\infty} \hat{u}_{xx}^i(x,t) E [\xi L^i(\xi) L^j(\xi)] \\
& \quad + 0.1 \left(\sum_{i=1}^{\infty} \hat{u}^i(x,t) E [L^i(\xi) L^j(\xi)] \right. \\
& \quad \left. - E \left[\left| \sum_{i=1}^{\infty} \hat{u}_x^i(x,t) L^i(\xi) \right|^{\frac{3}{2}} L^j(\xi) \right] \right) \\
\implies \hat{u}_t^j &= \sum_{i=1}^{\infty} \hat{u}_{xx}^i(x,t) E [\xi L^i(\xi) L^j(\xi)] \\
& \quad + 0.1 \hat{u}^j - 0.1 E \left[\left| \sum_{i=1}^{\infty} \hat{u}_x^i(x,t) L^i(\xi) \right|^{\frac{3}{2}} L^j(\xi) \right]
\end{aligned}$$

Letting

$$A_{ji} = E [\xi L_j L_i]$$

$$\hat{f}_j = 0.1 E \left[\left| \sum_{i=1}^{\infty} \hat{u}_x^i(x,t) L^i(\xi) \right|^{\frac{3}{2}} L^j(\xi) \right]$$

$$\hat{u} = \begin{pmatrix} \hat{u}^1(x,t) \\ \hat{u}^2(x,t) \\ \vdots \end{pmatrix}$$

simplifies the previous system to:

$$\hat{u}_t = A \hat{u}_x + \hat{u} - \hat{f}. \quad (2.26)$$

Since the initial condition is deterministic,

$$\hat{u}^1(x,0) = 3I_{[2,4]}, \text{ and } \hat{u}^i(x,0) = 0 \text{ for } i > 1.$$

We can then truncate the infinite system at some finite value N and solve the resulting deterministic system of PDEs.

The stochastic Galerkin system in equation (2.26) is more difficult to solve than the original SPDE system in equation (2.24) due to the nonlinear \hat{f} term. The expectations inside cannot be pre-computed since they depend on the values of the \hat{u}^i coefficients at each point in space and in time. We can compute \hat{f} at each timestep with numerical quadrature, but it requires us to compute N expectations, where N is the number of polynomial basis functions. If we solve the stochastic Galerkin system using a method of lines discretization or some other finite difference based approach, we will need to compute N expectations

for every timestep of the numerical solver. In order to compute the expectations in the \hat{f} vector we use a composite trapezoidal quadrature method that uses 200 Chebyshev nodes on the interval $[0.001, 1]$. The Legendre polynomials and the A matrix in equation (2.26) are pre-computed using symbolic arithmetic to avoid any error. Unlike the reaction-advection system in section 2.5, however, the solutions to this system will converge, which means that we do not have to constantly increase the number of polynomial basis functions as we increase the final integration time.

To solve the original SPDE in equation (2.24) for fixed values of ξ , we use a method of lines discretization coupled with an multistep implicit ODE solver (*ode15s* in Matlab). For the stochastic Galerkin system, however, the nonlinear coupling requires a different approach to efficiently solve. We implement the IIF2 integrator from [55, 9], which is a semi-implicit integration technique for nonlinear reaction-diffusion systems. It uses the method of lines to convert the PDE into a system of ODES, treats the diffusion component exactly with an exponential integrator, and then treats the reaction component implicitly to construct a nonlinear system. The nonlinear system is then solved with a fixed point iteration at each timestep.

To examine the accuracy of the solution we can look at the mean square expectation at $x = 1$, computed from the numerical solution to the stochastic Galerkin system in equation (2.26). Figures 2.40, 2.41, and 2.42 show the numerical gPC results compared to exact solutions generated by performing 100,000 Monte Carlo iterations. From the results we can see that it takes about 10 polynomial basis functions to accurately capture the mean square expectation out to time 10, and we only need to increase to 15 polynomial basis functions to accurately capture the mean square expectation out to time 100.

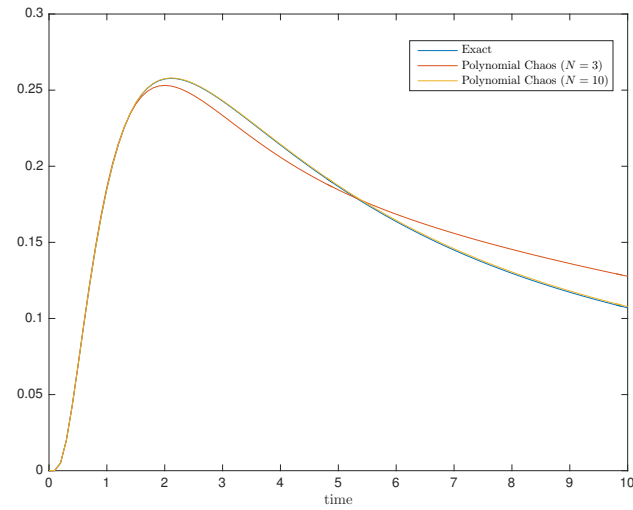


Figure 2.40: Mean square expectation $x = 1$ of solution to (2.24), computed using gPC with stochastic Galerkin, using Legendre polynomials of varying order N . The exact solution was generated by performing Monte Carlo sampling with 100,000 realizations.

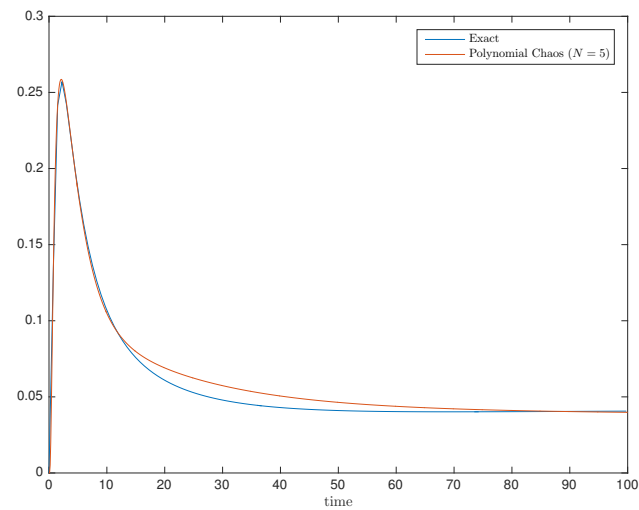


Figure 2.41: Mean square expectation $x = 1$ of solution to (2.24), computed using gPC with stochastic Galerkin, using Legendre polynomials of order 5. The exact solution was generated by performing Monte Carlo sampling with 100,000 realizations.

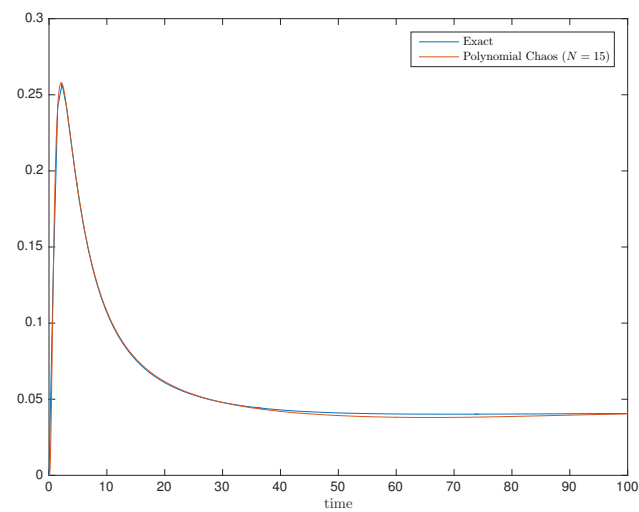


Figure 2.42: Mean square expectation $x = 1$ of solution to (2.24), computed using gPC with stochastic Galerkin, using Legendre polynomials of order 10. The exact solution was generated by performing Monte Carlo sampling with 100,000 realizations.

2.6.2 Empirical Chaos Expansion

If we let $\{\Psi^i(\xi)\}_{i=1}^N$ be the set of empirical basis functions, we can perform a stochastic Galerkin method as in section 1.1.1. This is essentially the same derivation as section 2.6.1, except that the Ψ^i coefficients are not orthogonal. The true solution to equation (2.24) is approximated as:

$$u(x, t, \xi) = \sum_{i=1}^N \hat{u}^i(x, t) \Psi^i(\xi).$$

Substituting this into equation (2.24), then multiplying by a test function $\Psi^j(\xi)$, and taking the expectation of both sides gives:

$$\begin{aligned}
\sum_{i=1}^N \hat{u}_t^i(x,t) \Psi^i(\xi) &= \xi \sum_{i=1}^N \hat{u}_{xx}^i(x,t) \Psi^i(\xi) \\
&\quad + 0.1 \left(\sum_{i=1}^N \hat{u}^i(x,t) \Psi^i(\xi) - \left| \sum_{i=1}^N \hat{u}^i(x,t) \Psi^i(\xi) \right|^{\frac{3}{2}} \right) \\
\implies E \left[\sum_{i=1}^N \hat{u}_t^i(x,t) \Psi^i(\xi) \Psi^j(\xi) \right] &= E \left[\xi \sum_{i=1}^N \hat{u}_x^i(x,t) \Psi^i(\xi) \Psi^j(\xi) \right] \\
&\quad + 0.1 \left(E \left[\sum_{i=1}^N \hat{u}_x^i(x,t) \Psi^i(\xi) \Psi^j(\xi) \right] \right. \\
&\quad \left. - \left| \sum_{i=1}^N \hat{u}_x^i(x,t) \Psi^i(\xi) \right|^{\frac{3}{2}} \Psi^j(\xi) \right) \\
\implies \sum_{i=1}^N \hat{u}_t^i(x,t) E [\Psi^i(\xi) \Psi^j(\xi)] &= \sum_{i=1}^N \hat{u}_x^i(x,t) E [\xi \Psi^i(\xi) \Psi^j(\xi)] \\
&\quad + 0.1 \left(\sum_{i=1}^N \hat{u}^i(x,t) E [\Psi^i(\xi) \Psi^j(\xi)] \right. \\
&\quad \left. - E \left[\left| \sum_{i=1}^N \hat{u}_x^i(x,t) \Psi^i(\xi) \right|^{\frac{3}{2}} \Psi^j(\xi) \right] \right)
\end{aligned}$$

Letting

$$\begin{aligned}
 A_{ji} &= E [\xi \Psi_j \Psi_i] \\
 M_{ji} &= E [\Psi_j \Psi_i] \\
 \hat{f}_j &= 0.1 E \left[\left| \sum_{i=1}^N \hat{u}_x^i(x, t) \Psi^i(\xi) \right|^{\frac{3}{2}} \Psi^j(\xi) \right] \\
 \hat{u} &= \begin{pmatrix} \hat{u}^1(x, t) \\ \hat{u}^2(x, t) \\ \vdots \end{pmatrix}
 \end{aligned}$$

simplifies the previous system to:

$$M \hat{u}_t = A \hat{u}_x + M \hat{u} - \hat{f}. \quad (2.27)$$

We can follow the method in section 2.1 to construct empirical basis functions by sampling trajectories and applying POD, and then using those empirical basis functions to compute the M and A matrices and the \hat{f} vector in Equation 2.27. We use 200 Chebyshev nodes on the interval $[0.001, 1]$ as the set of values for ξ . We compute the intermediate expectations of the \hat{f} vector using the same composite trapezoidal quadrature rule that we used for standard polynomial chaos in order to have a fair comparison of the running times. To solve this system we generate the empirical basis functions by sampling the solution over a small time interval (in this case from $t = 0$ to $t = 1$) and we then use those basis functions without updating them for the entire time interval. This produces accurate solutions since the reaction-diffusion equation eventually converges, and we do not need to resample trajectories at later time intervals.

To solve the stochastic Galerkin system we use the same IIF2 semi-implicit integrator described in the previous section [55, 9].

To examine the accuracy of the solution we can look at the mean square expectation at $x = 1$, computed from the numerical solution to the stochastic Galerkin system in equation (2.27). Figures 2.43 and 2.44 show the numerical empirical chaos expansion results compared to exact solutions generated by performing 100,000 Monte Carlo iterations. The sampling points were 200 Chebyshev nodes on the interval $[0.001, 1]$.

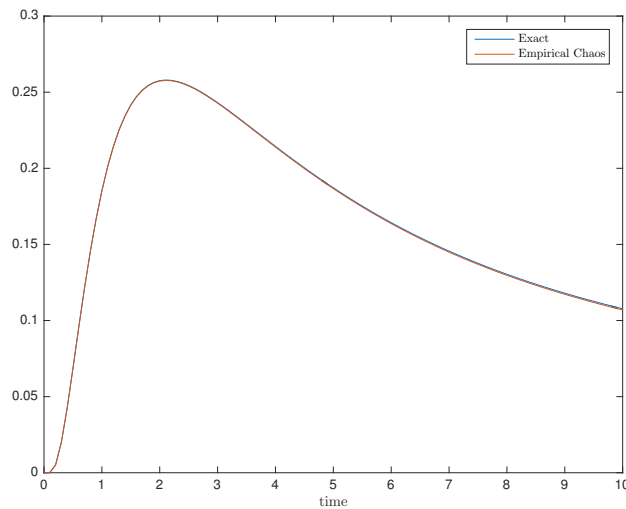


Figure 2.43: Mean Square Expectation $x = 1$ of the solution to (2.24) computed using an empirical chaos expansion with stochastic Galerkin. The timestep of size was 2, the basis functions were computed by solving the deterministic equation at 200 Chebyshev nodes on the interval $[0.001, 1]$, and the number of basis functions was 12. The exact solution was generated by performing Monte Carlo sampling with 100,000 realizations.

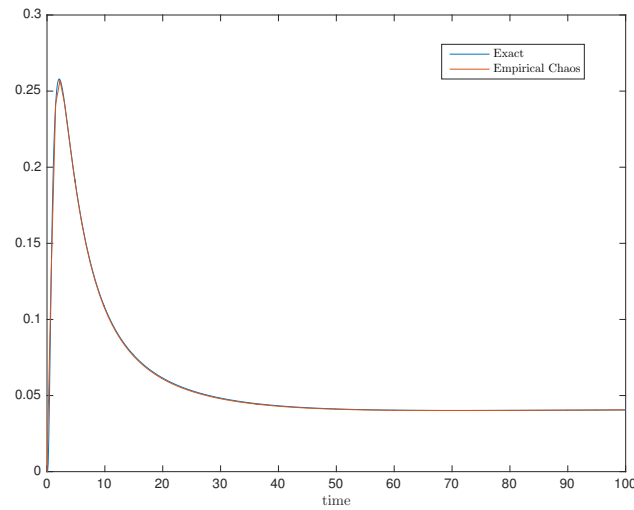


Figure 2.44: Mean Square Expectation $x = 1$ of the solution to (2.24) computed using an empirical chaos expansion with stochastic Galerkin. The timestep of size was 2, the basis functions were computed by solving the deterministic equation at 200 Chebyshev nodes on the interval $[0.001, 1]$, and the number of basis functions was 12. The exact solution was generated by performing Monte Carlo sampling with 100,000 realizations.

Just as in previous sections, we choose the number of empirical basis functions by examining the magnitude of the scaled singular values from POD. The difference is that we do not need to update the basis functions from their initial values by resampling trajectories. Figure 2.45 shows the magnitude of the singular values from the POD that was computed at $t = 0$. There is a marked drop in the magnitude from the first to the second singular value, and by the sixth singular value the scaled magnitude has gotten quite small.

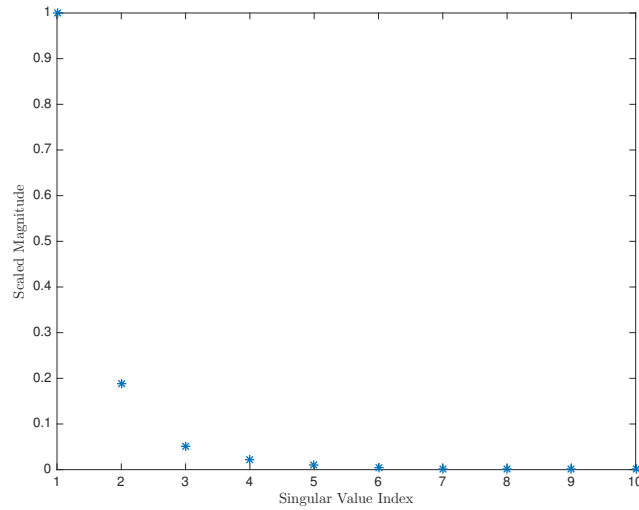


Figure 2.45: Singular values from POD for the time interval $t = 0$ to $t = 2$ when performing empirical chaos expansion to solve (2.24). Singular values are scaled so that the maximum singular value has magnitude 1.

2.6.3 Running Time

Since the number of empirical basis functions does not dramatically grow as the number of timesteps increases, the execution time for the empirical expansion method scales linearly with the final integration time (see figure 2.46). But since the solution to the reaction-diffusion equation converges, we also do not need to greatly increase the number of polynomial basis functions in standard polynomial chaos either, which leads to its computational time also scaling roughly linearly with the final integration time. The empirical chaos expansion outperforms standard polynomial chaos towards the end because it uses a total of 12 basis functions to accurately integrate to time 100, whereas polynomial chaos needs about 15 basis functions to accurately integrate to time 100.

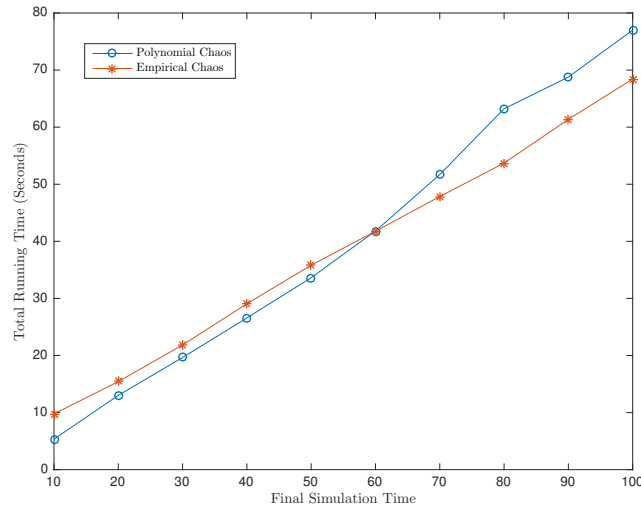


Figure 2.46: Comparison of total running times for solutions of (2.24) computed to the same accuracy using empirical chaos expansion and gPC with stochastic Galerkin.

2.6.4 Basis Function Evolution

We do not need to evolve the empirical basis in order to accurately compute the solution to the reaction-diffusion equation, so as in previous sections we fix the empirical basis functions to their initial values for computational efficiency. However, we can still evolve the basis functions and monitor their evolution. We set the timestep size for the reaction-diffusion equation (2.24) to 0.1, and examine the values of the basis functions over time. Figure 2.47 shows the values of the basis function that corresponds to the largest singular value from POD for the first 5 timesteps (each timestep is of size 0.1). The basis functions smoothly evolve, and in figure 2.48 we see that the empirical basis functions converge for later timesteps. The evolution of the first three singular values from POD are plotted in figure 2.49. Similar to the standard diffusion equation there are not any singular value crossings.

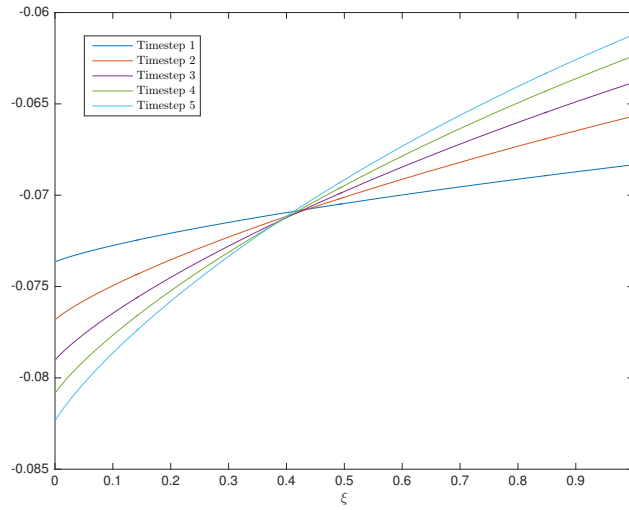


Figure 2.47: Evolution of the first basis function from POD for the first five timesteps in the solution to (2.24) using empirical chaos expansion.

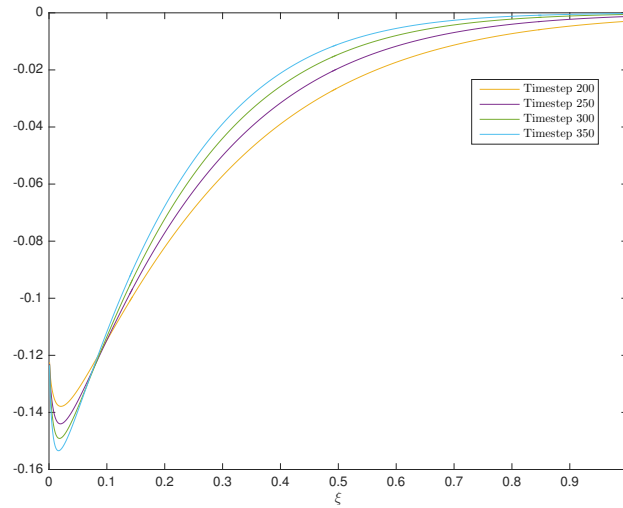


Figure 2.48: Evolution of the first basis function from POD for timesteps 200 to 350 in the solution to (2.24) using empirical chaos expansion.

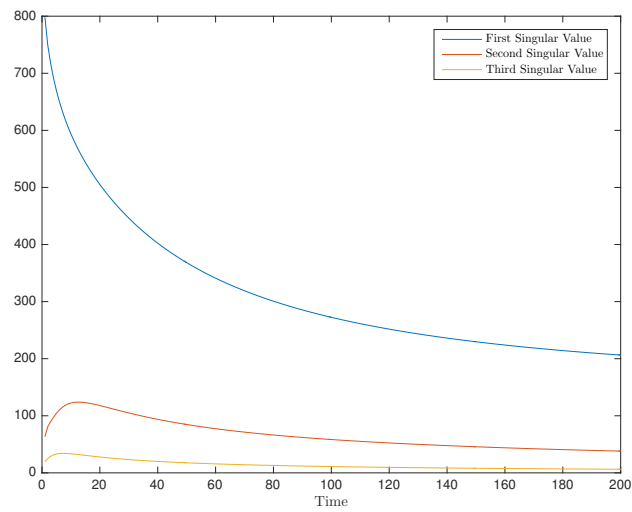


Figure 2.49: Evolution of the magnitude of the first three singular values from POD in the solution to (2.24) using empirical chaos expansion.

2.7 Acknowledgements

This work was conducted with Professor Melvin Leok at the University of California, San Diego and is currently being prepared for publication.

Chapter 3

Empirical Basis Evolution Operator

3.1 Empirical Basis Evolution

The smooth evolution of the empirical basis functions derived from POD suggests that the empirical basis functions can be computed through an analytic approach that involves the dynamics of the SPDE. In gPC methods we construct a basis that is orthogonal to the distribution of the random variables, then project the exact solution onto this basis and solve for the deterministic coefficients which are functions of space and time. If we wish to examine how the dynamics of a particular SPDE influence the basis functions for the random space, we can first take a specific basis—in this case one generated empirically—then project that basis onto a set of deterministic basis functions that only have a spatial dependence. After doing so the basis functions of the random variables will have a time dependence and we will have a DAE whose solution will evolve the basis functions in time.

For the model SPDEs that we analyze, we use the approximation:

$$u(x, t, \xi) \approx \sum_{i=1}^N \hat{u}^i(x) \Psi^i(\xi, t). \quad (3.1)$$

The values for $\Psi^i(\xi, t_0)$ will be the values of empirically generated basis functions, and the values of the $\hat{u}^i(x)$ basis functions will be the values $\hat{u}^i(x, t_0)$ of the deterministic coefficients from the empirical chaos expansion at time t_0 . In this new approximation the spatial component is fixed in time, but the random basis functions can vary.

In order to evolve the basis functions in time we can perform a Galerkin method, this time integrating over the spatial component. We multiply by a test function \hat{u}^j , then integrate over the spatial domain, R . If we work with the general model problem in Equation 1.1,

then this becomes:

$$\begin{aligned}
& \sum_{i=1}^N \hat{u}^i(x) \Psi^i(\xi, t) = L \left(\sum_{i=1}^N \hat{u}^i(x) \Psi^i(\xi, t), x, t, \xi \right) \\
\implies & \sum_{i=1}^N \hat{u}^i(x) \hat{u}^j(x) \Psi^i(\xi, t) = L \left(\sum_{i=1}^N \hat{u}^i(x) \Psi^i(\xi, t), x, t, \xi \right) \hat{u}^j(x) \\
\implies & \sum_{i=1}^N \int_R \hat{u}^i(x) \hat{u}^j(x) dx \Psi^i(\xi, t) = \int_R L \left(\sum_{i=1}^N \hat{u}^i(x) \Psi^i(\xi, t), x, t, \xi \right) \hat{u}^j(x) dx. \quad (3.2)
\end{aligned}$$

In practice this system can usually be simplified, but it depends on the form of the differential operator L . This provides a DAE whose solution will evolve the basis functions of the random variable in time. The general approach we follow is to generate a set of empirical basis functions over a short time interval using POD, solve the resulting stochastic Galerkin system, and use the final values of the $\hat{u}^i(x, t)$ coefficients as the fixed spatial basis in (3.2). We use the empirical basis functions as the initial values of the $\Psi^i(\xi, t)$ coefficients, and then solve (3.2) over a short time interval and use the final values of the $\Psi^i(\xi, t)$ coefficients as the new empirical basis for the next stochastic Galerkin step.

3.1.1 One Dimensional Wave Equation

If we substitute equation (3.1) into equation (2.2) for the one dimensional wave, then we get:

$$\begin{aligned} \sum_{i=1}^N \hat{u}^i(x) \Psi_t^i(\xi, t) &= \xi \sum_{i=1}^N \hat{u}_x^i(x) \Psi^i(\xi, t) \\ \implies \sum_{i=1}^N \hat{u}^i(x) \hat{u}^j(x) \Psi_t^i(\xi, t) &= \xi \sum_{i=1}^N \hat{u}_x^i(x) \hat{u}^j(x) \Psi^i(\xi, t) \\ \implies \sum_{i=1}^N \int_0^{2\pi} \hat{u}^i(x) \hat{u}^j(x) dx \Psi_t^i(\xi, t) &= \xi \sum_{i=1}^N \int_0^{2\pi} \hat{u}_x^i(x) \hat{u}^j(x) dx \Psi^i(\xi, t). \end{aligned}$$

Letting

$$\Psi = \begin{pmatrix} \Psi^1 \\ \Psi^2 \\ \vdots \\ \Psi^N \end{pmatrix} \quad \hat{u} = \begin{pmatrix} \hat{u}^1 \\ \hat{u}^2 \\ \vdots \\ \hat{u}^N \end{pmatrix} \quad A_{ji} = \int_0^{2\pi} \hat{u}^i(x) \hat{u}^j(x) dx \quad M_{ji} = \int_0^{2\pi} \hat{u}_x^i(x) \hat{u}^j(x) dx$$

implies:

$$A \Psi_t(\xi, t) = \xi M \Psi(\xi, t), \quad (3.3)$$

which is a DAE whose solution can be used to evolve basis functions in time. The general approach we use is to first generate a set of empirical basis functions up to a particular time t^* , using the method of section 2.1. Then the set of empirical basis functions is evolved in time by solving equation (3.3). In particular, if the matrix A is invertible, then the exact

solution to equation (3.3) is:

$$\Psi(\xi, t) = \exp [\xi A^{-1} M(t - t_0)] \Psi(\xi, t_0), \quad (3.4)$$

where \exp is the matrix exponential operator. The issue in practice is that A is singular. To deal with this we can decompose the full system into subsystems where the A matrix is nonsingular. To accomplish this we can first choose the largest nonsingular square submatrix of A whose upper left corner is the $(1, 1)$ entry of A . If that submatrix has lower right corner (k, k) where $k < n$, then we repeat this procedure by constructing another such matrix whose upper left corner is $(k + 1, k + 1)$. In practice we calculate the condition number of the submatrices and use that to determine if the matrix is close to singular. At this point each subsystem has a nonsingular A matrix, which allows us to directly apply the matrix exponential operator in equation (3.4) to update the basis functions.

Figure 3.1 shows the result of applying this method to the one-way wave equation (2.2). The basis functions up to time $t = 1$ are empirically generated using the standard method from Section 2.2. For times $1 < t \leq 10$, the empirical basis functions that were generated at $t = 1$ are evolved using the exponential operator from Equation 3.4. The numerical solution closely matches the exact solution up to about $t = 4$. Past that time the numerical solution begins to diverge from the exact solution, but still follows the general pattern. For comparison, we can examine Figure 3.2, where the basis functions are empirically generated up to time $t = 1$, and then the basis functions are kept fixed for times $1 < t \leq 10$. When the basis functions are not evolved at all then the numerical solution matches the exact solution up to about $t = 3$, but past that point it wildly diverges from the exact solution, in much the same way as the standard polynomial chaos expansion.

The basis evolution operator involves computing a matrix exponential, and has the

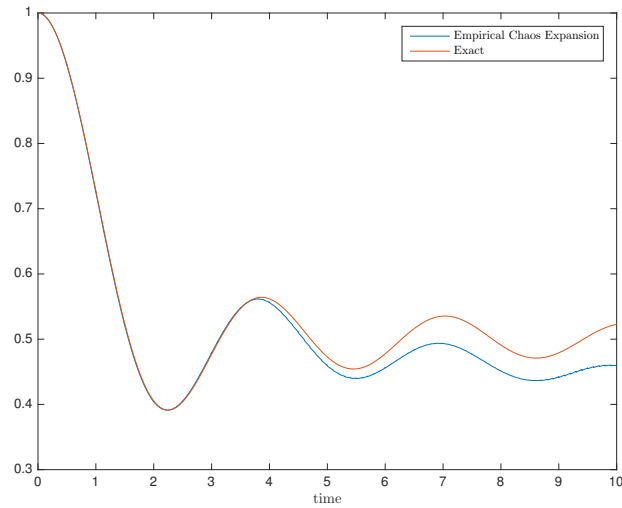


Figure 3.1: Mean square expectation at $x = 0$ of solution to (2.2), computed using empirical chaos expansion with stochastic Galerkin. The basis functions up to time $t = 1$ are empirically generated. For times $1 < t \leq 10$, the empirical basis functions that were generated at $t = 1$ are evolved using the exponential operator in (3.4).

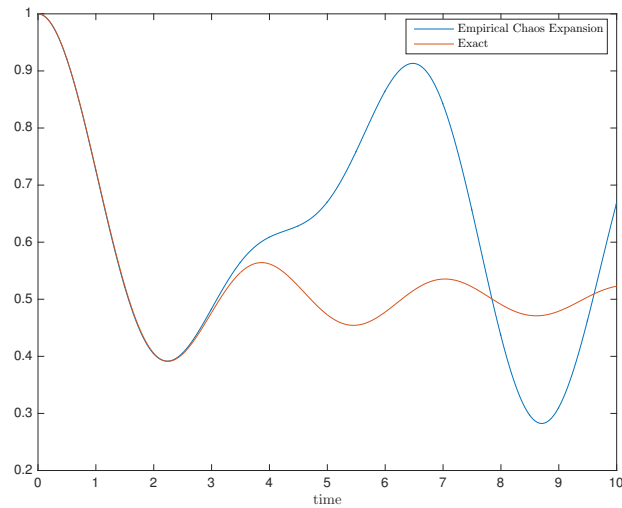


Figure 3.2: Mean square expectation at $x = 0$ of solution to (2.2), computed using empirical chaos expansion with stochastic Galerkin. The basis functions up to time $t = 1$ are empirically generated. For times $1 < t \leq 10$, the basis functions remain fixed at the empirical basis functions that were generated for time $t = 1$.

potential to be much cheaper to compute than the trajectory sampling approach, and it suggests the following general strategy:

1. Sample a set of trajectories and use POD to generate a set of empirical basis functions
2. Use the exponential basis evolution operator to update the basis functions for a few additional timesteps without resampling the trajectories
3. Repeat

Although we do not resample the trajectories at each timestep, we need to use smaller timesteps when applying the matrix exponential operator. In the case of the one dimensional wave, this results in a slight increase in the running time since the stochastic Galerkin system is already straightforward to solve. Figure 3.3 shows the result of applying the alternating timestep strategy, where the first timestep generates empirical basis functions by sampling trajectories, the second timestep evolves the basis functions using the exponential operator from 3.4, the third timestep resamples trajectories to generate a new set of empirical basis functions, the fourth timestep evolves the empirical basis functions using the exponential operator from 3.4, and so on. We can observe that the solution retains the same accuracy as when we used trajectory sampling on every timestep. If we do not use the exponential operator from 3.4 to update the basis functions on alternating timesteps, then the solution quickly loses accuracy, as we can see in figure 3.4.

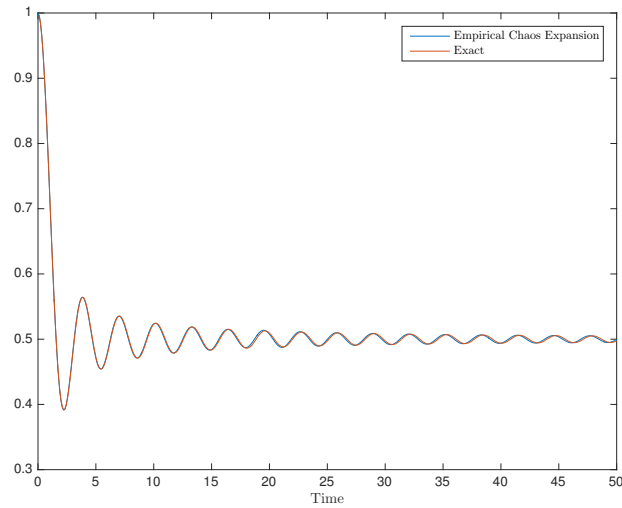


Figure 3.3: Mean square expectation at $x = 0$ of solution to (2.2), computed using empirical chaos expansion with stochastic Galerkin with timestep size of 1. The basis functions on even timesteps are empirically generated using POD. The basis functions on odd timesteps are evolved using the exponential operator in (3.4)

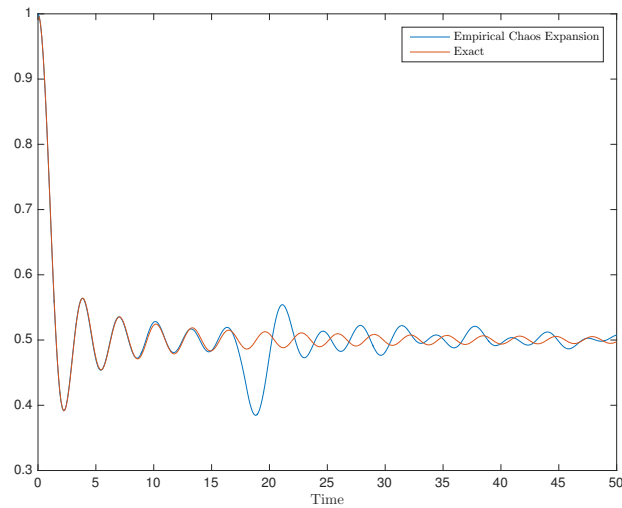


Figure 3.4: Mean square expectation at $x = 0$ of solution to (2.2), computed using empirical chaos expansion with stochastic Galerkin with timestep size of 1. The basis functions on even timesteps are empirically generated using POD. The basis functions on odd timesteps are not evolved from their previous values.

3.1.2 Diffusion Equation

In section 2.4 we showed that the empirical basis functions for the diffusion equation do not need to be evolved from their initial values in order to accurately compute the solution. It is still useful, however, to verify that the empirical basis continues to accurately capture the solution after we apply the exponential basis evolution operator.

If we substitute equation (3.1) into equation (2.14) for the diffusion equation, then we get:

$$\begin{aligned} \sum_{i=1}^N \hat{u}^i(x) \Psi_t^i(\xi, t) &= \xi \sum_{i=1}^N \hat{u}_{xx}^i(x) \Psi^i(\xi, t) \\ \implies \sum_{i=1}^N \hat{u}^i(x) \hat{u}^j(x) \Psi_t^i(\xi, t) &= \xi \sum_{i=1}^N \hat{u}_{xx}^i(x) \hat{u}^j(x) \Psi^i(\xi, t) \\ \implies \sum_{i=1}^N \int_0^{2\pi} \hat{u}^i(x) \hat{u}^j(x) dx \Psi_t^i(\xi, t) &= \xi \sum_{i=1}^N \int_0^{2\pi} \hat{u}_{xx}^i(x) \hat{u}^j(x) dx \Psi^i(\xi, t). \end{aligned}$$

Letting

$$\Psi = \begin{pmatrix} \Psi^1 \\ \Psi^2 \\ \vdots \\ \Psi^N \end{pmatrix} \quad \hat{u} = \begin{pmatrix} \hat{u}^1 \\ \hat{u}^2 \\ \vdots \\ \hat{u}^N \end{pmatrix} \quad A_{ji} = \int_0^{2\pi} \hat{u}^i(x) \hat{u}^j(x) dx \quad M_{ji} = \int_0^{2\pi} \hat{u}_{xx}^i(x) \hat{u}^j(x) dx$$

implies:

$$A \Psi_t(\xi, t) = \xi A \Psi(\xi, t), \quad (3.5)$$

which is a DAE whose solution can be used to evolve basis functions in time. The general

approach we use is to first generate a set of empirical basis functions up to a particular time t^* , using the method of section 2.1. Then the set of empirical basis functions is evolved in time by solving equation (3.3). In particular, if the matrix A is invertible, then the exact solution to equation (3.5) is:

$$\Psi(\xi, t) = \exp[\xi A^{-1} M(t - t_0)] \Psi(\xi, t_0), \quad (3.6)$$

where \exp is the matrix exponential operator. Unlike the case with the one dimensional wave equation, the A matrix in this case is nonsingular and we can directly apply the exponential operator in equation (3.6) to update the basis functions.

Figure 3.5 shows the result of applying this method to the diffusion equation (2.14). The basis functions up to time $t = 1$ are empirically generated using the standard method from section 2.4. For times $1 < t \leq 10$, the empirical basis functions that were generated at $t = 1$ are evolved using the exponential operator from equation (3.6). The numerical solution closely matches the exact solution. Recall, however, that the empirical basis functions accurately captured the solution even if they are not evolved at all. We can examine figure 3.6, where the basis functions are empirically generated up to time $t = 1$, and then the basis functions are kept fixed for times $1 < t \leq 10$, which also accurately captures the solution.

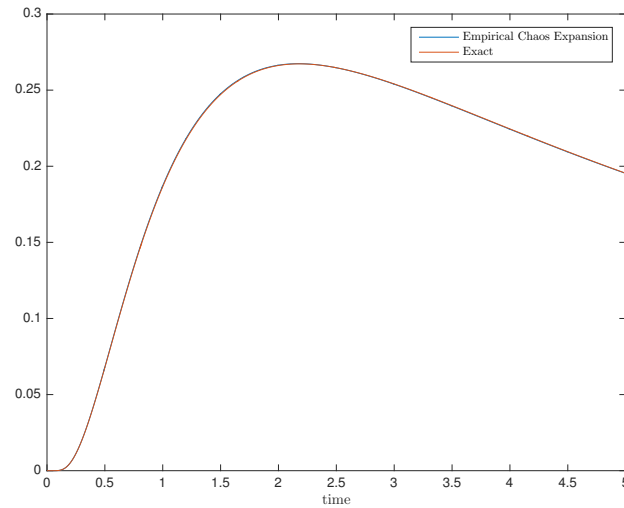


Figure 3.5: Mean square expectation at $x = 1$ of solution to (2.14), computed using empirical chaos expansion with stochastic Galerkin. The basis functions up to time $t = 1$ are empirically generated. For times $1 < t \leq 10$, the basis functions that were generated at $t = 1$ are evolved using the exponential operator in (3.6)

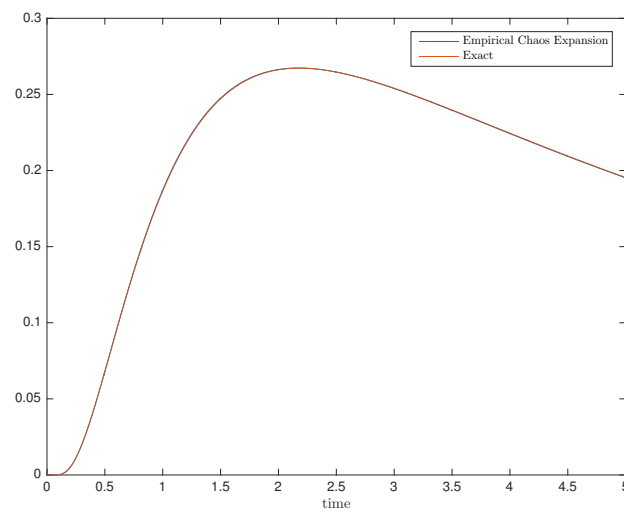


Figure 3.6: Mean square expectation at $x = 1$ of solution to (2.14), computed using empirical chaos expansion with stochastic Galerkin. The basis functions up to time $t = 1$ are empirically generated. For times $1 < t \leq 10$, the basis functions remain fixed at the empirical basis functions that were generated for time $t = 1$.

3.2 Acknowledgements

This work was conducted with Professor Melvin Leok at the University of California, San Diego and is currently being prepared for publication.

Chapter 4

Stochastic Collocation

In polynomial chaos, we first choose a basis $\{P^i(\xi)\}_{i=1}^N$ for the random space, and then express the solution to the SPDE as:

$$u(x, t, \xi) \approx \sum_{i=1}^N \hat{u}^i(x, t) P^i(\xi).$$

The stochastic Galerkin method presented in previous sections to compute the unknown $\hat{u}^i(x, t)$ coefficients can prove difficult to apply in practice. One of the principal issues is that the Galerkin system must be derived analytically, and there are as yet no sufficiently powerful algorithms to automate this process for fully general problems. Another issue is that implementing the stochastic Galerkin method usually requires new code to be written in order to solve the coupled deterministic Galerkin PDE. Finally, in many cases the Galerkin PDE is significantly more challenging to solve than the original SPDE.

In an attempt to deal with these issues, a class of methods termed *nonintrusive* were developed. Nonintrusive methods typically require the original SPDE system to be solved for fixed values of the random variables and then apply post-processing in order to compute various moments of the solution distribution. Thus, no new codes need to be developed beyond a deterministic solver for fixed values of the random variable, and such codes often already exist. Monte-Carlo methods are an example of a nonintrusive method, where the solution is computed for fixed values of the random variable, and then moments of the discrete distribution are used to approximate moments of the continuous distribution (e.g. the average of the computed solutions is used as an approximation to the mean of the continuous distribution).

Another commonly used nonintrusive method is stochastic collocation, which was formalized in [86]. The general approach of stochastic collocation involves choosing a set of collocation nodes in the random space and picking values for the unknown $\hat{u}^i(x, t)$

coefficients such that the error of the polynomial chaos expansion is zero at the collocation nodes. This can be accomplished by solving the original SPDE where the random variable is set to the value of the collocation nodes and/or neighboring nodes, then using those solutions either for interpolation or numerical integration. In the interpolation approach, a high order interpolating polynomial is constructed in the random variable space so that it passes through the computed numerical solutions at all of the collocation points. The polynomial can then be used to solve for the $\hat{u}^i(x, t)$ coefficients in the polynomial chaos expansion. In the numerical integration approach (also known as discrete projection or the pseudospectral approach [84]), the solutions at the collocation nodes are used with numerical quadrature to evaluate:

$$\hat{u}^i(x, t) = \int_{\Omega} u(x, t, \xi) P^i(\xi) d\xi,$$

for each of the unknown $\hat{u}^i(x, t)$ coefficients.

Another approach, which we use here, is called the Stochastic Response Surface Method (SRSM) [33, 34] or matrix inversion approach [85]. With this method, we construct and solve the following system for a set of discrete x and t values:

$$\begin{pmatrix} P^1(\xi_1) & P^2(\xi_1) & \dots & P^N(\xi_1) \\ P^1(\xi_2) & P^2(\xi_2) & \dots & P^N(\xi_2) \\ \vdots & & & \\ P^1(\xi_k) & P^2(\xi_k) & \dots & P^N(\xi_k) \end{pmatrix} \begin{pmatrix} \hat{u}^1(x, t) \\ \hat{u}^2(x, t) \\ \vdots \\ \hat{u}^N(x, t) \end{pmatrix} = \begin{pmatrix} u(x, t, \xi_1) \\ u(x, t, \xi_2) \\ \vdots \\ u(x, t, \xi_k) \end{pmatrix} \quad (4.1)$$

where $\{\xi_i\}_{i=1}^k$ is the set of collocation points, and the right hand side is the numerical solution at each of the collocation points. The SRSM has been applied as part of stochastic

collocation to solve SPDEs in multiple settings [52, 35, 31, 30, 5], and stochastic collocation in general is a very active field [2, 57, 18, 50, 17, 67, 72], in no small part due to the relative ease of implementation relative to stochastic Galerkin.

The system can be constructed so that $k = N$ and there is a unique solution. In practice, however, we usually create the system so that $k > N$, causing it to be overdetermined and then solve it in least squares sense. Just like stochastic Galerkin, SRSM may also be applied using empirical basis functions generated from POD. The advantage, just as with SRSM applied to gPC, is that it does not require new code that is specific to a given problem, beyond code that can solve the problem for a fixed value of the random variable. In the following sections we show the result of applying SRSM to some model problems using gPC expansions as well as empirical chaos expansions.

4.1 One Dimensional Wave Equation

4.1.1 Polynomial Chaos Expansion

For the one dimensional wave equation (2.2), we can apply SRSM to the standard polynomial chaos expansion, choosing the collocation points to be the set of k Chebyshev nodes on the interval $[-1, 1]$. Each of the k collocation nodes requires one solution to the original equation, for a fixed value of ξ . These computations can trivially be run in parallel. After computing the numerical solutions at the collocation nodes we then compute the least squares solution to the linear system in (4.1) at each fixed value of x and t . The total computational cost is thus the cost of computing the k solutions of the original system, plus the cost of inverting a $k \times N$ system.

Just like the stochastic Galerkin method, capturing solution behavior for long time intervals requires N to continually grow. Effectively solving equation (4.1) requires k to be at least as large as N , so this increases the cost of computing the solution at the collocation nodes, and also increases the cost of inverting the resulting $k \times N$ matrix. Figure 4.1 shows the result of applying SRSM using gPC for polynomial orders of 10, 20, and 30, and using the expansions to compute the mean square expectation of the solution at $x = 0$. Past a certain point in time all of the numerical solutions diverge from exact value.

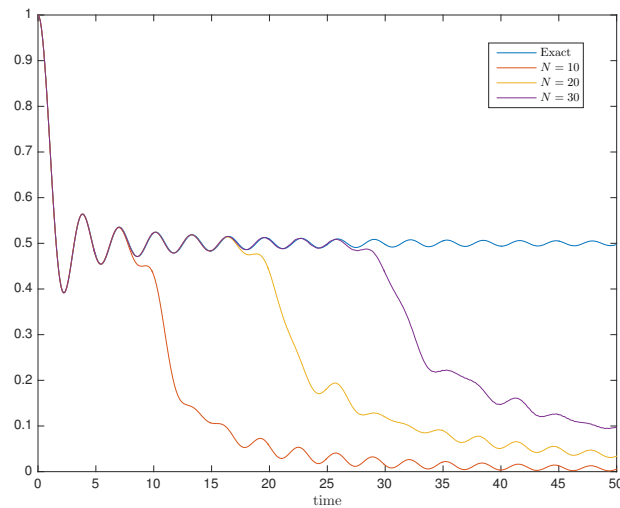


Figure 4.1: Mean Square Expectation at $x = 0$ of solution to (2.2), computed using gPC with SRSM using Legendre polynomials of varying order, N . The collocation nodes were chosen to be 600 Chebyshev nodes on the interval $[-1, 1]$

4.1.2 Empirical Chaos Expansion

We can apply SRSM to the empirical chaos expansion in a similar way to standard polynomial chaos. Before solving Equation (4.1), however, we must generate a set of empirical basis functions. This step also requires solving the original system for a set of fixed values of ξ , so we may solve the equation for a fixed set once, and then use that set both for generating the empirical basis and also for estimating the values of the unknown $\hat{u}^i(x, t)$ coefficients.

We begin by fixing the value of ξ to the collocation points, and solving the deterministic PDE from the starting time up to the first timestep. The solutions are then used to construct an empirical basis, following the method of Section 2.1. After the basis functions are generated, we use them to evaluate the left side of equation (4.1). The values of the solutions are also used to determine the right side of equation (4.1). The system is then solved to determine the unknown $\hat{u}^i(x, t)$ coefficients. This provides a solution up to the

first timestep. The solution at the first timestep is then used as the initial condition, and we again solve the deterministic PDE at the collocation points from the first timestep to the second timestep. We use the values of the solutions from timestep one to timestep two to construct a new set of empirical basis functions, which again lets us evaluate the left side of equation (4.1). The values of the solutions also provide the right side of equation (4.1). The system is then solved to determine the unknown $\hat{u}^i(x, t)$ coefficients up to timestep two. This process is iteratively repeated out to the final timestep, at which point the full solution is available. Figure 4.2 shows the result of applying SRSM with an empirical chaos expansion using a timestep of $t = 1$, using 240 Chebyshev nodes on the interval $[-1, 1]$ as the collocation points, and using the expansion to compute the mean square expectation of the solution at $x = 0$. The expansion used at most 9 empirical basis functions for any given timestep. Similar to stochastic Galerkin, it very faithfully reproduces the behavior of the mean square expectation of the exact solution while keeping the total number of basis functions low.

The singular values from POD show a marked drop off, just as in the case of the stochastic Galerkin method. We use the same singular value cutoff of 10^{-4} to decide the total number of empirical basis functions after performing a POD. Figure 4.3 shows the first ten scaled singular values from POD at the fifth timestep. There is a noticeable drop from the second to third singular value, and the singular values are very close to zero past the sixth.

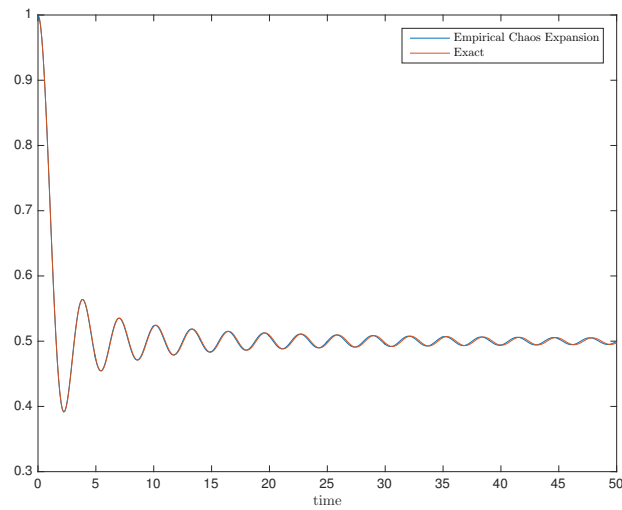


Figure 4.2: Mean square expectation at $x = 0$ computed using an empirical chaos expansion with SRSM. The collocation nodes were chosen to be 240 Chebyshev nodes on the interval $[-1, 1]$, and the timestep length was $t = 1$. The maximum number of basis functions used on any individual timestep was 9.

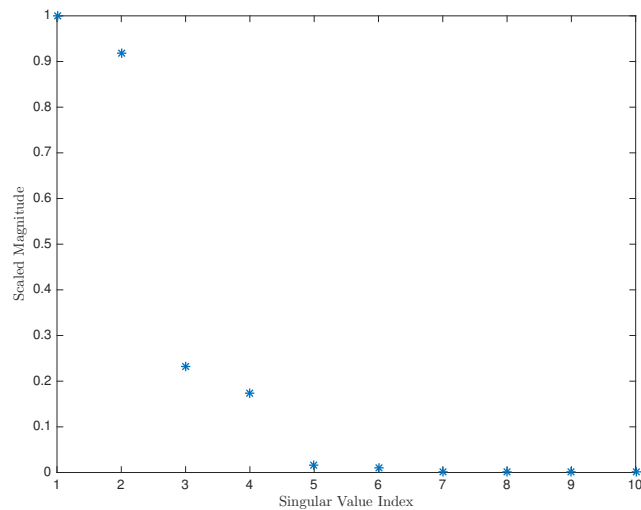


Figure 4.3: Singular values from POD for the first timestep when performing empirical chaos expansion with SRSM to solve (2.2). Singular values are scaled so that the maximum singular value has magnitude 1.

4.1.3 Running Time

We expect the computational time of the empirical chaos expansion with SRSM to scale linearly as we increase the final time. If the number of basis functions does not noticeably grow as the final time increases, and the number of collocation points remains relatively fixed, then the total amount of computational work done at every timestep is fixed. Thus we expect doubling the final simulation time to result in roughly double the total amount of computational time. The situation with polynomial chaos is different, since increasing the number of basis functions also increases the cost of solving the SRSM system. Figure 4.4 shows a comparison of the running times. Note that the polynomial chaos running time scales superlinearly with the final time, while the empirical chaos expansion running time scales linearly with the final running time. The polynomial chaos method used 600 collocation nodes in order to accurately compute the solution, while the empirical chaos method required 240 collocation nodes.

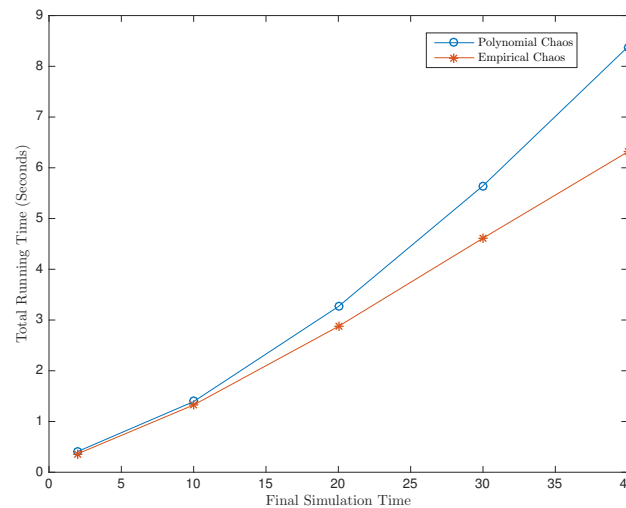


Figure 4.4: Comparison of total running times for solutions of (2.2) computed to the same accuracy using empirical chaos expansion and gPC with SRSM.

4.1.4 Basis Function Evolution

We now examine how the empirical basis functions evolve between timesteps. We set the timestep length to 0.1 for this section to closely monitor how the basis functions change. Figure 4.5 shows how the basis function corresponding to the largest singular value evolves over the first five timesteps.

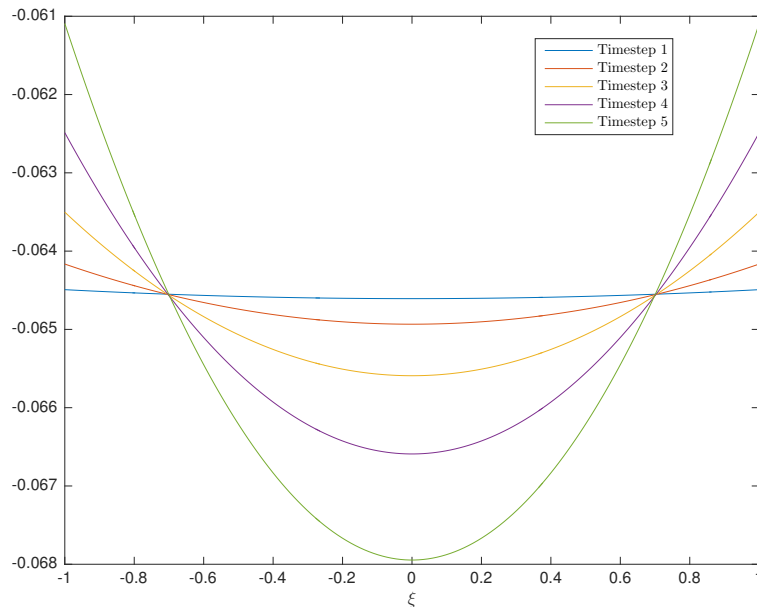


Figure 4.5: Evolution of the first basis function from POD for the first five timesteps in the solution to (2.2) using empirical chaos expansion with SRSM.

This basis function evolves smoothly, but since the first and second singular values cross multiple times, it can also become the basis function associated with the second singular value. See Figure 4.6, which shows the magnitudes of the first and second singular values over 100 timesteps. Figure 4.7 shows a three dimensional view of the evolution of the first basis function, where time is the third axis.

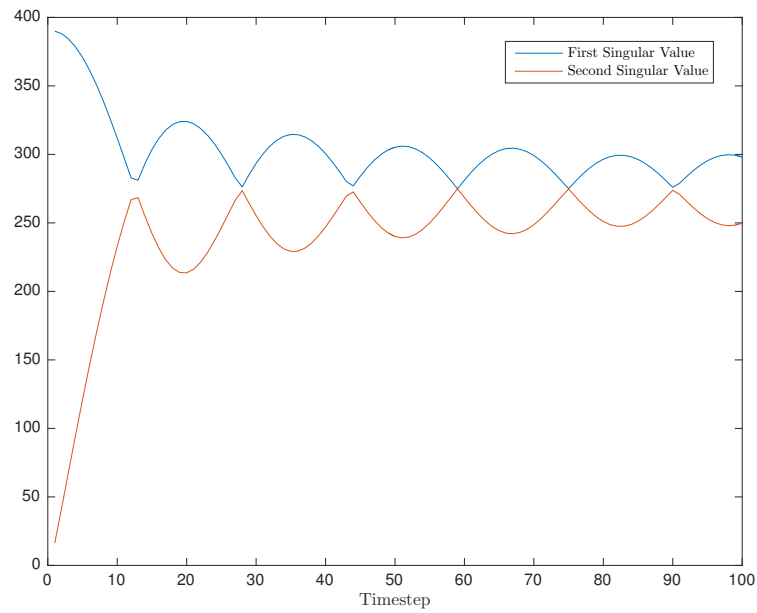


Figure 4.6: Evolution of the magnitude of the first two singular values from POD in the solution to (2.2) using empirical chaos expansion with SRSM.

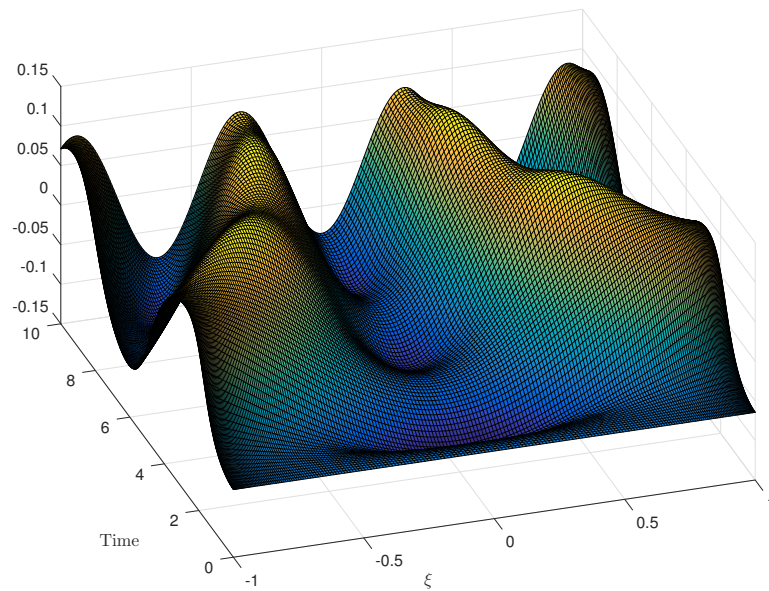


Figure 4.7: Evolution of the first basis function from POD for the first 100 timesteps in the solution to (2.2) using empirical chaos expansion with SRSM.

4.2 Diffusion Equation

4.2.1 Polynomial Chaos Expansion

For the diffusion equation (2.14), we can apply SRSM to the gPC expansion, choosing the collocation nodes to be the set of k Chebyshev nodes on the interval $[0, 1]$. Each of the k collocation points requires one solution to the original equation, for a fixed value of ξ .

Since the solution to the diffusion equation converges, we do not need to dramatically increase the number of Legendre basis polynomials in order to accurately capture the solution behavior out to long final integration times. Figure 4.8 shows the result of applying SRSM using standard polynomial chaos for polynomial orders of 3, 5, and 10, and using the expansions to compute the mean square expectation of the solution at $x = 1$. The exact solution was computed using 75,000 Monte Carlo iterations. All of the computed solutions follow the general trend of the exact solution, and once we have added 10 polynomial basis functions the exact solution is visually indistinguishable from the solution computed using polynomial chaos.

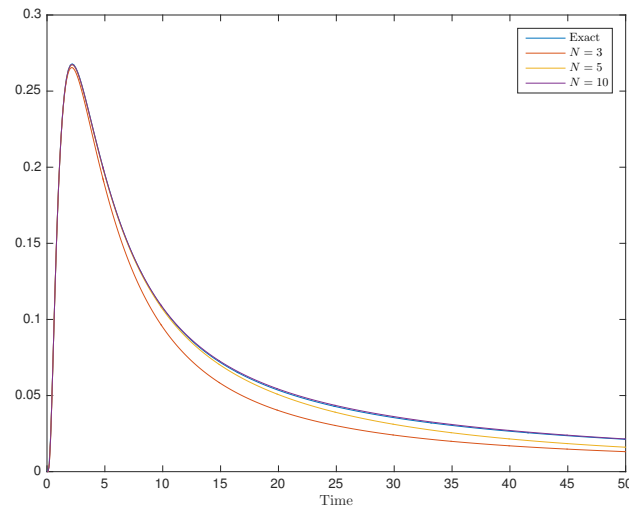


Figure 4.8: Mean Square Expectation at $x = 1$ of solution to (2.14), computed using gPC with SRSM using Legendre polynomials of varying order N . The collocation nodes were chosen to be 200 Chebyshev nodes on the interval $[0, 1]$.

4.2.2 Empirical Chaos Expansion

We can apply SRSM to the empirical chaos expansion in a similar way to standard polynomial chaos. Before solving equation (4.1), however, we must generate a set of empirical basis functions. This step also requires solving the original system for a set of fixed values of ξ , so we may solve the equation for a fixed set once, and then use that set both for generating the empirical basis and also for estimating the values of the unknown $\hat{u}^i(x, t)$ coefficients. Since the solution to the diffusion equation converges, we can generate a single set of empirical basis functions by solving the original system up to time 1, and then using that same set of basis functions for the entire integration time.

Figure 4.9 shows the result of applying SRSM with an empirical chaos expansion using a timestep of $t = 1$, with 200 Chebyshev nodes on the interval $[0, 1]$ as the collocation points, and using the expansion to compute the mean square expectation of the solution at $x = 1$. The expansion used 12 empirical basis functions. Similar to stochastic Galerkin, it

very faithfully reproduces the behavior of the mean square expectation of the exact solution while keeping the total number of basis functions low.

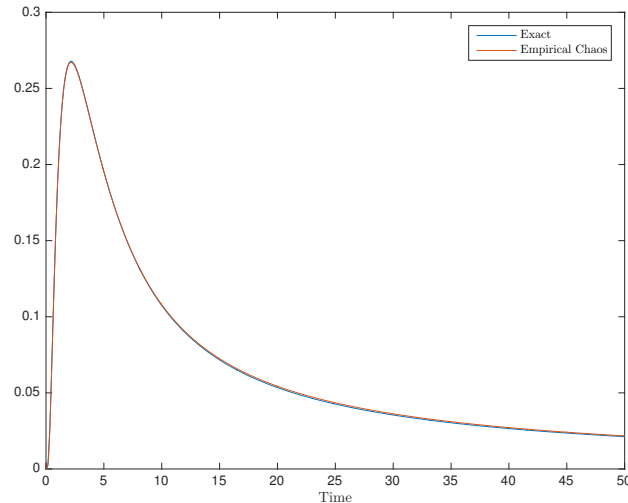


Figure 4.9: Mean Square Expectation at $x = 1$ of solution to (2.14), computed using empirical chaos expansion with SRSM. The collocation points were chosen to be 200 Chebyshev nodes on the interval $[0, 1]$, and the timestep length was $t = 1$. The basis functions were generated by sampling solutions up to the first timestep and then fixing them for the rest of the integration. There were 12 basis functions total.

The singular values from POD show a marked drop off, just as in the case of the stochastic Galerkin method. We use the same singular value cutoff of 10^{-4} to decide the total number of empirical basis functions after performing a POD. Figure 4.10 shows the first ten scaled singular values from POD at the first timestep. There is a dramatic decay over the first three singular values, and the singular values are very close to zero past the fifth.

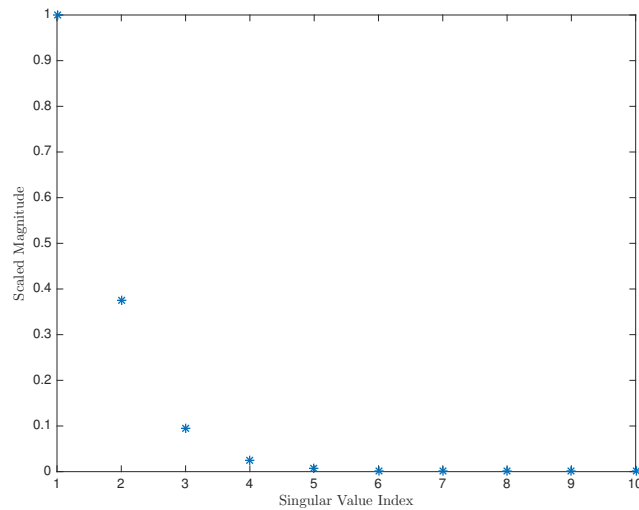


Figure 4.10: Singular values from POD for first timestep when performing empirical chaos expansion with SRSM to solve (2.14). Singular values are scaled so that the maximum singular value has magnitude 1.

4.2.3 Running Time

Since the diffusion equation converges and we can use a fixed basis for both the polynomial chaos expansion as well as for the empirical chaos expansion, we expect both methods to perform well. In particular, since we can rely on a fixed number of basis functions in both methods, both their running times scale linearly with the final integration time. Figure 4.11 shows a comparison of the running times. The running times for both methods are nearly identical, since both rely on sampling the solution at 200 fixed values of ξ , and both use roughly the same number of basis functions (14 for empirical chaos and 15 for polynomial chaos). While the empirical chaos expansion incurs some extra overhead from performing a singular value decomposition and also performing numerical quadrature, the cost of the extra operations is insignificant compared to the cost of numerically solving the original equation for 200 fixed values of ξ and the cost of solving the SRSM system.

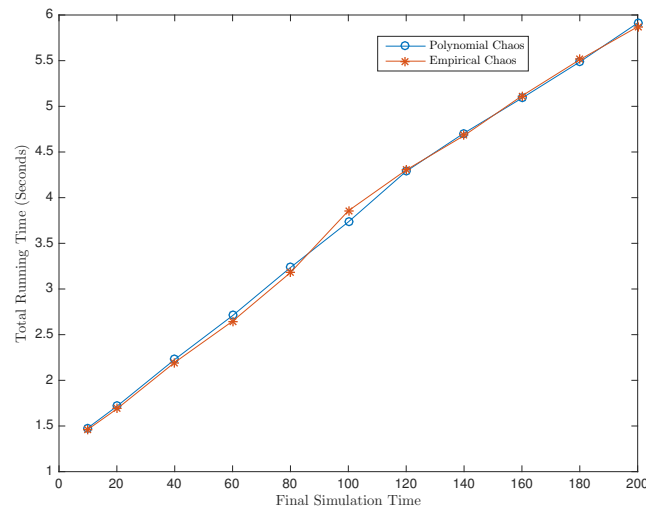


Figure 4.11: Comparison of total running times for solutions of (2.14) computed to the same accuracy using empirical chaos expansion and gPC with SRSM.

4.2.4 Basis Function Evolution

We now examine how the empirical basis functions evolve between timesteps. For the computations in the previous sections we fixed the initial basis and did not evolve it at all, but for this section we resample the trajectories in order to see how the basis functions evolve. This is to verify that the basis functions do in fact converge, just as they do when we solve the diffusion equation using a stochastic Galerkin method. We set the timestep length to 0.1 for this section to closely monitor how the basis functions change. Figures 4.12 and 4.13 show how the basis functions corresponding to the first two singular values evolve over the first five timesteps. Figures 4.14 and 4.15 show the basis functions corresponding to the first two singular values between timesteps 400 and 500. They only slightly change between those 100 timesteps, indicating that they are converging, just as they did when we solved the diffusion equation using a stochastic Galerkin method.

We can also track how the magnitudes of the singular values from POD change between timesteps. Just as is the case with the stochastic Galerkin solution of the diffusion

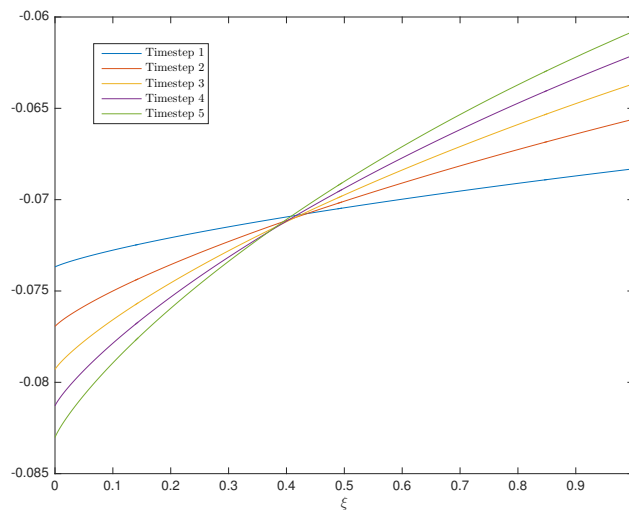


Figure 4.12: Evolution of the first basis function from POD for the first five timesteps in the solution to (2.14) using empirical chaos expansion with SRSM.

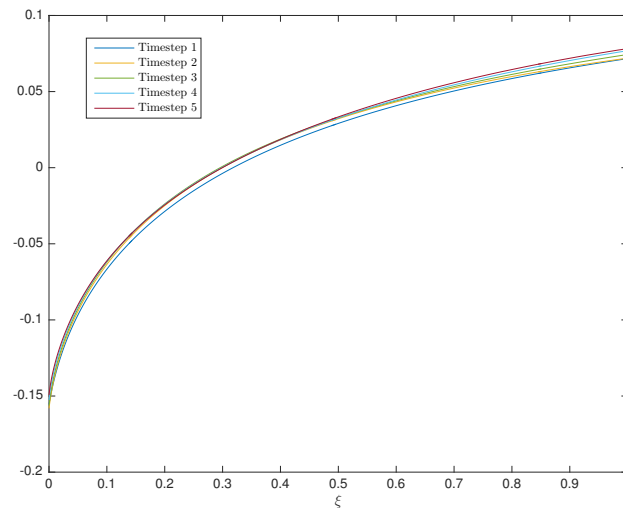


Figure 4.13: Evolution of the second basis function from POD for the first five timesteps in the solution to (2.14) using empirical chaos expansion with SRSM.

equation, the largest singular values from POD with stochastic collocation do not seem to cross, which makes it easier to track the evolution of individual basis functions (see Figure 4.16).

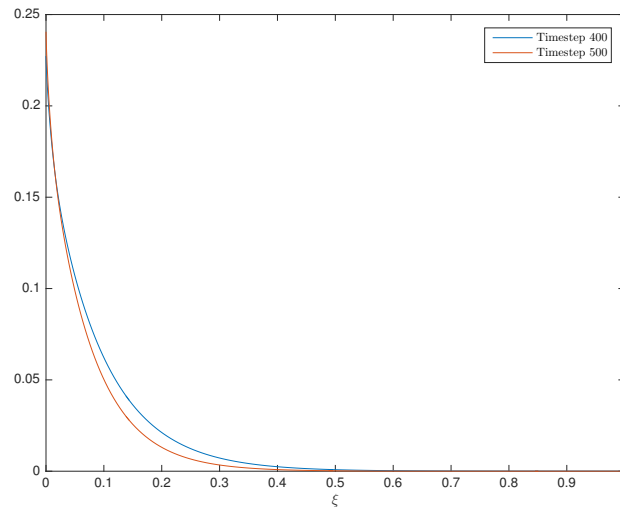


Figure 4.14: Evolution of the first basis function from POD for timesteps 400 and 500 in the solution to (2.14) using empirical chaos expansion with SRSM.

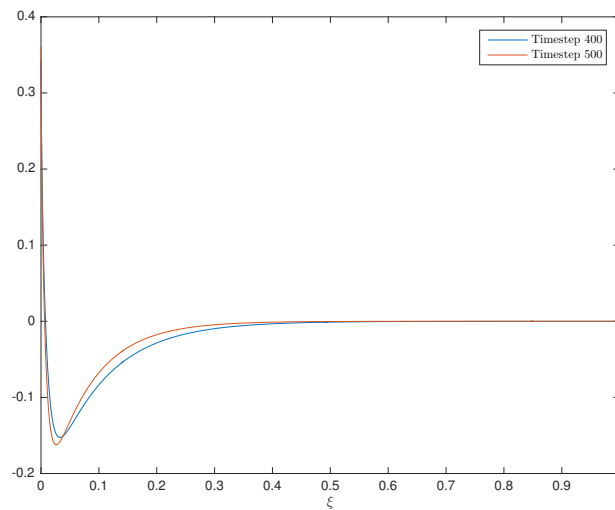


Figure 4.15: Evolution of the second basis function from POD for timesteps 400 and 500 in the solution to (2.14) using empirical chaos expansion with SRSM.

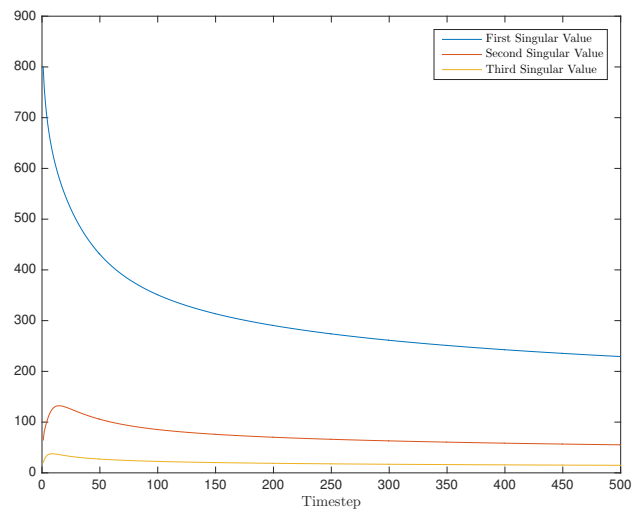


Figure 4.16: Evolution of the magnitude of the first three singular values from POD in the solution to (2.2) using empirical chaos expansion.

4.3 Advection-Reaction Equation

4.3.1 Polynomial Chaos Expansion

For the advection-reaction equation (2.20), we can apply SRSM to the standard polynomial chaos expansion, choosing the collocation points to be the set of k Chebyshev nodes on the interval $[-1, 1]$. Each of the k collocation points requires one solution to the original equation, for a fixed value of ξ . These computations can trivially be run in parallel. After computing the numerical solutions at the collocation points we then compute the least squares solution to the linear system in (4.1) at each fixed value of x and t . The total computational cost is thus the cost of computing the k solutions of the original system, plus the cost of inverting a $k \times N$ system.

Just as with the stochastic Galerkin method, capturing solution behavior for long time intervals requires N to continually grow. Effectively solving (4.1) requires k to be at least as large as N , so this increases the cost of computing the solution at the collocation points, and also increases the cost of inverting the resulting $k \times N$ matrix. Figure 4.17 shows the result of applying SRSM using standard polynomial chaos for polynomial orders of 5 and 10 and using the expansions to compute the mean square expectation of the solution at $x = 0$. Past a certain point in time all of the numerical solutions diverge from exact value.

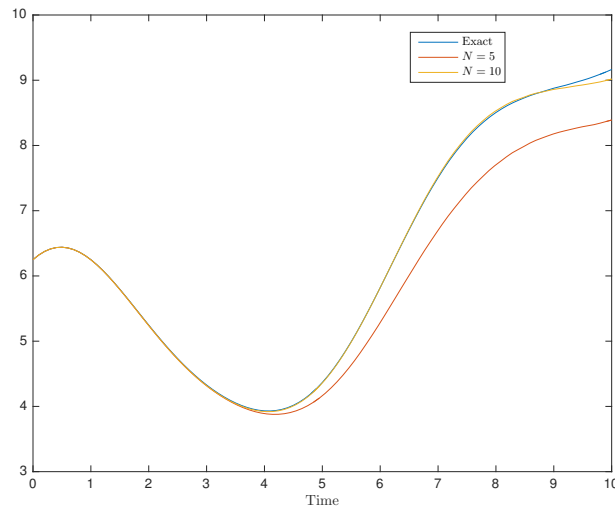


Figure 4.17: Mean square expectation $x = 0$ of solution to (2.20), computed using gPC with SRSM. N is the total number of polynomial basis functions that were used. The collocation points were chosen to be 240 Chebyshev nodes on the interval $[-1, 1]$.

4.3.2 Empirical Chaos Expansion

We can apply SRSM to the empirical chaos expansion in a similar way to standard polynomial chaos. Before solving equation (4.1), however, we must generate a set of empirical basis functions. This step also requires solving the original system for a set of fixed values of ξ , so we may solve the equation for a fixed set once, and then use that set both for generating the empirical basis and also for estimating the values of the unknown $\hat{u}^i(x, t)$ coefficients.

We begin by fixing the value of ξ to the collocation points, and solving the deterministic PDE from the starting time up to the first timestep. The solutions are then used to construct an empirical basis, following the method of section 2.1. After the basis functions are generated, we use them to evaluate the left side of equation (4.1). The values of the solutions are also used to determine the right side of (4.1). The system is then solved to determine the unknown $\hat{u}^i(x, t)$ coefficients. This provides a solution up to the first timestep.

The solution at the first timestep is then used as the initial condition, and we again solve the deterministic PDE at the collocation points from the first timestep to the second timestep. We use the values of the solutions from timestep one to timestep two to construct a new set of empirical basis functions, which again lets us evaluate the left side of equation (4.1). The values of the solutions also provide the right side of (4.1). The system is then solved to determine the unknown $\hat{u}^i(x, t)$ coefficients up to timestep two. This process is iteratively repeated out to the final timestep, at which point the full solution is available. Figure 4.18 shows the result of applying SRSM with an empirical chaos expansion using a timestep of $t = 1$, using 240 Chebyshev nodes on the interval $[-1, 1]$ as the collocation points, and using the expansion to compute the mean square expectation of the solution at $x = 0$. The expansion used at most 22 empirical basis functions for any given timestep. Similar to stochastic Galerkin, it very faithfully reproduces the behavior of the mean square expectation of the exact solution while keeping the total number of basis functions low.

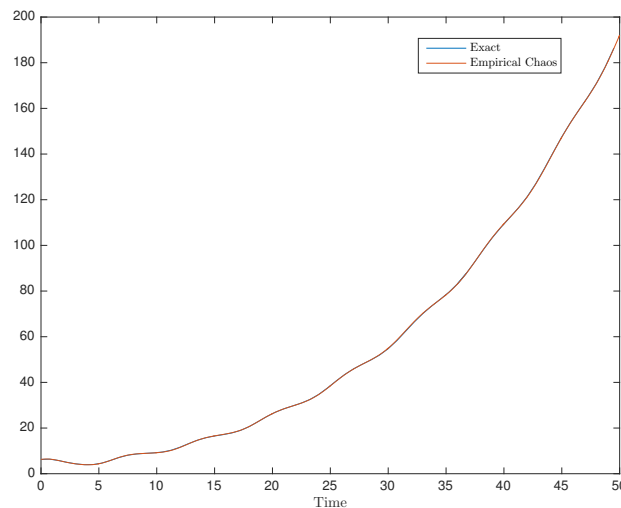


Figure 4.18: Mean square expectation at $x = 0$ of the solution to (2.20) computed using an empirical chaos expansion with SRSM with a timestep size of 1. The collocation points were chosen to be 240 Chebyshev nodes on the interval $[-1, 1]$. The maximum number of basis functions used on any individual timestep was 22.

The singular values from POD show a marked drop off, just as in the case of the stochastic Galerkin method. We use the same singular value cutoff of 10^{-4} to decide the total number of empirical basis functions after performing a POD. Figure 4.19 shows the first ten scaled singular values from POD at the fifth timestep. There is a noticeable drop from the second to third singular value, and the singular values are very close to zero past the sixth.

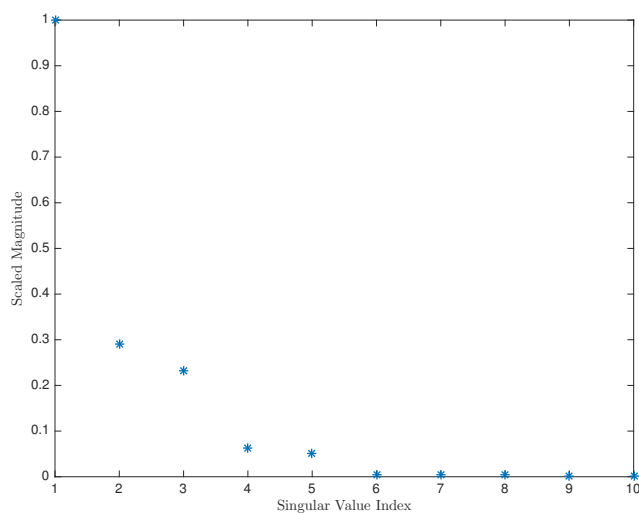


Figure 4.19: Singular values from POD for the fifth timestep when performing empirical chaos expansion to solve (2.20). Singular values are scaled so that the maximum singular value has magnitude 1.

4.3.3 Running Time

We expect the computational time of the empirical chaos expansion with SRSM to scale linearly as we increase the final time. If the number of basis functions does not noticeably grow as the final time increases, and the number of collocation points remains relatively fixed, then the total amount of computational work done at every timestep is fixed. Thus we expect doubling the final simulation time to result in roughly double the

total amount of computational time. The situation with polynomial chaos is different, since increasing the number of basis functions also increases the cost of solving the SRSM system. We also need to steadily increase the number of collocation nodes for polynomial chaos as the final integration time increases. Figure 4.20 shows a comparison of the running times. Note that the polynomial chaos running time scales superlinearly with the final time, while the empirical chaos expansion running time scales linearly with the final running time. The polynomial chaos method used 800 collocation nodes for the final time in order to accurately compute the solution, while the empirical chaos method requires 200 collocation nodes.

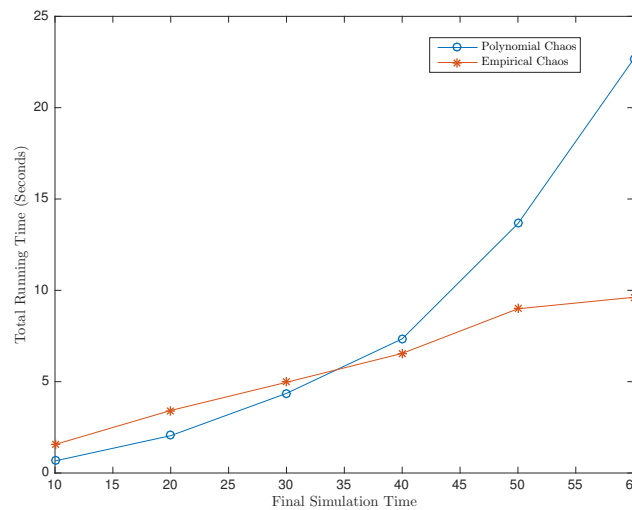


Figure 4.20: Comparison of total running times for solutions of (2.20) computed to the same accuracy using empirical chaos expansion and gPC with SRSM.

4.3.4 Basis Function Evolution

We now examine how the empirical basis functions evolve between timesteps. We set the timestep length to 0.1 for this section to closely monitor how the basis functions change. Figure 4.21 shows how the basis function corresponding to the largest singular value evolves over the first five timesteps. Figure 4.22 shows the evolution of the magnitudes

of the first, second, and third singular values over 100 timesteps.

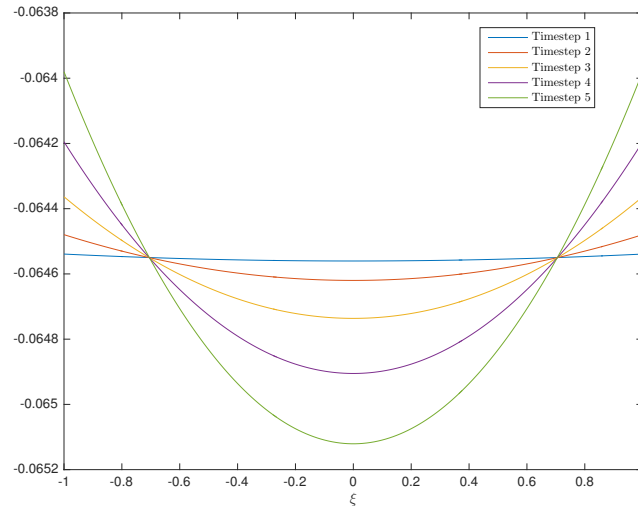


Figure 4.21: Evolution of the first basis function from POD for the first five timesteps in the solution to (2.20) using empirical chaos expansion.

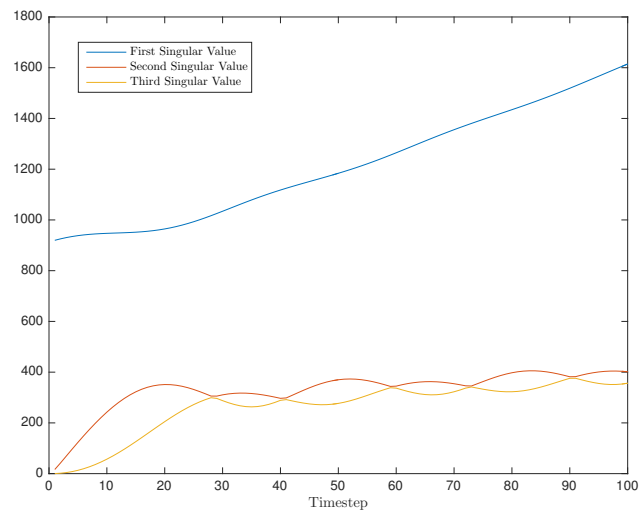


Figure 4.22: Evolution of the magnitude of the first, second, and third singular values from POD in the solution to (2.20) using empirical chaos expansion with SRSM.

4.4 Reaction-Diffusion Equation

4.4.1 Polynomial Chaos Expansion

For the reaction-diffusion equation (2.24), we can apply SRSM to the gPC expansion, choosing the collocation points to be the set of k Chebyshev nodes on the interval $[0, 1]$. Each of the k collocation points requires one solution to the original equation, for a fixed value of ξ .

Since the solution to the diffusion equation converges, we do not need to dramatically increase the number of Legendre basis polynomials in order to accurately capture the solution behavior out to long final integration times. Figure 4.23 shows the result of applying SRSM using gPC for polynomial orders of 4 and 10, and using the expansions to compute the mean square expectation of the solution at $x = 1$. The exact solution was computed using 100,000 Monte Carlo iterations. All of the computed solutions follow the general trend of the exact solution, and once we have added 10 polynomial basis functions the exact solution is visually indistinguishable from the solution computed using polynomial chaos.

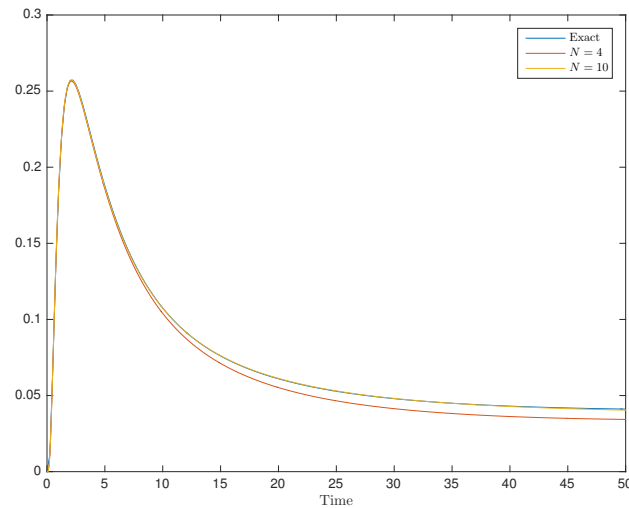


Figure 4.23: Mean square expectation $x = 1$ of solution to (2.24), computed using gPC with SRSM, using Legendre polynomials of varying order N . The collocation points were chosen to be 300 Chebyshev nodes on the interval $[0.00001, 1]$

4.4.2 Empirical Chaos Expansion

We can apply SRSM to the empirical chaos expansion in a similar way to standard polynomial chaos. Before solving (4.1), however, we must generate a set of empirical basis functions. This step also requires solving the original system for a set of fixed values of ξ , so we may solve the equation for a fixed set once, and then use that set both for generating the empirical basis and also for estimating the values of the unknown $\hat{u}^i(x, t)$ coefficients. Since the solution to the diffusion equation converges, we can generate a single set of empirical basis functions by solving the original system up to time 1, and then using that same set of basis functions for the entire integration time.

Figure 4.24 shows the result of applying SRSM with an empirical chaos expansion using a timestep of $t = 2$, with 300 Chebyshev nodes on the interval $[0.01, 1]$ as the collocation points, and using the expansion to compute the mean square expectation of the solution at $x = 1$. The expansion used 14 empirical basis functions. Similar to stochastic Galerkin, it

very faithfully reproduces the behavior of the mean square expectation of the exact solution while keeping the total number of basis functions low.

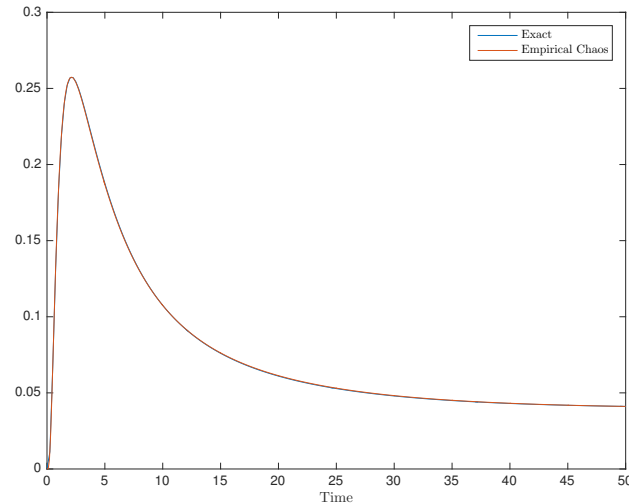


Figure 4.24: Mean square expectation at $x = 1$ of the solution to (2.24) computed using an empirical chaos expansion with SRSM. The collocation points were chosen to be 300 Chebyshev nodes on the interval $[0.01, 1]$, and the timestep length was $t = 2$. The basis functions were generated by sampling solutions up to the first timestep and then fixing them for the rest of the integration. There were 14 basis functions total.

The singular values from POD show a marked drop off, just as in the case of the stochastic Galerkin method. We use the same singular value cutoff of 10^{-4} to decide the total number of empirical basis functions after performing a POD. Figure 4.25 shows the first ten scaled singular values from POD at the first timestep. There is a dramatic decay over the first three singular values, and the singular values are very close to zero past the eighth.

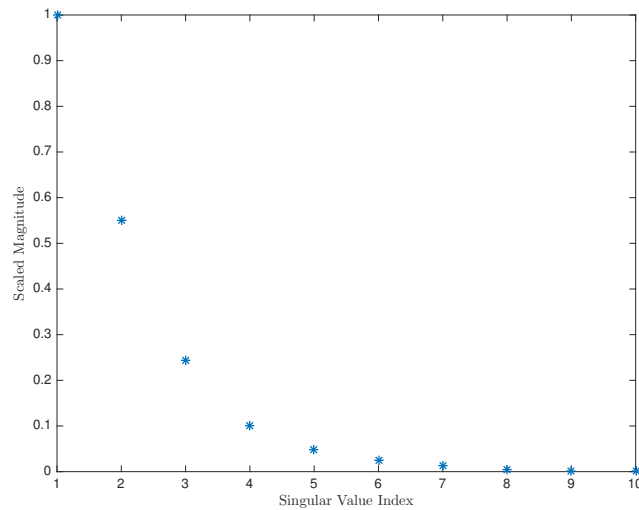


Figure 4.25: Singular values from POD for the time interval $t = 0$ to $t = 2$ when performing empirical chaos expansion to solve (2.24). Singular values are scaled so that the maximum singular value has magnitude 1.

4.4.3 Running Time

Since the solution to the reaction-diffusion equation converges and we can use a fixed basis for both the polynomial chaos expansion as well as for the empirical chaos expansion, we expect both methods to perform well. In particular, since we can rely on a fixed number of basis functions in both methods, both their running times scale linearly with the final integration time. Figure 4.26 shows a comparison of the running times. The running times for both methods are nearly identical, since both rely on sampling the solution at 300 fixed values of ξ , and both use roughly the same number of basis functions (14 for empirical chaos and 15 for polynomial chaos). While the empirical chaos expansion incurs some extra overhead from performing a singular value decomposition and also performing numerical quadrature, the cost of the extra operations is insignificant compared to the cost of numerically solving the original equation for 300 fixed values of ξ and the cost of solving the SRSM system.

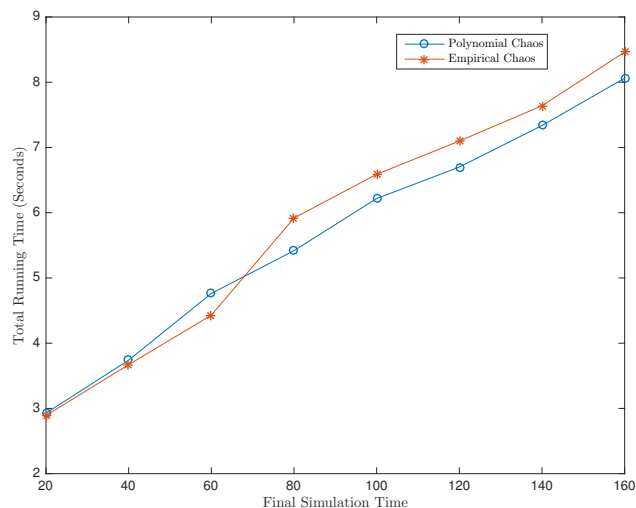


Figure 4.26: Comparison of total running times for solutions of (2.24) computed to the same accuracy using empirical chaos expansion and gPC with SRSM.

4.4.4 Basis Function Evolution

We now examine how the empirical basis functions evolve between timesteps. For the computations in the previous sections we fixed the initial basis and did not evolve it at all, but for this section we resample the trajectories in order to see how the basis functions evolve. This is to verify that the basis functions do in fact converge, just as they do when we solve the diffusion equation using a stochastic Galerkin method. We set the timestep length to 0.1 for this section to closely monitor how the basis functions change. Figure 4.27 shows how the basis function corresponding to the first singular value evolves over the first five timesteps. Figure 4.28 shows the basis function corresponding to the first singular value between timesteps 400 and 500. There is only a slight change between those 100 timesteps, indicating that the basis function is converging, just as it did when we solved the reaction-diffusion equation using a stochastic Galerkin method.

We can also track how the magnitudes of the singular values from POD change between timesteps. Just as is the case with the stochastic Galerkin solution of the reaction-

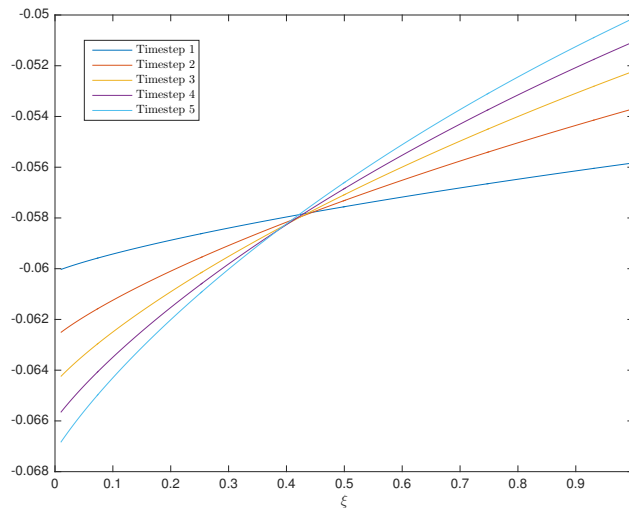


Figure 4.27: Evolution of the first basis function from POD for the first five timesteps in the solution to (2.24) using empirical chaos expansion with SRSM.

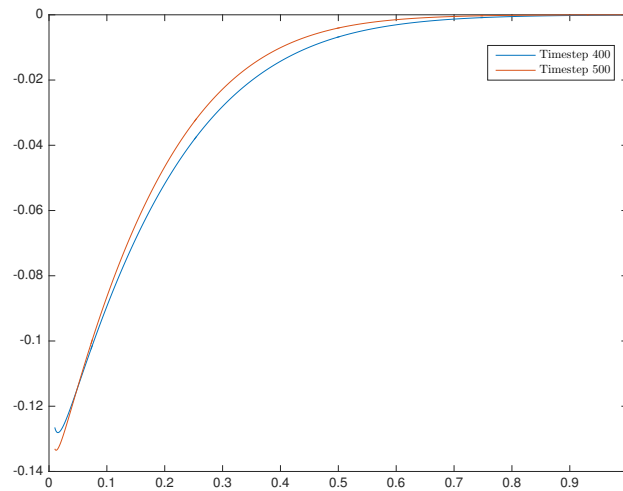


Figure 4.28: Evolution of the first basis function from POD for timesteps 400 to 500 in the solution to (2.24) using empirical chaos expansion.

diffusion equation, the largest singular values from POD with stochastic collocation do not seem to cross, which makes it easier to track the evolution of individual basis functions (see figure 4.29).

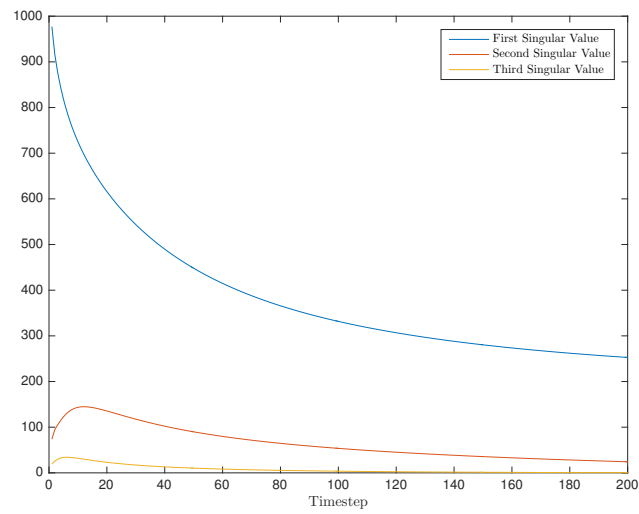


Figure 4.29: Evolution of the magnitude of the first three singular values from POD in the solution to (2.24) using empirical chaos expansion with SRSM.

4.5 Acknowledgements

This work was conducted with Professor Melvin Leok at the University of California, San Diego and is currently being prepared for publication.

Chapter 5

Conclusion

5.1 Future Work

Since their inception, polynomial chaos techniques have been successfully applied to a number of numerical problems that arise in uncertainty quantification. This work introduces a method to generate a set of empirical basis functions that varies with time to take the place of the standard orthogonal polynomial basis that remains fixed for the entire integration time. We demonstrate its numerical accuracy and efficiency over long-term integrations with multiple model problems. We also introduce a method to numerically evolve the empirical basis functions without needing to resample solutions of the original SPDE. We demonstrate that the running time of the empirical chaos method scales linearly with the final integration time. Thus, it has the potential to address one of the two principal issues with applying polynomial chaos techniques—solving problems out to long-term integrations is often inefficient due to the need to continually increase the number of polynomial basis functions.

This work does not, however, present a solution to the second and most fundamental issue—the curse of dimensionality. Namely, if the number of random variables is large then polynomial chaos techniques run slower than Monte Carlo methods. While empirical basis functions can be used in order to try to limit the size of such a basis, performing numerical integrations (which are a necessary component of the empirical chaos expansion) over a very high dimensional space still poses significant challenges, both in terms of computational time and accuracy. We currently use sparse grid quadrature, which allows us to achieve accurate solutions over higher dimensional spaces, but at the cost of sampling a large number of solutions of the original SPDE. Past a certain point it becomes more practical to use Monte Carlo methods instead. Some techniques such as multi-element polynomial chaos have shown some promise when faced with larger numbers of random variables, and it is

possible that using the basis decomposition employed by multi-element polynomial chaos methods coupled with empirical basis functions might allow higher dimensional SPDEs to be solved more efficiently.

Another open question is to what degree the empirical chaos expansion algorithms can be made adaptive. Recall that the number of basis functions is selected by examining the scaled magnitude of the singular values from POD, and there are two values that we can adjust.

1. The length of each timestep.
2. The number of solutions of the SPDE to sample.

The length of the timestep can be altered depending on the number of basis functions that we desire. In general, choosing a shorter timestep will result in the singular values from POD decaying faster, and thus will result in fewer empirical basis functions. The number of solutions to sample is a bit harder to determine. An approach that could be employed is to generate a set of empirical basis functions by sampling a fixed number of solutions to the SPDE, and then comparing the span of that basis to one that is generated by sampling a smaller number of solutions to the SPDE. If the difference in span is small then we would conclude that the number of solutions that we sampled is sufficient. If the difference in span is large, then we would conclude that the number of solutions that we sampled is insufficient, and proceed to sample additional solutions before repeating the process. Another, and perhaps more attractive, approach would be to develop robust error estimates that could be used instead of generating two separate empirical bases.

The method of empirical basis expansion has the potential to be coupled with gPC expansions as well. We could use a set of N orthogonal polynomial functions and perform the same trajectory sampling that we do for an empirical chaos expansion. We could then

project the trajectories onto the polynomial basis, and construct an empirical basis for the residuals of the trajectories. The empirical basis should be numerically orthogonal to the polynomial basis, which might allow the two systems to be propagated independently. Even in the case that the two sets of basis functions need to be coupled, this work has demonstrated that it is feasible to solve such systems through the inclusion of a mass matrix that turns the system of propagation PDEs into a DAE.

Recent work [64] has also shown that when gPC is applied to SPDEs with Hamiltonian structure, the resulting stochastic Galerkin system retains the Hamiltonian structure. Future work could attempt to determine whether the Hamiltonian structure is also retained when the original system is expanded using the empirical chaos method presented here.

We have shown the empirical chaos to be a robust and accurate solution method for the model problems presented. Further work is needed to demonstrate its efficacy for additional problems.

Bibliography

- [1] R Askey and J Wilson. Some basic hypergeometric polynomials that generalize jacobi polynomials, vol. 319. *Mem. Amer. Math., Providence, RI*, 1985.
- [2] Ivo Babuška, Fabio Nobile, and Raul Tempone. A stochastic collocation method for elliptic partial differential equations with random input data. *SIAM Journal on Numerical Analysis*, 45(3):1005–1034, 2007.
- [3] Volker Barthelmann, Erich Novak, and Klaus Ritter. High dimensional polynomial interpolation on sparse grids. *Advances in Computational Mathematics*, 12(4):273–288, 2000.
- [4] A Bensoussan and R Temam. Equations stochastiques du type navier-stokes. *Journal of Functional Analysis*, 13(2):195–222, 1973.
- [5] Marc Berveiller, Bruno Sudret, and Maurice Lemaire. Stochastic finite element: a non intrusive approach by regression. *European Journal of Computational Mechanics/Revue Européenne de Mécanique Numérique*, 15(1-3):81–92, 2006.
- [6] Robert H Cameron and William T Martin. Transformations of weiner integrals under translations. *Annals of Mathematics*, pages 386–396, 1944.
- [7] Anindya Chatterjee. An introduction to the proper orthogonal decomposition. *Current science*, 78(7):808–817, 2000.
- [8] Alexandre Joel Chorin. Gaussian fields and random flow. *Journal of Fluid Mechanics*, 63(01):21–32, 1974.
- [9] C Chou, Y Zhang, Rui Zhao, and Qing Nie. Numerical methods for stiff reaction-diffusion systems. *Discrete and Continuous Dynamica Systems Series B*, 7(3):515, 2007.
- [10] P-L Chow. Stochastic partial differential equations in turbulence related problems. *NASA STI/Recon Technical Report A*, 79:26135, 1978.
- [11] Charles W Clenshaw and Alan R Curtis. A method for numerical integration on an automatic computer. *Numerische Mathematik*, 2(1):197–205, 1960.

- [12] Giuseppe Da Prato and Arnaud Debussche. Ergodicity for the 3d stochastic navier–stokes equations. *Journal de mathématiques pures et appliquées*, 82(8):877–947, 2003.
- [13] Giuseppe Da Prato, Arnaud Debussche, and Roger Temam. Stochastic burgers’ equation. *Nonlinear Differential Equations and Applications NoDEA*, 1(4):389–402, 1994.
- [14] Manas K Deb, Ivo M Babuška, and J Tinsley Oden. Solution of stochastic partial differential equations using galerkin finite element techniques. *Computer Methods in Applied Mechanics and Engineering*, 190(48):6359–6372, 2001.
- [15] Alireza Doostan, Roger G Ghanem, and John Red-Horse. Stochastic model reduction for chaos representations. *Computer Methods in Applied Mechanics and Engineering*, 196(37):3951–3966, 2007.
- [16] Alireza Doostan and Gianluca Iaccarino. A least-squares approximation of partial differential equations with high-dimensional random inputs. *Journal of Computational Physics*, 228(12):4332–4345, 2009.
- [17] Michael Scott Eldred. Recent advances in non-intrusive polynomial chaos and stochastic collocation methods for uncertainty analysis and design. *AIAA Paper*, 2274(2009):37, 2009.
- [18] MS Eldred and John Burkardt. Comparison of non-intrusive polynomial chaos and stochastic collocation methods for uncertainty quantification. *AIAA paper*, 976(2009):1–20, 2009.
- [19] Hermann Engels. Numerical quadrature and cubature. 1980.
- [20] Oliver G Ernst, Antje Mugler, Hans-Jörg Starkloff, and Elisabeth Ullmann. On the convergence of generalized polynomial chaos expansions. *ESAIM: Mathematical Modelling and Numerical Analysis*, 46(02):317–339, 2012.
- [21] Jasmine Foo and George Em Karniadakis. Multi-element probabilistic collocation method in high dimensions. *Journal of Computational Physics*, 229(5):1536–1557, 2010.
- [22] W Morven Gentleman. Implementing clenshaw-curtis quadrature, i methodology and experience. *Communications of the ACM*, 15(5):337–342, 1972.
- [23] Marc Gerritsma, Jan-Bart Van der Steen, Peter Vos, and George Karniadakis. Time-dependent generalized polynomial chaos. *Journal of Computational Physics*, 229(22):8333–8363, 2010.
- [24] Roger Ghanem. Ingredients for a general purpose stochastic finite elements implementation. *Computer Methods in Applied Mechanics and Engineering*, 168(1):19–34, 1999.

- [25] Roger Ghanem, George Saad, and Alireza Doostan. Efficient solution of stochastic systems: application to the embankment dam problem. *Structural safety*, 29(3):238–251, 2007.
- [26] Roger G Ghanem and Pol D Spanos. *Stochastic finite elements: a spectral approach*. Courier Corporation, 2003.
- [27] David Gottlieb and Dongbin Xiu. Galerkin method for wave equations with uncertain coefficients. *Commun. Comput. Phys*, 3(2):505–518, 2008.
- [28] Vincent Heuveline and Michael Schick. A local time-dependent generalized polynomial chaos method for stochastic dynamical systems. *Preprint Series of the Engineering Mathematics and Computing Lab*, (04), 2011.
- [29] Thomas Y Hou, Wuan Luo, Boris Rozovskii, and Hao-Min Zhou. Wiener chaos expansions and numerical solutions of randomly forced equations of fluid mechanics. *Journal of Computational Physics*, 216(2):687–706, 2006.
- [30] Shuping Huang, Sankaran Mahadevan, and Ramesh Rebba. Collocation-based stochastic finite element analysis for random field problems. *Probabilistic Engineering Mechanics*, 22(2):194–205, 2007.
- [31] SP Huang, B Liang, and KK Phoon. Geotechnical probabilistic analysis by collocation-based stochastic response surface method: An excel add-in implementation. *Georisk*, 3(2):75–86, 2009.
- [32] Michael B Isichenko. Percolation, statistical topography, and transport in random media. *Reviews of modern physics*, 64(4):961, 1992.
- [33] Sastry S Isukapalli. *Uncertainty analysis of transport-transformation models*. PhD thesis, Citeseer, 1999.
- [34] Sastry S Isukapalli, Suhrid Balakrishnan, and Panos G Georgopoulos. Computationally efficient uncertainty propagation and reduction using the stochastic response surface method. In *Decision and Control, 2004. CDC. 43rd IEEE Conference on*, volume 2, pages 2237–2243. IEEE, 2004.
- [35] SS Isukapalli, A Roy, and PG Georgopoulos. Stochastic response surface methods (srsms) for uncertainty propagation: application to environmental and biological systems. *Risk analysis*, 18(3):351–363, 1998.
- [36] Kari Karhunen. *Über lineare Methoden in der Wahrscheinlichkeitsrechnung*, volume 37. Universitat Helsinki, 1947.
- [37] Gaetan Kerschen, Jean-claude Golinval, Alexander F Vakakis, and Lawrence A Bergman. The method of proper orthogonal decomposition for dynamical characterization and order reduction of mechanical systems: an overview. *Nonlinear dynamics*, 41(1-3):147–169, 2005.

- [38] VI Kliatskin. Stochastic equations and waves in randomly inhomogeneous media. *Moscow Izdatel Nauka*, 1, 1980.
- [39] Andreas Klimke. Sparse Grid Interpolation Toolbox – user’s guide. Technical Report IANS report 2007/017, University of Stuttgart, 2007.
- [40] Andreas Klimke and Barbara Wohlmuth. Algorithm 847: spinterp: Piecewise multilinear hierarchical sparse grid interpolation in MATLAB. *ACM Transactions on Mathematical Software*, 31(4), 2005.
- [41] DD Kosambi. Statistics in function space. *J. Indian Math. Soc.*, 7(1):76–88, 1943.
- [42] OP Le Maître, HN Najm, RG Ghanem, and OM Knio. Multi-resolution analysis of wiener-type uncertainty propagation schemes. *Journal of Computational Physics*, 197(2):502–531, 2004.
- [43] YC Liang, HP Lee, SP Lim, WZ Lin, KH Lee, and CG Wu. Proper orthogonal decomposition and its applications part i: Theory. *Journal of Sound and vibration*, 252(3):527–544, 2002.
- [44] YC Liang, WZ Lin, HP Lee, SP Lim, KH Lee, and H Sun. Proper orthogonal decomposition and its applications part ii: Model reduction for mems dynamical analysis. *Journal of Sound and Vibration*, 256(3):515–532, 2002.
- [45] Guang Lin, C-H Su, and George E Karniadakis. Predicting shock dynamics in the presence of uncertainties. *Journal of Computational Physics*, 217(1):260–276, 2006.
- [46] Yiming Lou and Panagiotis D Christofides. Estimation and control of surface roughness in thin film growth using kinetic monte-carlo models. *Chemical Engineering Science*, 58(14):3115–3129, 2003.
- [47] Yiming Lou and Panagiotis D Christofides. Feedback control of growth rate and surface roughness in thin film growth. *AIChE Journal*, 49(8):2099–2113, 2003.
- [48] Yiming Lou and Panagiotis D Christofides. Feedback control of surface roughness of gas (0 0 1) thin films using kinetic monte carlo models. *Computers & chemical engineering*, 29(1):225–241, 2004.
- [49] D Lucor, D Xiu, and G Karniadakis. Spectral representations of uncertainty in simulations: Algorithms and applications. In *Proceedings of the International Conference on Spectral and High Order Methods (ICOSAHOM-01)*, Uppsala, Sweden, 2001.
- [50] Youssef Marzouk and Dongbin Xiu. A stochastic collocation approach to bayesian inference in inverse problems. 2009.
- [51] R Mikulevicius and BL Rozovskii. Stochastic navier–stokes equations for turbulent flows. *SIAM Journal on Mathematical Analysis*, 35(5):1250–1310, 2004.

- [52] Guilhem Mollon, Daniel Dias, and Abdul-Hamid Soubra. Probabilistic analysis of pressurized tunnels against face stability using collocation-based stochastic response surface method. *Journal of Geotechnical and Geoenvironmental Engineering*, 137(4):385–397, 2010.
- [53] Habib N Najm. Uncertainty quantification and polynomial chaos techniques in computational fluid dynamics. *Annual Review of Fluid Mechanics*, 41:35–52, 2009.
- [54] Dong Ni and Panagiotis D Christofides. Multivariable predictive control of thin film deposition using a stochastic pde model. *Industrial & Engineering Chemistry Research*, 44(8):2416–2427, 2005.
- [55] Qing Nie, Yong-Tao Zhang, and Rui Zhao. Efficient semi-implicit schemes for stiff systems. *Journal of Computational Physics*, 214(2):521–537, 2006.
- [56] Bernd R Noack, Konstantin Afanasiev, Marek Morzynski, Gilead Tadmor, and Frank Thiele. A hierarchy of low-dimensional models for the transient and post-transient cylinder wake. *Journal of Fluid Mechanics*, 497:335–363, 2003.
- [57] Fabio Nobile, Raúl Tempone, and Clayton G Webster. A sparse grid stochastic collocation method for partial differential equations with random input data. *SIAM Journal on Numerical Analysis*, 46(5):2309–2345, 2008.
- [58] Anthony Nouy. A generalized spectral decomposition technique to solve a class of linear stochastic partial differential equations. *Computer Methods in Applied Mechanics and Engineering*, 196(45):4521–4537, 2007.
- [59] Anthony Nouy. Generalized spectral decomposition method for solving stochastic finite element equations: invariant subspace problem and dedicated algorithms. *Computer Methods in Applied Mechanics and Engineering*, 197(51):4718–4736, 2008.
- [60] Steven A Orszag and LR Bissonnette. Dynamical properties of truncated wiener-hermite expansions. *Physics of Fluids (1958-1988)*, 10(12):2603–2613, 1967.
- [61] George C Papanicolaou. Wave propagation in a one-dimensional random medium. *SIAM Journal on Applied Mathematics*, 21(1):13–18, 1971.
- [62] George C Papanicolaou. Diffusion in random media. In *Surveys in applied mathematics*, pages 205–253. Springer, 1995.
- [63] E Pardoux. Stochastic partial differential equations and filtering of diffusion processes. *Stochastics*, 3(1-4):127–167, 1980.
- [64] Jose Miguel Pasini and Tuhin Sahai. Polynomial chaos based uncertainty quantification in hamiltonian and chaotic systems. In *Decision and Control (CDC), 2013 IEEE 52nd Annual Conference on*, pages 1113–1118. IEEE, 2013.

- [65] K Person. On lines and planes of closest fit to system of points in space. *philosophical magazine*, 2, 559-572, 1901.
- [66] Matthew T Reagan, HN Najm, PP Pebay, OM Knio, and RG Ghanem. Quantifying uncertainty in chemical systems modeling. *International journal of chemical kinetics*, 37(6):368–382, 2005.
- [67] Sethuraman Sankaran and Alison L Marsden. A stochastic collocation method for uncertainty quantification and propagation in cardiovascular simulations. *Journal of biomechanical engineering*, 133(3):031001, 2011.
- [68] Ya Sinai. Burgers system driven by a periodic stochastic flow. *Itô's stochastic calculus and probability theory*, Springer, Tokyo, pages 347–353, 1996.
- [69] Ya G Sinai. Two results concerning asymptotic behavior of solutions of the burgers equation with force. *Journal of statistical physics*, 64(1-2):1–12, 1991.
- [70] Sergey A Smolyak. Quadrature and interpolation formulas for tensor products of certain classes of functions. In *Dokl. Akad. Nauk SSSR*, volume 4, page 123, 1963.
- [71] Pol D Spanos and Roger Ghanem. Stochastic finite element expansion for random media. *Journal of engineering mechanics*, 115(5):1035–1053, 1989.
- [72] Aretha L Teckentrup, Peter Jantsch, Clayton G Webster, and Max Gunzburger. A multilevel stochastic collocation method for partial differential equations with random input data. *SIAM/ASA Journal on Uncertainty Quantification*, 3(1):1046–1074, 2015.
- [73] Jonathan H Tu and Clarence W Rowley. An improved algorithm for balanced pod through an analytic treatment of impulse response tails. *Journal of Computational Physics*, 231(16):5317–5333, 2012.
- [74] Manuel Villegas, F Augustin, Albert Gilg, A Hmadi, and Utz Wever. Application of the polynomial chaos expansion to the simulation of chemical reactors with uncertainties. *Mathematics and Computers in Simulation*, 82(5):805–817, 2012.
- [75] Xiaoliang Wan and George Em Karniadakis. An adaptive multi-element generalized polynomial chaos method for stochastic differential equations. *Journal of Computational Physics*, 209(2):617–642, 2005.
- [76] Xiaoliang Wan and George Em Karniadakis. Multi-element generalized polynomial chaos for arbitrary probability measures. *SIAM Journal on Scientific Computing*, 28(3):901–928, 2006.
- [77] Grzegorz W Wasilkowski and Henryk Wozniakowski. Explicit cost bounds of algorithms for multivariate tensor product problems. *Journal of Complexity*, 11(1):1–56, 1995.

- [78] E Weinan and Eric Vanden Eijnden. Statistical theory for the stochastic burgers equation in the inviscid limit. *Commun. Pure Appl. Math.*, 53:852–901, 2000.
- [79] E Weinan, K Khanin, A Mazel, and Ya Sinai. Invariant measure for burgers equation with stochastic forcing. *Annals of Mathematics-Second Series*, 151(3):877–960, 2000.
- [80] E Weinan, Konstantin Khanin, Alexandre Mazel, and Yakov Sinai. Probability distribution functions for the random forced burgers equation. *Physical Review Letters*, 78(10):1904, 1997.
- [81] Norbert Wiener. The homogeneous chaos. *American Journal of Mathematics*, 60(4):897–936, 1938.
- [82] Norbert Wiener. Nonlinear problems in random theory. *Nonlinear Problems in Random Theory*, by Norbert Wiener, pp. 142. ISBN 0-262-73012-X. Cambridge, Massachusetts, USA: The MIT Press, August 1966.(Paper), 1, 1966.
- [83] Karen Willcox and Jaime Peraire. Balanced model reduction via the proper orthogonal decomposition. *AIAA journal*, 40(11):2323–2330, 2002.
- [84] Dongbin Xiu. Efficient collocational approach for parametric uncertainty analysis. *Commun. Comput. Phys*, 2(2):293–309, 2007.
- [85] Dongbin Xiu. *Numerical Methods for Stochastic Computations*. Princeton University Press, 2010.
- [86] Dongbin Xiu and Jan S Hesthaven. High-order collocation methods for differential equations with random inputs. *SIAM Journal on Scientific Computing*, 27(3):1118–1139, 2005.
- [87] Dongbin Xiu and George Em Karniadakis. Modeling uncertainty in steady state diffusion problems via generalized polynomial chaos. *Computer Methods in Applied Mechanics and Engineering*, 191(43):4927–4948, 2002.
- [88] Dongbin Xiu and George Em Karniadakis. The wiener–askey polynomial chaos for stochastic differential equations. *SIAM journal on scientific computing*, 24(2):619–644, 2002.
- [89] Dongbin Xiu and George Em Karniadakis. Modeling uncertainty in flow simulations via generalized polynomial chaos. *Journal of computational physics*, 187(1):137–167, 2003.
- [90] Dongbin Xiu, Didier Lucor, C-H Su, and George Em Karniadakis. Stochastic modeling of flow-structure interactions using generalized polynomial chaos. *Journal of Fluids Engineering*, 124(1):51–59, 2002.

- [91] Thomas A Zang, Michael J Hensch, Mark W Hilburger, Sean P Kenny, James M Luckring, Peiman Maghami, Sharon L Padula, and W Jefferson Stroud. Needs and opportunities for uncertainty-based multidisciplinary design methods for aerospace vehicles. 2002.